Review

Recent Advances and Prospects of FeOOH-Based Electrode Materials for Supercapacitors

Youness El Issmaeli [1], Amina Lahrichi [1], Shankara S. Kalanur [1,*], Sadesh Kumar Natarajan [1] and Bruno G. Pollet [1,2,*]

1   GreenH2Lab, Hydrogen Research Institute (HRI), Department of Chemistry, Biochemistry and Physics, Université Du Québec à Trois-Rivières (UQTR), 3351 Boulevard des Forges, Trois-Rivières, QC G9A 5H7, Canada
2   Hydrogen Energy and Sonochemistry Research Group, Department of Energy and Process Engineering, Faculty of Engineering, Norwegian University of Science and Technology (NTNU), NO-7491 Trondheim, Norway
*   Correspondence: shankara.kalanur@uqtr.ca (S.S.K.); bruno.pollet@uqtr.ca (B.G.P.)

Abstract: Supercapacitors (SCs) offer a potential replacement for traditional lithium-based batteries in energy-storage devices thanks to the increased power density and stable charge–discharge cycles, as well as negligible environmental impact. Given this, a vast array of materials has been explored for SCs devices. Among the materials, iron oxyhydroxide (FeOOH) has gained significant attention in SC devices, owing to its superior specific capacitance, stability, eco-friendliness, abundance, and affordability. However, FeOOH has certain limitations that impact its energy storage capabilities and thus implicate the need for optimizing its structural, crystal, electrical, and chemical properties. This review delves into the latest advancements in FeOOH-based materials for SCs, exploring factors that impact their electrochemical performance. To address the limitations of FeOOH's materials, several strategies have been developed, which enhance the surface area and facilitate rapid electron transfer and ion diffusion. In this review, composite materials are also examined for their synergistic effects on supercapacitive performance. It investigates binary, ternary, and quaternary Fe-based hydroxides, as well as layered double hydroxides (LDHs). Promising results have been achieved with binder-free Fe-based binary LDH composites featuring unique architectures. Furthermore, the analysis of the asymmetric cell performance of FeOOH-based materials is discussed, demonstrating their potential exploitation for high energy-density SCs that could potentially provide an effective pathway in fabricating efficient, cost-effective, and practical energy storage systems for future exploitations in devices. This review provides up-to-date progress studies of novel FeOOH's based electrodes for SCs applications.

Keywords: iron oxyhydroxide (FeOOH); capacitive performance; supercapacitors; hybrid supercapacitors; energy storage

1. Introduction

Energy is a vital ingredient for human advancement. Hence, factors such as the source of energy, production, storage, and transportation hold the key to fulfilling the growing demand for energy and its management for stable development. Currently, there is an energy crisis triggered primarily by the exhaustion of fossil fuels, environmental pollution, and the increasing use of electric cars, portable electronics, and wireless devices [1,2]. Until now, the fossil fuel-derived energy sector has been at the forefront of human development due to its availability, cost, and ease of utilization in a wide range of applications. However, the burning of fossil fuels releases approximately 34 billion tons of carbon dioxide (CO_2) into the atmosphere each year [3], implicating serious environmental concerns associated with fossil fuels. To address this, governments around the world are introducing policies to decrease the use of fossil fuels and encourage the use of renewable energy sources.

Increasingly, countries are pledging to achieve net zero emissions over the next few decades. For example, more than 70 countries, including the biggest polluters—China, the United States, and the European Union—have set a net zero target, covering about 76% of global emissions [4]. However, the commitments so far are far from what is needed to achieve net zero CO_2 emissions by 2050 and ensure a 1.5 °C limit on the rise of global temperatures [5]. Even if all countries were to meet their current commitments, global emissions would still be higher than what is necessary to achieve the objectives of the Paris Agreement [6]. Therefore, more ambitious commitments are essential to reach the goal of net zero emissions by 2050. Hence, the development of clean and renewable energy systems is under intensive research, with advanced energy storage being one of the key components [7–12]. Therefore, a low-cost, energy-efficient, and eco-friendly energy storage system is essential [13–15].

Because of their simple structure, safety, and versatility, SCs are promising types of energy storage systems that may revolutionize the mode of storage and harvesting of renewable energy sources. In addition to having increased power density, high capacitance, rapid charging/discharging rates, extended shelf life, and high cycling performance, they have a minimal environmental impact and intrinsic safety [13,16–20]. SCs are composed of non-toxic, recyclable materials and can operate in a variety of temperatures and environmental conditions. They also require minimal maintenance and have an extremely long life, indicating a prolonged life cycle with no degradation in performance [21–23]. Supercapacitors are composed of a negative and positive electrode divided using a separator immersed in the electrolyte medium for charge diffusion/transfer. As such, supercapacitors are ideal for energy storage in a variety of devices including portable electronics and industrial machinery. In supercapacitors, electrodes play a significant role in electrochemical properties because they are responsible for reversible adsorption/desorption or electrochemical reactions [18,24,25]. Recently, supercapacitors have attracted much attention worldwide because they have several benefits over conventional capacitors and batteries [26–28]. There is no doubt that batteries possess a high energy density. However, their charging and discharge rates, as well as their service life, are severely restricted by cation diffusion in the crystalline framework [29,30]. It is not uncommon for conventional capacitors to possess a practically infinite life cycle, but their energy density, on the other hand, is quite low [31–33]. According to the Ragone plot as presented in Figure 1a, SCs have a higher energy and power density in comparison to standard capacitors and batteries/fuel cells, respectively, and thus act as a bridge between these three common energy storage devices. Consequently, supercapacitors are well suited to behave as advanced energy storage devices, as they combine the advantages of conventional dielectric capacitors (electrostatic) with the advantages of rechargeable batteries (electrochemical) [19,21,34,35].
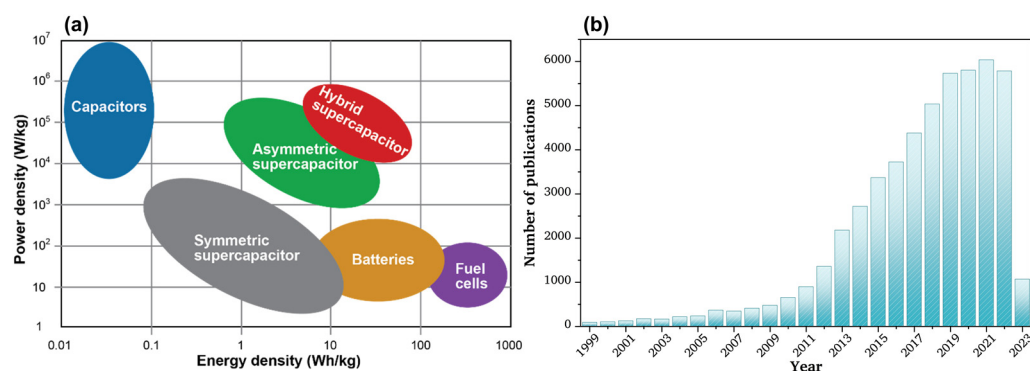

Figure 1. (**a**) Ragone plot showing different types of energy storage materials [36]. (**b**) Evolution of the yearly number of publications on FeOOH-based materials for supercapacitors from 1999 to February 2023 (from CAS-SciFinder, access 27 February 2023). Search terms in the topic: "FeOOH-based materials for supercapacitors".

1.1. Types of Supercapacitors

Based on the mechanism of charge storage, the SCs are classified as shown below [13,16,19,21,37]:

- Electric double-layer capacitor (EDLC) or so-called non-faradaic EDLC;
- Pseudo-capacitor (PC) or faradaic supercapacitor;
- Hybrid capacitor of hybrid supercapacitor (HSC).

According to the type and configuration of employed electrodes, each type of super-capacitor is subcategorized into different classes, as shown in Figure 2. The same figure displays a schematic representation of the three types of supercapacitors and their working mechanisms [38–40].
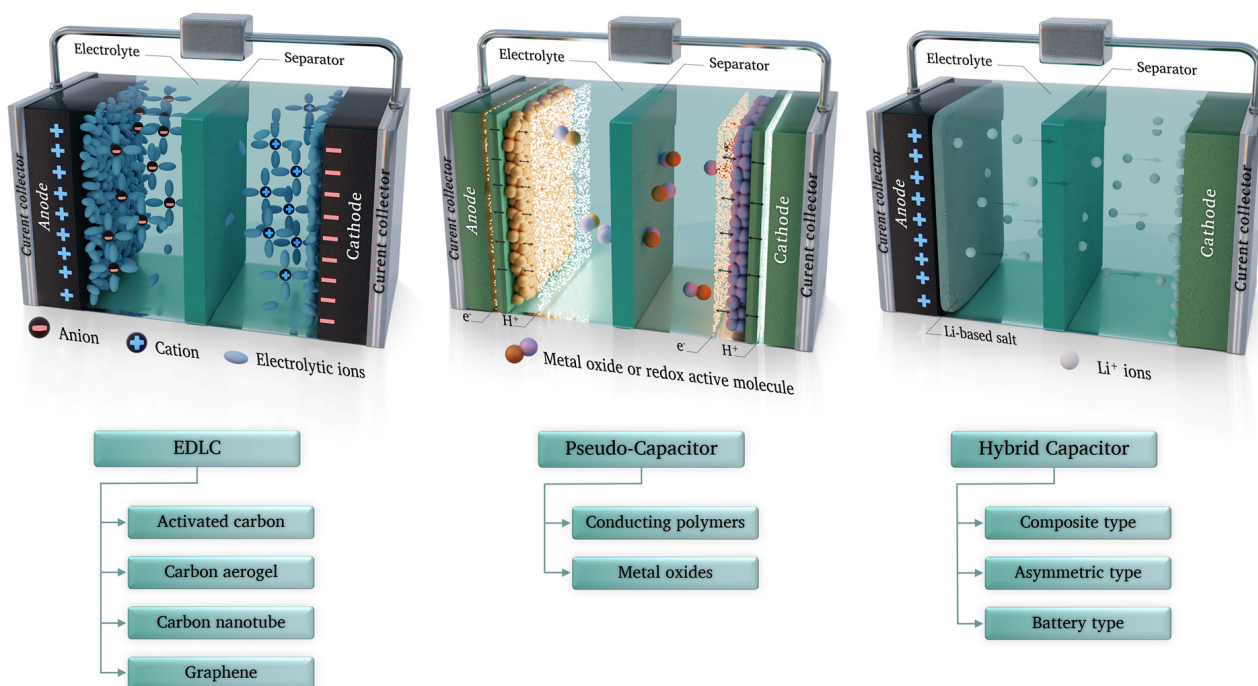
Figure 2. Schematic representation of the three types of supercapacitors with their taxonomy based on the mechanism of storing energy and on the most common types of electrodes they incorporate.

There are several carbon-based electrode materials used in electric double-layer capacitors, including activated carbon [41–46], carbon aerogels [47–52], carbon nanotubes [53–58], and carbon nanofibers [59–63]. Electrodes and electrolytes do not exchange charges in EDLCs, so the energy is stored electrostatically [19,38,64]. This means that non-faradaic EDLCs store energy in an ionic double layer (Helmholtz layer) as a result of electrostatic accumulation/adsorption of electrolytic ions at the electrode/electrolyte interface. Because of the absence of charge transfer in the non-faradaic method, no structural or chemical modification is required. EDLCs can therefore store charges highly reversibly, resulting in very high cycling stability [18,19,39].

A pseudo-capacitor is a device whose electrode materials contain metal oxides [24,65–69] and conductive polymers [35,63,70]. Through redox reactions, electrosorption, and intercalation on the surface and subsurface of the material, a PC works by transferring charge between each electrode and the electrolyte [21,39,64]. This is completed using the Faradaic approach. When compared to EDLCs, this increases capacitance and energy density. However, PCs are limited in their application due to their relatively low conductivity and poor cycle life [19,64], which means there is a relatively small number of charging/discharging cycles that an individual PC can complete before it starts to lose performance.

The newest and most advanced type of supercapacitor is the hybrid capacitor, which combines both Faradaic and non-Faradaic approaches to store energy [21,64]. On the one hand, the faradaic reaction occurs on the negative electrode, which is typically fabricated from pseudocapacitance electrode material. As a result, HCs have a higher energy density. On the other hand, charge carriers interact electrostatically with the electrode's surface on the positive electrode, which is typically made from carbon electrode material. Therefore,

HCs can deliver higher power density. In addition, HCs have a longer cycle life and improved stability compared to previous types of supercapacitors [21,35,40]. There are three types of hybrid supercapacitors, according to the configuration of their electrodes: composite, asymmetric, and battery type [38–40].

To compete with batteries in the future, hybrid supercapacitors will need significant breakthroughs in research to have enhanced energy storage capabilities. Such advances may come about through advancements in electrode materials [18,24,25], as pseudocapacitance electrode materials, hydroxides, and transition-metal oxides have attracted extensive research. This is because of the multiple valence states and unique crystal structures that enable rapid faradaic redox intercalation [55,65].

1.2. Iron-Based Materials for Supercapacitors

Iron-based/hydroxides are among the transition metal oxides and hydroxides that offer significant advantages as SC's electrodes due to iron's various valence states (Fe^0, Fe^{2+}, Fe^{3+}, etc.) and its rich oxidation-reduction reactions (Fe^{2+}/Fe^{3+}, Fe^0/Fe^{2+}, Fe^0/Fe^{3+}, etc.); they are capable of exhibiting high specific capacitances [71–73]. In addition, most transition metal oxides and hydroxides are utilized for positive electrodes; however, iron oxides/hydroxides have a wide and stable working window at a negative potential which is ideal for asymmetric supercapacitor (ASC) devices [74–76]. Furthermore, iron oxides and hydroxides are non-toxic and more eco-friendly compared to other transition metal oxides and hydroxides [77–79]. A final consideration is that iron oxides and hydroxides are abundant on Earth and inexpensive (under $1/kg for ferric oxide), making them suitable for pilot-scale production without affecting the supply chain [80–82]. During the past two decades, iron oxide-hydroxide-based supercapacitor materials have been published in a greater number, as depicted in Figure 1b (The data were obtained from the CAS-SciFinder database).

α-FeOOH, β-FeOOH, and γ-FeOOH (also known as Goethite, Akaganeite, and Lepidocrocite, respectively) are all polymorphs of iron oxyhydroxide (FeOOH) that have been investigated as supercapacitor electrodes [70,83–88] and other energy-storage systems [89–95]. Each of these polymorphs (the crystallographic representation is shown in Figure 3) has a unique crystalline structure and properties that make them promising candidates for SC's applications. To begin with, α-FeOOH appears to have a three-dimensional (3D) structure formed by $FeO_3(OH)_3$ octahedra that create large tunnels. Despite its wide range of shapes, goethite generally has an acicular morphology [96]. Second, Akaganeite, β-FeOOH, has a large tunnel-shaped structure with strongly bonded iron atoms. Finally, showing orthorhombic symmetry, γ-FeOOH is composed of layers of iron octahedra stacked upon each other, connected by hydrogen bonds. It is common to find lepidocrocites with a tabular or lath-like morphology [96].

Overall, FeOOH materials are considered exceptional anode materials for SCs due to their tunnel structures that facilitate efficient ion diffusion of the electrolyte [86]. However, when compared to other available materials, they exhibit numerous limitations and challenges that hinder their electrochemical properties. For example, the critical disadvantages of FeOOH-based materials include poor electrical conductivity and low specific surface area leading to restricted specific capacitance, rate capability, power density, and stability [24,66,97]. Additionally, the application of α-FeOOH nanoparticles and graphene oxide (GO) composites faces problems such as large particle size and broad size distribution in GO coating structures [85]. Furthermore, β-FeOOH has poor electrical conductivity, and its synthesis, which is typically conducted in acidic solutions, results in extra protonation of oxides within iron octahedra, causing structural destabilization [86]. Another issue is the degradation in the gravimetric capacitance of γ-FeOOH-based electrodes, which has been observed due to poor utilization of electroactive species and reduced active surface area at greater thicknesses [71]. Crystalline FeOOH materials also encounter difficulties in expanding or contracting, which in turn limits ion permeation and diffusion [97]. Although mixing FeOOH with a conducting polymer or graphene could potentially enhance its properties,

it would simultaneously increase the resistance between the active material and current collectors or raise costs. Preparing amorphous FeOOH directly on a substrate without a binder remains a challenge [98]. Conclusively, FeOOH's limitations have been addressed through significant research, and efforts have been made to improve its electrochemical properties [24,66–68,84,85,87,88,97–136].
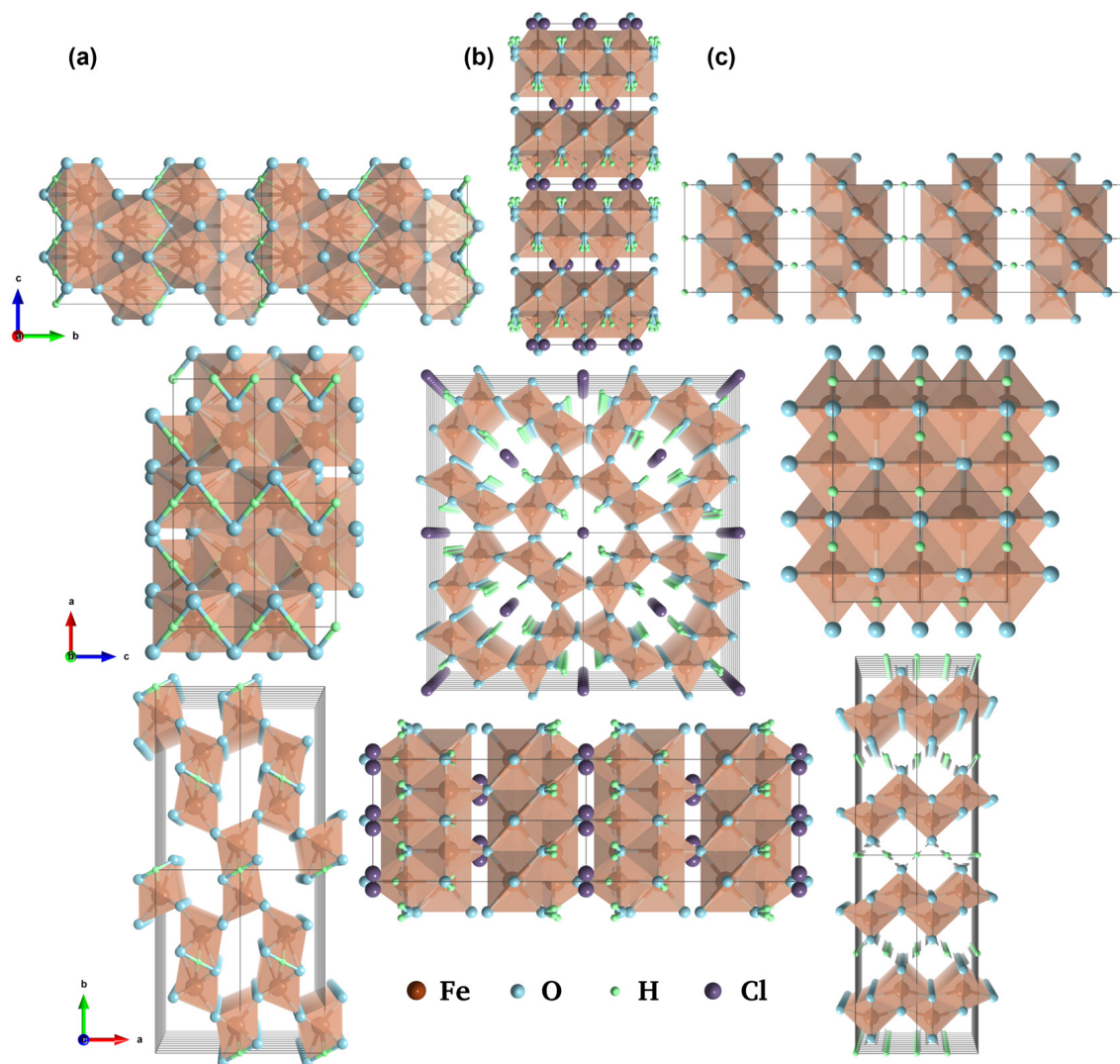
Figure 3. Crystal structure schematic representation of (**a**) α-FeOOH, (**b**) β-FeOOH, and (**c**) γ-FeOOH from three different views.

Herein, we summarize the recent advancements in the utilization of FeOOH in SC systems, delving into essential rational design, synthesis, and capacitive performance of various FeOOH-based electrodes (e.g., FeOOH, Co-Fe Layered Double Hydroxide (LDH), Ni-Fe LDH, Ni-Co-Fe LDH, Ternary and Quaternary LDH) as well as their composites for SC application. The review investigates factors influencing the electrochemical performance of FeOOH electrodes and provides an up-to-date overview of unique FeOOH-based electrodes for SCs. In addressing the inherent limitations of FeOOH materials, the review explores strategies that include the synergistic effects of composite materials and the development of Fe-based binary, ternary, and quaternary hydroxides and LDHs. Promising results achieved with binder-free Fe-based binary LDH composites featuring unique architectures are presented, and the enhancement of supercapacitive performance through synergistic effects is discussed. Furthermore, this review provides a comprehensive analysis of the asymmetric cell performance of FeOOH-based materials, highlighting their potential

for constructing next-generation, cost-effective, high energy density devices. Additionally, FeOOH-based materials are discussed as potential electrode materials for SCs, offering insight into their development and optimization in the future.

2. FeOOH

2.1. Low-Crystalline and Crystalline FeOOH

There is generally a higher mobility of charge carriers in crystalline materials compared to amorphous materials. Despite this, amorphous materials have a variety of structural defects, including vacancies, that help the diffusion of electrolyte ions [137,138]. In the process of charging and discharging, amorphous materials present isotropic strain. The electrochemical system's long-term stability is thus enhanced. Therefore, many material systems will perform better with amorphous or low-crystalline phases [68,88,97,98,101] compared to the pure crystalline forms. This section highlights the advancements of low-crystalline and crystalline FeOOH in SC applications.

As demonstrated by Liu et al., FeOOH quantum dots could be elaborated by using a simple method [97]. The developed scheme successfully produces FeOOH QDs/functionalized graphene sheets (FGS) and FeOOH quantum dots (QDs) of 2 nm, as shown in Figure 4a. The synthesized FeOOH/FGS hybrid nanosheets display an unusual heterostructure (Figure 4b) that consists of mesoporous FeOOH nanofilms tightly anchored to the surface of graphene nanosheets. This study presents the first investigation of amorphous FeOOH-based electrode materials for supercapacitors. It has been shown that the hybrid FeOOH/FGS nanosheets have superior pseudocapacitive properties, which outperform the crystalline iron oxide/hydroxide-based materials in terms of pseudocapacitive performance. Electrodes made from amorphous FeOOH/FGS exhibit at 1 A g^{-1} significant specific capacitances of approximately 365 F g^{-1} at a voltage ranging between -0.8 and 0 V vs. Ag/AgCl, superb cycling stability (89.7% capacitance retention over 20,000 charge–discharge cycles), and at a current density of 128 A g^{-1} a superior rate capability of 189 F g^{-1}. Furthermore, the FeOOH/FGS hybrid nanosheets were conducted at broad voltage intervals ranging from -1 to 0 V and from -1.25 to 0 V. It was found that the poor-rate and cycling performances of FeOOH-based electrodes make them unsuitable for use in broad voltage windows despite reaching the 1243 F g^{-1} of enhanced specific capacitance.

Amorphous nanostructured fish-scale-like FeOOH were produced using a one-step electrodeposition method that is simple, cost-effective, scalable, and environmentally friendly, as shown in Figure 4c [88]. The hydroxides' unique nanostructures provide ample active sites, efficient electronic and ionic transport, and the ability to handle strain and distortion effectively. The material's amorphous nature allows for easy diffusion of electrolyte ions and their reaction, allowing for the isotropic charging and discharging mechanism. FeOOH electrodes demonstrate a pseudocapacitance of 867 F g^{-1} at 5 mV s^{-1} due to these advantages. In the same study, flower-like Co-Ni DH was elaborated using the same method to serve as a cathode material. The Co-Ni DH electrode exhibited a large pseudocapacitance (at 5 mV s^{-1}) of 1201 F g^{-1}. At an elevated scan rate of 50 mV s^{-1}, both Co-Ni DH and FeOOH electrodes maintained increased capacitances of 0.595 and 0.702 F cm^{-2}, respectively, indicating excellent rate capabilities. With FeOOH and Co-Ni DH as an anode and a cathode, respectively, an ASC was engineered and displayed a superior energy and power density of 86.4 W h kg^{-1} and 11.6 kW kg^{-1}, respectively. Moreover, a stable charge/discharge cycle was absorbed that retained to 92.3% at the 200th cycle, as well as low impedance with an upper limit of 30 Ω for both Z' and -Z''.

A one-pot hydrothermal route has also been used to produce amorphous FeOOH without the need for a binder, which was directly deposited onto Ni foam (NF) [98]. The amorphous FeOOH flakes formed on the surface of NF appear to have a 3D porous structure. Such a unique structure offers facile penetration of liquid electrolytes, enabling rapid ion diffusion and electron transfer. In addition, it mitigates the volume change of FeOOH/NF electrodes through the charge–discharge process. At 2 A g^{-1} current density, an optimized

FeOOH/NF electrode was observed to have a large specific capacitance of 1300 F g^{-1}, with an impressive capacity retention of 91% at a 4 A g^{-1} current density.

It was reported by Owusu et al. [66] that a low-crystalline nanoparticle FeOOH anode displayed excellent electrochemical performance across a wide potential window. The researchers employed a unique approach to produce low-crystalline FeOOH nanoparticles, involving the hydrothermal synthesis of α-Fe_2O_3, followed by an electrochemical transformation to FeOOH having low crystallinity on carbon fiber cloth (CFC). With 1.6 and 9.1 mg cm^{-2} mass loadings at a current density of 1 A g^{-1}, the FeOOH nanoparticles demonstrated capacitances of 1066 and 716 F g^{-1}, respectively. It was found to be retained at 74.6% (at 30 A g^{-1} of current density) and maintained at 91% of capacitance after 10,000 cycles were demonstrated, indicating the superior stability of the electrodes. A primary capacitive charge storage mechanism is responsible for the impressive performance. Furthermore, using the hydrothermal method, the researchers designed $NiMoO_4$ electrode (cathode electrode for battery-type configuration) to construct a $NiMoO_4$//FeOOH aqueous hybrid supercapacitor. The HSC demonstrated a 1.27 kW kg^{-1} power density and an energy density of 104.3 Wh kg^{-1} in an extended potential range of 1.7 V, a 273 F g^{-1} of capacitance at 1.5 A g^{-1} current density, and superior stability during the float voltage test for 450 h.
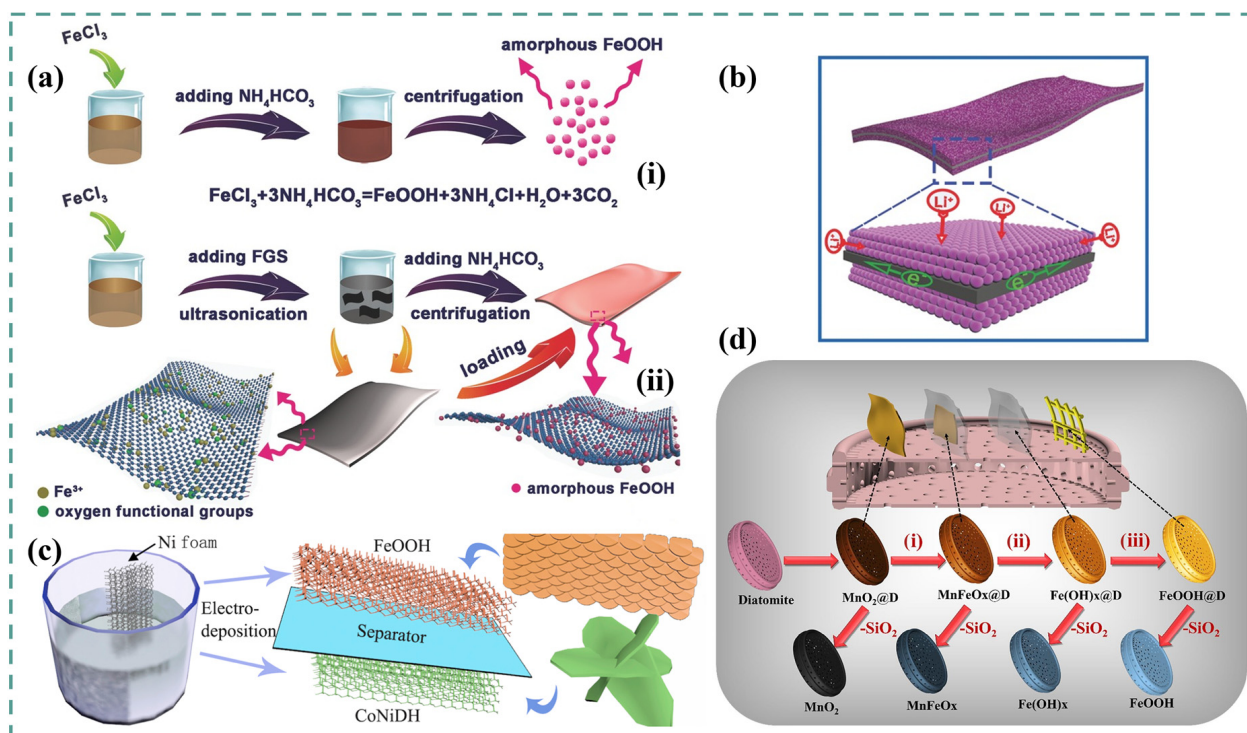
Figure 4. Schematic representation about (**a**) the fabrication of (i) amorphous FeOOH QDs and (ii) amorphous FeOOH/FGS hybrid nanosheets, and about (**b**) The FeOOH/FGS hybrid nanosheet heterostructure. Reprinted from Ref. [97], Copyright (2023), with permission from John Wiley and Sons. (**c**) Graphical illustration about the fabrication of FeOOH and Co-Ni DH. Reprinted from Ref. [88], Copyright (2023), with permission from Elsevier. (**d**) Scheme about the transition from MnO_2@D to FeOOH@D and replicas after removing the template of diatomite: (i) Fe(OH)x layer covering MnO_2; (ii) Fe^{2+} replacing MnO_2; (iii) Fe(OH)x grown into nanorods. Reprinted from Ref. [24], Copyright (2023), with permission from Elsevier.

Amorphous iron oxides/hydroxides tend to exhibit greater electrochemical activity due to their disorganized structures; however, significant studies have focused on crystalline phases instead [24,84,85,87]. On the carbon nanofoam paper (CNFP), the fact that the amorphous Ni-Mn hydroxide and γ-FeOOH were electrodeposited to create negative

and positive electrodes, respectively, has been reported by Nguyen et Montemor [87]. The γ-FeOOH on CNFP demonstrated a porous morphology with fluffy nanoflakes and ameliorated redox response in the -1.5–0 V vs. SCE negative working potential range, achieving a storage capacity of 3.48 C cm^{-2} at 10 mA cm^{-2} and a 71% rate of response while current density rose to 50 from 10 mA cm^{-2}. The amorphous Ni-Mn hydroxide on CNFP exhibited fine nanoflakes with porous morphology and improved redox response at 0–0.5 V. At a current density of 10 mA cm^{-2}, the storage capacity of SCE was 1.54 C cm^{-2}, and there was a 73% rate of response with the rise in current density to 50 from 10 mA cm^{-2}. At 50 mA cm^{-2}, FeOOH-CNFP electrodes retained 92% of capacity after 3000 charge–discharge cycles. Ni-Mn hydroxide electrodes retained 94% of capacity. The SC device attained 1515 mW h cm^{-2} of energy density at a power density of 9 mW cm^{-2} with the 1.8 V working voltage and extended cycle life, maintaining capacitance of 95% after 10,000 cycles of charge and discharge. It self-discharged from 1.8 V to 1 V in 10 h. The negative FeOOH-CNFP electrode primarily contributed to the cell's self-discharge, with self-discharge processes in this electrode being mainly activation-controlled. On the other hand, the positive Ni-Mn hydroxide-CNFP electrode's self-discharge processes were controlled by both activation and diffusion.

2.2. FeOOH Replica from MnO$_2$

Diatomite is a mineral composed of bio-silica produced by single cell algae called diatoms. It is considered a highly desirable template for creating three-dimensional structures. Because diatoms possess a distinctive 3D silica shell structure with micro- to nano-porous walls, their hierarchical silica layers can offer intricate and orderly pore patterns and complexity that cannot be achieved by current fabrication technologies [139]. Due to these exceptional characteristics, researchers have invested significant efforts into exploring the potential of diatoms for energy storage applications [24,140]. Li et al. have controlled the elaboration of Mn-Fe-oxide hybrids (Mn-FeOx) through a customizable porous three-dimensional structure containing diatoms for efficient SCs [24]. The process involved a two-step hydrothermal method for transitioning from MnO$_2$ to FeOOH on diatomite, followed by an etching process to obtain replicas with 3D diatom morphology. By varying the dosages of FeSO$_4$·7H$_2$O, the researchers were able to tune the MnFeOx replicas to different forms with either MnO$_2$ nanosheets or FeOOH nanorods structures created on diatom structures, as depicted in Figure 4d. All replicas were derived from the removal of diatom silica while maintaining their unique 3D morphology and porosity. The MnFeOx replica with MnO$_2$ nanosheets as anodes showed the best electrochemical properties, exhibiting a superior stability of 94.3% over 4000 cycles, a rate capability of 74.6% retention at an increased current density to 10 A g^{-1}, a 228.6 F g^{-1} specific capacitance at 1 A g^{-1} of current density, and a coulombic efficiency of approximately 93.1% at 10 A g^{-1}. MnFeOx-110, as a cathode material containing completely transitioned FeOOH nanorods, demonstrated exceptional properties, including 224.6 F g^{-1} specific capacitance at a current density of 1 A g^{-1}, a coulombic efficiency of about 80% at 10 A g^{-1}, and a stable cathode retention of 92.5% at the 4000th cycle. An ASC was fabricated using MnFeOx-0 and MnFeOx-110 as positive and negative electrodes, respectively, which delivered an extended potential window (2 V) with a maximum energy density of 51.5 Wh kg^{-1} and a power density of 9.1 kW kg^{-1}. Figure 5a shows an illustration of the different components of the assembled ASC. The unique nanostructure and removal of diatomite enlarged the active sites and surface area that contacted the electrolyte, avoiding accumulation and making the electrochemical properties outstanding. This facile transition process can prepare positive and negative materials by a simple preparation process, and the replica has greater energy storage properties, opening an opportunity for the rational design of diatomite morphology electrode material for advanced supercapacitors.

Inspired by the process of conversion of MnO$_2$ to FeOOH, Wang et al. have recently introduced a novel and uncomplicated approach to obtain FeOOH with retained morphology by transforming MnO$_2$ into FeOOH (Figure 5b) [99]. This strategy produced a hollow

parallel FeOOH, which can be employed as the negative electrode in ASCs. The key factors for achieving the preserved morphology are low-temperature and dropwise strategies, which were determined through a series of controlled experiments. At 0.5 A g^{-1} the hollow parallel FeOOH exhibited an exceptional specific capacitance of 186.8 F g^{-1} as well as a 93.1% capacitance retention at the 4000th cycle. The electrochemical characterization of the ASC with parallel MnO$_2$ and FeOOH (hollow parallel) as the positive electrode and negative electrodes, respectively, outperformed those having FeOOH or activated graphene as negative electrodes. The negative and positive electrodes have a high electrochemical matching effect owing to the advantages of parallel nanostructures. At a power density of 0.5 kW kg^{-1}, the energy density was recorded as high as 46.8 Wh kg^{-1}, while it remained at 20.7 Wh kg^{-1} at the maximum power density of 10 kW kg^{-1}. It is also highly versatile and thus applied to all the MnO$_2$ research areas as a suitable negative electrode that are structurally and electrochemically identical, resulting in improved electrochemical performance of ASCs.
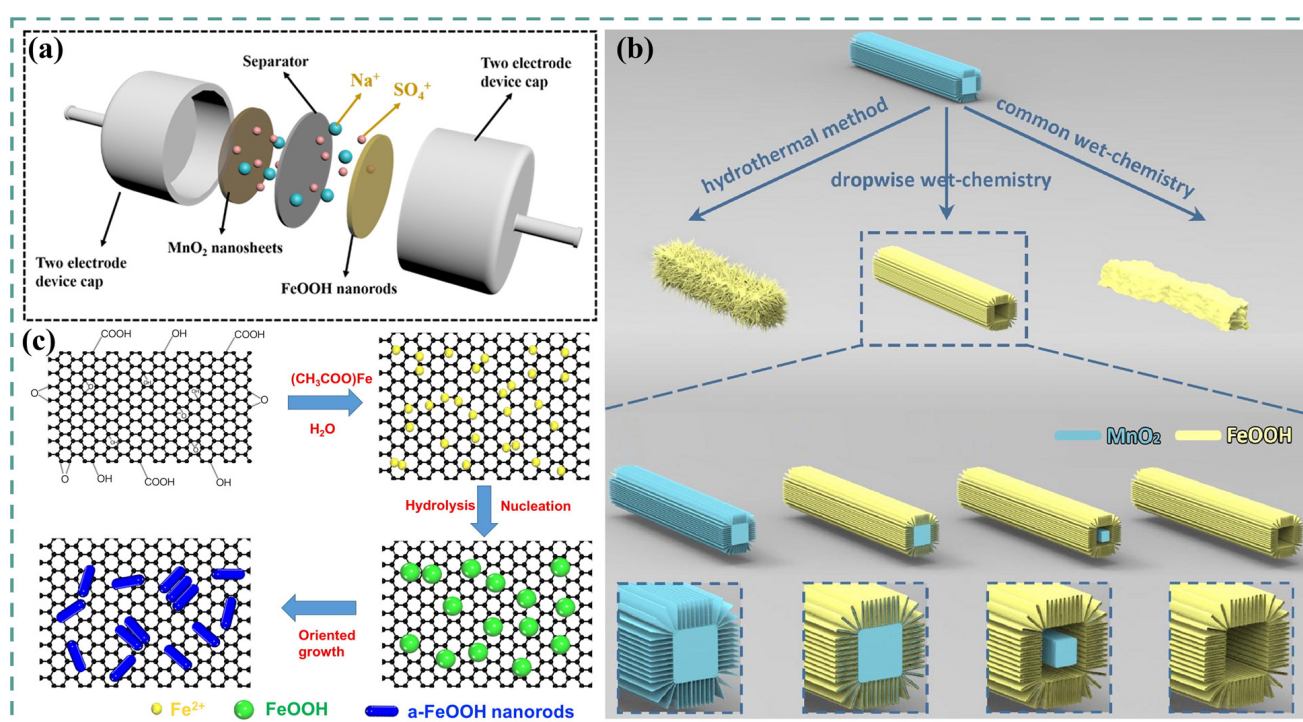
Figure 5. (**a**) Illustration of FeOOH and MnO$_2$ electrodes device assembly in 1M Na$_2$SO$_4$. Reprinted from Ref. [24], Copyright (2023), with permission from Elsevier. (**b**) Illustration of the transition from parallel MnO$_2$ nanosheets to hollow parallel FeOOH. Reprinted from Ref. [99], Copyright (2023), with permission from Elsevier. (**c**) Schematic representation of the possible formation mechanism of α-FeOOH/GO composites. Reprinted from Ref. [85], Copyright (2023), with permission from Elsevier.

2.3. FeOOH Composites

Graphene consists of a nanosheet of honeycomb pattern of carbon atoms, along with its byproducts, reduced graphene oxide (rGO) and GO, which have piqued the interest of researchers globally in both materials science and chemistry due to their impressive thermal, mechanical, electronic, and optical characteristics, as well as their extensive surface area [141]. Graphene's unique properties offer optimal support for metal deposition, which stabilizes metal nanoparticles and preserves the required structural, electrical, and chemical characteristics [142]. Furthermore, GO, which contains various oxygen-containing groups, can serve as an anchoring site for metal nanoparticles, preventing the formation of clusters and particle growth. In particular, iron oxyhydroxide composites with graphene, such as

nanoparticles, nanorices, nanorods, and nanowires, have been extensively used in supercapacitors [85,97,99,102,103,105,108,110,114,125,134]. Wei et al. devised a facile approach to obtain ultrathin α-FeOOH nanorods/GO composites [85]. The composites are produced directly from iron acetate and GO in a water solution without any inorganic or organic additives. The resulting composites' nanorods are single crystallites 6 nm in diameter and 75 nm in length, significantly smaller than those of α-FeOOH nanorods without GO, due to GO's confinement effect and distinctive electronic influence. The influence of experimental conditions, such as reactant concentration and reaction time, on nanorod size was explored, revealing that the initial Fe^{2+} concentration and reaction time were critical factors in the synthesis method. Moreover, as illustrated in Figure 5c, a potential nucleation growth mechanism was suggested. The proposed technique is more economical and eco-friendlier than the reported methods that utilize iron acetate and GO aqueous solution as reactants, leading to enhanced material purity. Furthermore, the method demonstrates the viability of the scaling strategy. When employed as supercapacitor electrode materials, the α-FeOOH nanorods/GO composite containing 20% Fe displayed a specific capacitance of 127 F g^{-1} at 10 A g^{-1}, accompanied by 2000 of cycling stability (at 85% retention), and exceptional rate capability at 20 A g^{-1} of 100 F g^{-1}, outperforming α-FeOOH nanorods without GO. This unique structure facilitates swift electron transport, rapid electrolyte ion diffusion, and a high charge–discharge rate.

Sun et al. proposed a facile and scalable approach to fabricate the composites of amorphous FeOOH nanoflowers (NFs) and multiwalled carbon nanotubes (MWCNTs) (FeOOH NFs@MWCNTs) [101]. The resultant hybrid structures display a unique heterostructure made up of MWCNT and self-assembled amorphous FeOOH nanofilms. At pH 8, FeOOH NFs@MWCNTs low-crystalline composites show excellent performance, owing to their favorable structural characteristics. When tested between −0.85 and 0 V (vs. Ag/AgCl), the fabricated electrode exhibited a 1 A g^{-1} of current density a 345 F g^{-1} specific capacitance, good cycling performance (76.4% capacitance retention at the 5000th cycle), and a current density of 11.4 A g^{-1} remarkable rate performance of 167 F g^{-1}. The exhibited electrochemical capabilities can be linked to these key factors: primarily, the capacitive effect of amorphous FeOOH NFs, which led to a significantly increased specific capacitance; additionally, the mesoporous arrangement and large effective electrode area contributed to a greater number of storage sites; and finally, the direct connection between the MWCNTs and FeOOH NFs ensures rapid ion/charge diffusion and straightforward exposure of storage sites components to the electrolytes.

The limited capacitance of iron-based negative electrodes compared to advanced positive electrodes presents a challenge in developing high-performance ASC devices with a wide voltage range and improved power energy properties. To address this issue, Chen et al. have created negative supercapacitor electrodes exhibiting large capacitance, which can be on par with the capabilities of sophisticated positive electrodes. This performance is maintained even at elevated loading of active material [84]. The proposed approach involves the new extraction mechanism called particle extraction using a liquid–liquid interface (PELLI) to prepare α-FeOOH as well as β-FeOOH electrode materials, that yielded agglomerate-free powders which could be utilized for the effective mixing with MWCNTs leading to the better electrolyte access at the particle surface. Results indicated the feasibility as an effective negative electrode when composited with α-FeOOH-MWCNT with an extractor; 16-phosphonohexadecanoic acid (PHDA) provided a low impedance and a high capacitance. Additionally, PHDA can serve multiple purposes, including serving as a capping agent in the process of synthesizing particles and functioning as an extractor within the PELLI approach. The electrochemical performance of their asymmetric SC device was shown to be promising for a high potential window (1.6 V), as confirmed via cyclic voltammetry (CV), impedance spectroscopy, and galvanostatic charging and discharging analysis.

Molybdenum diselenide composites are considered suitable materials for SC energy storage systems owing to their enhanced dynamic contact area, conductivity properties,

and variable oxidation states. A recent study [100] reported the formation of a composite consisting of FeOOH nanorods and molybdenum diselenide ($MoSe_2$) nanoflowers, utilizing a hydrothermal route assisted by a room temperature chemical blending technique. The suggested procedure is found to be simple and cost effective and effectively reduces the agglomeration of both nanoflowers and nanorods. When used as an electrode in a symmetric cell, the FeOOH-$MoSe_2$ composite displayed a 132 F g^{-1} specific capacitance at 1 A g^{-1} for 1 V voltage, with 100% capacitance retention for 3000 cycles and a coulombic efficiency of 100% for 10,000 cycles. The cell produces, at 1 A g^{-1}, 18.3 Wh kg^{-1} of energy density and 1174 W kg^{-1} of power density. Practical application of the symmetric cell based on the composite electrode was demonstrated by illuminating a panel of 42 red LEDs for 10 min without interruption. Additionally, the study proposes a suitable charge storage mechanism associated with the prepared symmetric supercapacitor, as illustrated in Figure 6a.
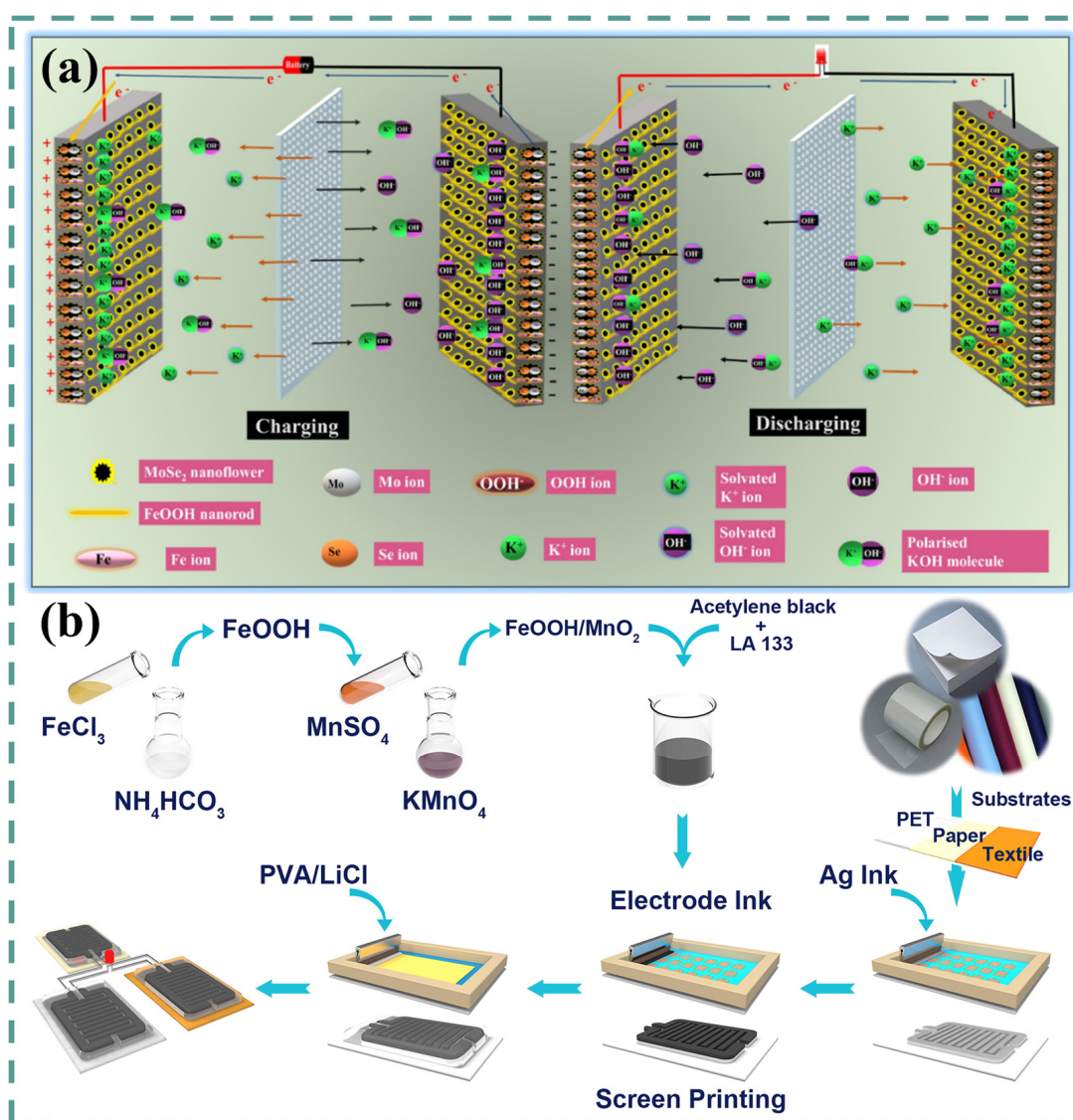
Figure 6. (**a**) The possible mechanism of charging–discharging process in the fabricated FeOOH-$MoSe_2$ symmetric cell. Reprinted from Ref. [100], Copyright (2023), with permission from Elsevier. (**b**) Schematic representation of the amorphous FeOOH/MnO_2 composites synthesis method and fabrication procedures of all printed SC devices. Reprinted from Ref. [68], Copyright (2023), with permission from Elsevier.

2.4. FeOOH for Solid-State Supercapacitors (SSSs)

SCs and HCs typically consist of a liquid electrolyte enclosed by two electrodes and a separator. However, their use in electronics viz., wearable optoelectronics, collapsible displays, etc., is limited due to safety concerns related to electrolyte leakage and challenges associated with large-scale manufacturing [143]. To overcome these limitations, flexible, solid-state, and transparent SCs have been developed. The main advantage of flexible/transparent solid-state SCs (FTSSSs) is the use of flexible/transparent electrodes and a solid-state gel electrolyte [143]. Carbon materials have been the focus of previous studies for the development of transparent electrode materials for FTSSSs [144–149]; however, their performance is often restricted by low mass loading and low theoretical specific capacitance.

The development of transparent microstructure electrodes made of large specific capacity pseudocapacitive transition metal oxide/hydroxide materials presents a significant challenge in enhancing the performance of FTSSSs. Improving the energy density by extending the operating voltage window is also crucial. Li et al. have successfully produced transparent films of amorphous FeOOH nanowires and Co $(OH)_2$ nanosheets using a bioinspired approach that is scalable and easy to execute in air-solution interactions [102]. By coating the nanostructures with graphene shells (Gr), Fe@Gr-TF and Co@Gr-TF are formed as transparent asymmetric pseudocapacitive negative and positive electrodes. The encapsulation structure of these materials offers numerous advantages, such as providing pseudocapacitive electrode materials, extending the potential window of the FeOOH cathode with minimal cycling stability degradation, forming three-dimensional pathways for efficient ion and electron transport, and reducing active material dissolution in the electrolyte. The Fe@Gr-TF//Co@Gr-TF-based asymmetric transparent and flexible supercapacitor (ATFS), which operates at 1.8 V, possesses increased transparency of 50.5% at 550 nm, 1.04 mWh cm^{-3} of energy density and 25.5 mF cm^{-2} of specific capacitance (similar to non-transparent devices), and a good cyclability of 83.5% over 10,000 cycles. Their study was further extended to create microstructured transparent films employing amorphous FeOOH nanowires and Ni$(OH)_2$ nanosheets using a scalable gas–liquid diffusion technique at the interface of air and solution [103]. Ni@Gr-TF and Fe@Gr-TF microstructures were coated with graphene shells to improve the electron/ion diffusion pathways and prevent the exfoliation and dissolution of active materials. As a result of such an approach, the voltage window of the FeOOH cathode could be prolonged to −1.25~0 V. Furthermore, ATFS was constructed using Fe@Gr-TF//Ni@Gr-TF, which demonstrated excellent performance. In addition to having a 52.3% transmittance at 550 nm, the ATFS also had a large specific capacity of 17.42 mF cm^{-2} at 0.2 mA cm^{-2} (compared to the maximum value reported for transparent graphene membranes, this value is one order higher), a high capacity retention (85%) after 20,000 cycles, and an energy density of 0.67 mWh cm^{-3} for the entire system.

In the case of solid-state flexible SCs (SSFSs), Lu et al. developed an amorphous FeOOH/MnO$_2$ composite that can be screen-printed as an electrode material [68], as shown in Figure 6b. Fabricated SSFSs with appealing designs were screen-printed on textile, paper, and PET substrates. The amorphous FeOOH/MnO$_2$ composite demonstrated at 0.5 A g^{-1} a large specific capacitance of 350.2 F g^{-1} and, at 20 A g^{-1}, a rate capability of 159.5 F g^{-1}, and an impressive cyclability of 95.6% at 10,000th cycle. The SSFS device also displayed a remarkable 5.7 mF cm^{-2} of area-specific capacitance and capacitance retention of 80% over 2000 cycles, along with excellent mechanical flexibility. The printed SCs were able to power a 1.9 V yellow LED, when connected in series, despite subjecting to bending and stretching tests. Furthermore, the printed SSFSs were revealed to be cost-effective, eco-friendly, visually appealing, and mechanically flexible.

As a promising candidate for lightweight, portable SSSs, Al $(OH)_3$/MnO$_2$/FeOOH (AMFO) binder-free composite electrodes have been fabricated on stainless steel (SS) substrates through a simple, eco-friendly, and low-cost Layer-by-Layer technique at room temperature [104]. The synthesized electrode exhibited a mesoporous morphology resembling reindeer moss, with ample open cavities as observed by high-resolution SEM. The

supercapacitive properties of the electrode were examined by electrochemical measurements in Na_2SO_4 solution (1 M) implicating 2557 C g^{-1} of specific capacity at 5 mV s^{-1} of scan-rate of over a broad voltage range from about -1.11 to 1.06 V. The long-term testing exhibited a cycle stability of around 70%, and the electrochemical impedance spectroscopy displayed a smaller charge transfer resistance of about 1.45 Ω. To realize the practical application of energy storage devices, a solid-state symmetric supercapacitive device (SSD-AMFO) was fabricated using the synthesized electrode in a planar configuration and sandwiched with PVA/1 M Na_2SO_4 gel electrolyte. The SSD-AMFO device demonstrated supercapacitive behavior having large specific capacitance of 511 F g^{-1} across a wide potential range of 0.0–2.5 V. Additionally, the assembled device exhibited an ultra-high specific energy density of 443.67 Wh kg^{-1} at a specific power density of 13.53 kW kg^{-1}. The practical application of SSD-AMFO was established by illuminating red, green, blue, and white LEDs.

3. Ni-Fe LDH

Two-dimensional (2D) layer double hydroxides (LDHs) are gaining popularity in electrochemical energy conversion and storage because of their customizable composition and morphology. LDHs have highly dispersed active species in layered arrays, making them easily exfoliated into monolayer nanosheets that can be chemically modified for use as active electrode materials in SCs. Efficient transport features, a high specific surface area, and interesting physicochemical properties make these materials attractive [150]. The structure of LDHs includes positively charged host layers and exchangeable hydrated anions located in the interlayer gallery, which provide a charge balance [151]. Interestingly, the host layer and interlayer negative ions can exchange without structural change, giving LDHs a variable nanostructure. However, LDH electrodes are relatively large in diameter (0.2–5 mm) and thickness (6–40 nm), with fewer surface atoms exposed, leading to capacity fading and poor electrochemical performance [150]. Although LDH materials with sheet-like morphology have been suggested for use in SCs [67,105–131], interparticle agglomeration and ineffective ion diffusion between active electrode materials and the current collector have hindered their practical application. Ultrathin NiFe-LDH nanosheet arrays were synthesized by facile hydrothermal approach on 3D NF (Figure 7a), with variations in Ni/Fe molar ratio and feeding contents of metal ions [106]. At a current density of 5 A g^{-1}, the nanosheets were vertically and homogeneously aligned on the Ni foam surface and displayed a high specific capacitance of 2708 F g^{-1} as a result of systematically oriented single crystal geometry and well-defined porous nanostructure. The study also investigated the impact of concentration and the molar ratio between Ni and Fe on the electrochemical behavior of the nanosheets. Furthermore, as a positive electrode in ASCs with negative active carbon electrode, the NiFe-LDH nanosheet film exhibited 50.2 Wh kg^{-1} of energy density and 800 W kg^{-1} of power density. In just one min, two aqueous ASCs stacked in series were charged and powered two green light-emitting diodes for over 5 min.

The hydrothermal procedures could also be extended to a two-step hydrothermal method to yield sulfidized NiFe-LDHs as demonstrated by Xiao et al. The process involves vulcanization of NiFe-LDHs followed by sulfidation. When used as a negative electrode for asymmetric supercapacitors, such treatment improves electrochemical performance [109]. As a result of the sulfidation treatment, the electrode's electrical conductivity is significantly increased, while its diffusion resistance is significantly reduced. Compared to the pristine NiFe-LDHs, the sulfidized NiFe-LDHs showed better electrochemical properties: 992 mF cm^{-2} of area-specific capacitance at 2 mA cm^{-2} and improved cycling performance, at a current density of 4 mA cm^{-2}, of 64.5% at the 2000th cycle. When used as a negative electrode in ASCs, a specific capacitance of 112.2 F g^{-1} was obtained at 2.25 mA cm^{-2}, and an energy density of 39.9 Wh kg^{-1} was achieved at a power density of 211.4 W kg^{-1}, whereas with $Ni(OH)_2$ as the positive electrode, a decreased power density of 13.5 Wh kg^{-1} at 2114 W kg^{-1} was obtained in the potential window of 0–1.6 V in an aqueous electrolyte containing 1 M KOH.

NiFe-LDH nanostructures could also be synthesized using ultrasound irradiation with varying molar ratios and reaction times [107]. The sonochemical method produces different NiFe-LDH nanostructure morphologies free of impurities or structural changes. During the optimization process, it was discovered that the reagent concentration and the sonication time at a fixed irradiation frequency were major factors influencing the nanostructures' size and morphology. Under ultrasound irradiation, non-aggregated and uniform spherical particles were obtained at 45 W for 180 min with a molar ratio of 4:1 (Ni:Fe) under ultrasound irradiation. The use of morphologically controlled NiFe-LDH samples led to the tuning of the pseudo-capacitive behavior of the nanostructures. When optimized, NiFe-LDH spherical nanostructures with a 4:1 M ratio produced after 3 h of ultrasonic irradiation showed the large value 168 F g^{-1} in specific capacitance.

Wang et al. have described an environmentally friendly method that utilizes ultrasonication to fabricate NiFe-LDH nanosheets, which exhibit improved capacitive performance [116]. In comparison, the bulky NiFe-LDHs were synthesized without ultrasonic treatment. Interestingly, the interlayer spacing of NiFe-LDHs was increased with the help of ultrasonic treatment during the synthesis process. Through a combination of experimental outcomes and cutting-edge characterization techniques, it was revealed that the ultrasonic treatments in the synthesis process exhibit a substantial influence on the thickness and nanostructure of the resulting NiFe-LDHs, as well as the capacitive behavior. NiFe-LDH nanosheets, produced with 2 h of ultrasonic treatment, displayed outstanding capacitive capabilities ascribed to the synergistic effect of their excellent specific surface area, extremely thin structure, and elevated mesoporous volume (0.080 cm^3 g^{-1}). However, excessive ultrasonication could decrease the number of active energy storage sites. The NiFe-LDH nanosheets, having a 7.39 nm thickness and a specific surface area of 77.16 m^2 g^{-1}, achieved a specific capacitance of 1923 F g^{-1} at 3 A g^{-1}, which is almost 1.4-fold and 1.7-fold that of bulky NiFe-LDHs and NiFe-LDHs nanosheets prepared with 3 h of ultrasonic treatment, respectively. The superior retention of the capacitance of 98% at 1000 cycles under the 10 A g^{-1} was revealed. Moreover, the maximum energy density of the assembled ASC, consisting of positive electrode NiFe-LDHs and an AC negative electrode (NiFe-LDHs//AC), was 49.13 Wh kg^{-1} at a power density of 400 W kg^{-1}. A key finding of the study is that it presents a green method for synthesizing LDH nanosheets, while also providing insights into the relationship between LDH nanosheet morphology/structure and capacitive properties, which could lead to the advancement of high-performance electrodes containing LDH systems.

2D nanostructures derived from different materials possess exceptional electrical and chemical properties and have demonstrated broader applicability in energy storage devices. Among the materials, MXene is a type of conductive 2D material derived from carbonitrides, transition metal carbides, and nitrides and includes Ti$_3$C$_2$, Ti$_2$C, Nb$_2$C, V$_2$C, and Ti$_3$CN. MXene has excellent characteristics including flexibility, good charge conductivity, large active storage sites, plentiful shallow functional groups, and good hydrophilicity, thereby proving to be a suitable material for the manufacture of highly efficient SCs. The utilization of MXene as a substrate for depositing NiFe-LDH nanosheets via a facile hydrothermal approach is reported to yield a 3D porous NiFe-LDH/MXene electrode [112]. Such a unique structure of NiFe-LDH/MXene was found to exhibit a higher specific capacitance (720.2 F g^{-1}) than that of NiFe-LDH (465 F g^{-1}) and a cycling performance of 86% capacitance retention at 1000th cycle, indicating excellent cycle stability (only 24% for NiFe-LDH). The enhanced electrochemical properties of the composites can be ascribed to the efficient sheet-like morphology throughout charging and discharging, the conductive network created by MXene, and the MXene's ability to improve the electrolyte ion transfer efficiency of composites. Importantly, MXene stabilizes the nanostructure of LDH and prevents the separation and aggregation of LDH, while the uniform anchoring of LDH nanosheets on MXene allows the composite to have a larger specific surface area. Moreover, an ASC utilizing a NiFe-LDH/MXene positive electrode demonstrated at 758.27 W kg^{-1} power density a 42.4 Wh Kg^{-1} energy density.

Despite the prevalent use of carbon materials as anodes in SCs, their reduced capacitance results in limited energy density for SC devices that use aqueous electrolytes. To overcome this challenge, Shakir et al. proposed a flexible and binder-free electrode for supercapacitor applications by directly decorating NiFe-LDH on carbon cloth (CC) [113]. The NiFe-LDH/CC electrode exhibited a large gravimetric capacitance of 984 F g^{-1} at 1 A g^{-1}, which can be attributed to the synergistic effect of the hybrid composition, porous structure, higher surface area, and binder-free design. The electrode also demonstrated good cyclic stability, with nearly 87.6% of capacity retention after 7000 consecutive galvanostatic charging–discharging cycles. The flexible substrate, layered morphology, and porous architecture of the fabricated electrode were found to protect from the expected pulverization and expansion processes, resulting in excellent cyclic activity. Additionally, the proposed electrode showed excellent rate performance, with only a 13.5% decrease in gravimetric capacitance when the applied current density was increased from 1 to 9 A g^{-1}. The numerous voids and pores in the NiFe-LDH sample acted as ion reservoirs, facilitating mass transport even at higher current densities.
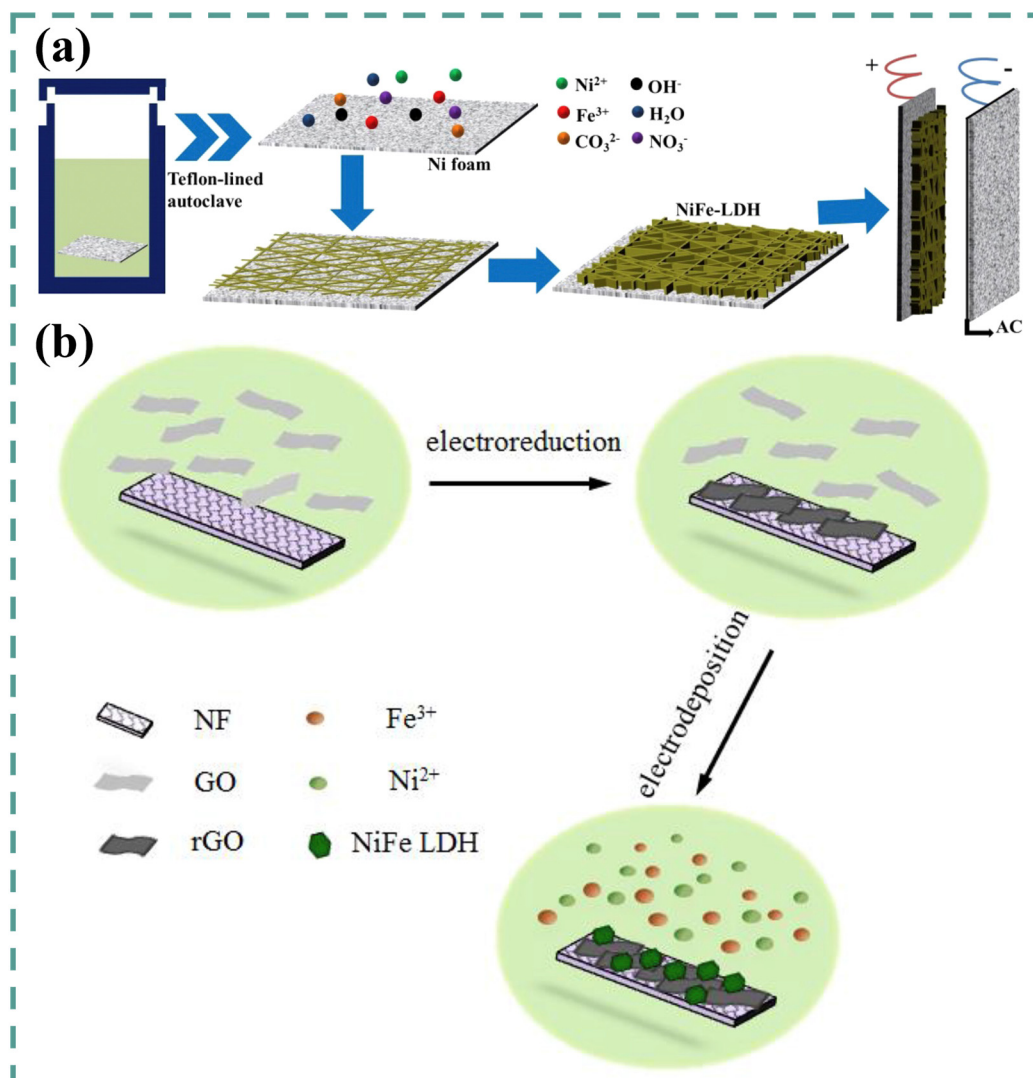
Figure 7. (**a**) Schematic illustration of the NiFe-LDH/NF formation mechanism of the ASC device. Reprinted from Ref. [106], Copyright (2023), with permission from Elsevier. (**b**) Preparation of NiFe-LDHs/rGO/NF by electrochemical reduction of GO to rGO and deposition onto NF, then electrodeposition of NiFe-LDHs. Reprinted from Ref. [110], Copyright (2023), with permission from Elsevier.

As previously mentioned, graphene is an ideal material for supporting metal deposition as it can stabilize metal nanoparticles while retaining their electronic structure and chemical properties [142]. In their study, Gao et al. created a 3D airgel by combining 2D graphene layer with a 2D Ni-Fe LDH hybrid using a simple hydrothermal method combined with freeze-drying [105]. The 3D hybrid aerogel has several benefits over the 2D structure, such as a distinctive porous framework, superior electrical conductivity, and a multidimensional electron transport pathway. As an SC electrode, the Ni-Fe LDH/graphene hybrid aerogel (Ni-Fe LDH/GHA) exhibited an 1196 F g^{-1} capacitance at 1 A g^{-1} current density, as well as exceptional stability of 80% at the 2000th cycle, owing to the mentioned features. Additionally, the ASC device having active carbon negative electrode and the Ni-Fe LDH/GHA positive electrode reached 17.6 Wh kg^{-1} of energy density at 650 W kg^{-1} of power density and exhibited excellent cycling performance of 87.2% capacitance retention at 3500th cycle with 91 F g^{-1} specific capacitance at 1 A g^{-1}.

An intertwined caterpillar-like NiFe-LDH bridged on rGO-modified NF (NiFe-LDH/rGO/NF) electrode could be fabricated through a simple two-step electrodeposition process to coat as shown in Figure 7b [110]. Initially, rGO is electrochemically coated on NF at −1.2 V versus SCE for 600 s, followed by NiFe-LDH electrodeposition at −1.2 V for 10 s using Ni/Fe-LDHs with different Ni/Fe ratios. When optimized, the resulting NiFe-LDHs/rGO/NF composites exhibited a 1462.5 F g^{-1} specific capacitance at 5 A g^{-1} and a cyclic stability of approximately 64.7% over 2000 cycles. Moreover, a flexible ASC is developed with mesoporous carbon (MC) coating on NF as the anode and NiFe-LDHs/rGO/NF as the cathode. This SC displayed a 17.71 Wh kg^{-1} energy density and 348.49 W kg^{-1} power density.

Hsiao et al. proposed an innovative method for synthesizing rGO-FeO-CNT-NiFeLDH electrodes using oyster shell powder to obtain a hierarchical structure and growing CNTs on the rGO surface [114], as displayed in Figure 8a. The elaboration method included the combination of oyster shell powder with GO and iron sulfate solution, followed by a hydrothermal reaction to reduce GO to rGO, forming rGO-FeOOH. Subsequently, CNTs were grown on the rGO surface through a chemical vapor deposition process (CVD) while using dried rGO-FeOOH as the framework. To prepare the rGO-FeO-CNT-NiFeLDH electrodes, electrochemical deposition (ECD) is used to deposit NiFe-LDH onto the rGO substrate. The deposition of FeO onto the rGO substrate provides both pseudocapacitance and catalytic support for CNT growth. The CNTs grown between the rGO sheets enhance conductivity and create a hierarchical structure that reduces the transport barriers for electrolyte ions during operation, significantly improving the electrode's electrochemical properties. The deposition of the NiFeLDH layered structure on the CNT surface of the rGO-FeO-CNT electrode offers a high surface area for redox reactions. These advantages create a synergistic effect that enhances the electrode's performance, which results in an excellent capacitance of 411.9 F g^{-1} tested at 5 mV s^{-1} for the rGO-FeO-CNT-700-NiFeLDH-60 electrode. In 1.7-volt operation, the ASC exhibited a maximum energy density of 41.4 W h kg^{-1} and a maximum power density of 5600 W kg^{-1} when paired with AC-NiO as the cathode. The capacitance decreased due to the collapse of the extruded petal-like structure generated during the initial charge/discharge operation after 3200 cycles. However, a good retention rate of 102.2% was attained after 5000 charge/discharge cycles.

Recently, nanostructured metal sulfides are emerging as a promising material for energy storage thanks to their outstanding electrical and catalytic properties. In particular, Cobalt sulfide (CoS$_2$) has desirable electroconductibility and thermal stability, making it an ideal candidate for supercapacitor devices [111,127]. Tian et al. developed a hydrothermal method of synthesizing CoS$_2$ nanosheet-coated flower-like NiFe-LDH nanospheres directly on a 3D nickel foam substrate (NiFe-LDH@CoS$_2$@Ni) [111] for high-performance supercapacitors, as displayed in Figure 8b,c. The opted hydrothermal process involves the preparation of CoS$_2$@Ni, followed by surface generation of flower-like NiFe-LDH nanospheres through a subsequent hydrothermal process, producing a binder-free electrode with an exceptional capacitance performance. The electrode displayed an impressive

3880 F g^{-1} specific capacitance at 1.17 A g^{-1} and a stability of 81.9% over 10,000 electrochemical cycles at 20 mA cm^{-2}. Furthermore, the electrodes were exploited in an all-solid-state ASC, utilizing the NiFe-LDH@CoS$_2$@Ni hybrid as the positive electrode and AC covered NF as the negative electrode; consequently, 375.16 W kg^{-1} power density yields 15.84 Wh kg−1 energy density. The as-fabricated ASC also demonstrated the ability to power a blue LED indicator for over 30 min (Figure 8e). The impressive electrochemical performance is due to the flower-like structure of the ultrathin nanosheet, that provides a large specific surface area and a high number of active sites, shortens the diffusion distance between electrolyte ions and substrates, and accelerates electron transport (Figure 8d). Consequently, the findings indicated that the NiFe-LDH@CoS$_2$@Ni hybrid is an ideal electrode material for advanced supercapacitors.
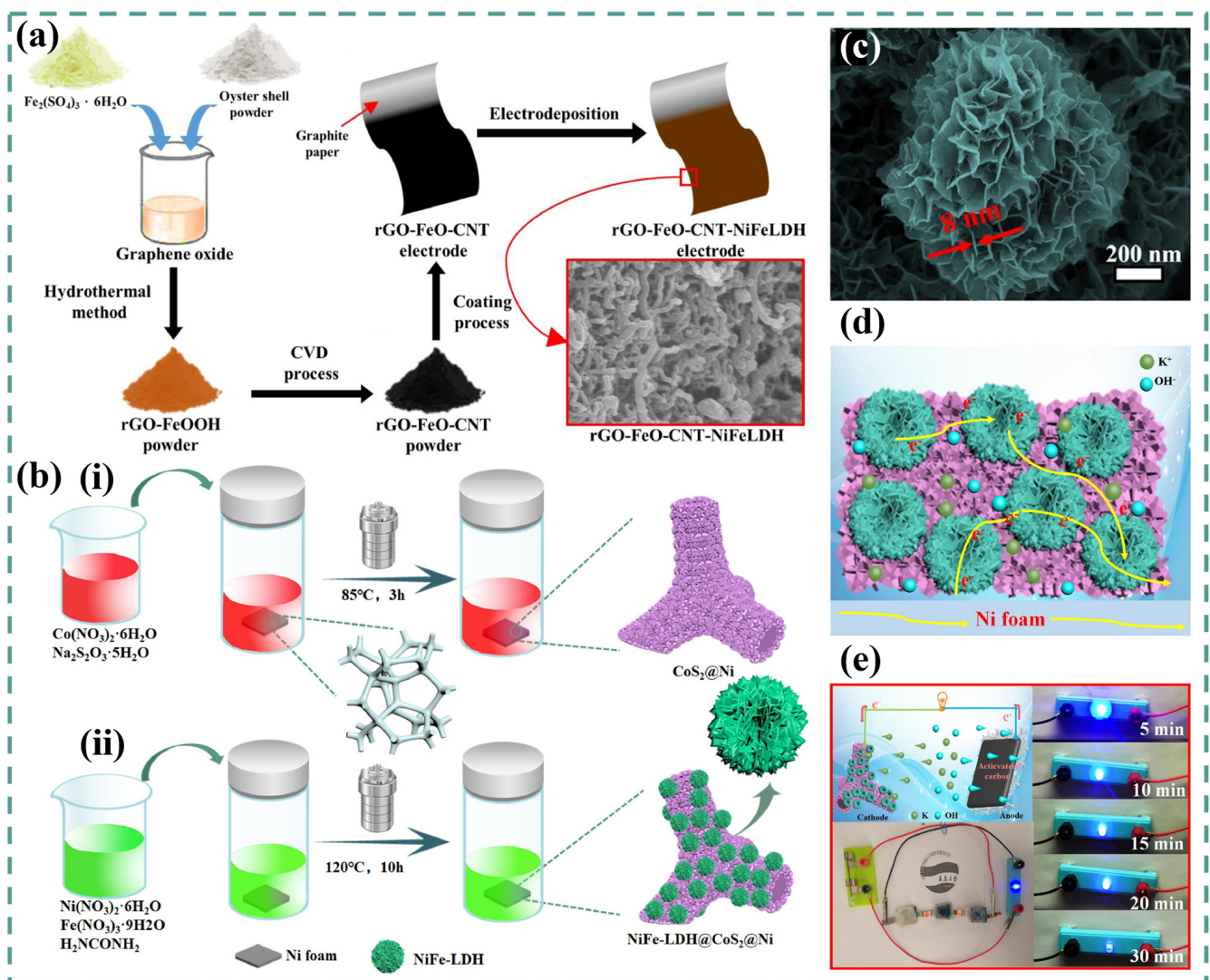
Figure 8. (**a**) The preparation process of the rGO-FeO-CNT-NiFeLDH electrode. Reprinted from Ref. [114], Copyright (2023), with permission from Elsevier. (**b**) The preparation process of (i) CoS$_2$@Ni nanosheets and (ii) NiFe-LDH@CoS$_2$@Ni. (**c**) High magnification SEM image of the NiFe-LDH@CoS$_2$@Ni flower-like nanospheres. (**d**) Schematic representation of electron transport in NiFe LDH@CoS$_2$@Ni. (**e**) Schematic configuration of the NiFe-LDH@CoS$_2$@Ni//AC ASC device and the corresponding images of the three ASC devices that connect in series that could illuminate the LEDs. (**b**–**e**) are reprinted from Ref. [111], Copyright (2023), with permission from Elsevier.

4. Co-Fe LDH

Among various LDHs, cobalt-iron LDHs (CoFe-LDHs) have triggered tremendous interest in recent years thanks to their potential use in energy storage systems [67,117–123]. CoFe-LDH is a family of lamellar materials made up of positively charged brucite-like host layers and interlayer regions. In this system, the metal cations occupy octahedral vacancies between alternate pairs of OH^- planes of the brucite-like sheets, and the interlayer regions are filled with charge-compensating anions and solution molecules [152–154]. Recently, the use of CoFe-LDH electrode materials has also received increasing attention because the co-existence of Co and Fe ions in the host layers can provide rich redox reactions due to their combined contributions during the electrochemical processes. Ma et al. showcased an innovative method for creating CoFe-LDHs with varying $Co/(Fe^{2+}, Fe^{3+})$ atomic proportions through precipitation and subsequent partial oxidation of I_2 [117]. Co/Fe ratios in the solution can be adjusted over a broad spectrum, significantly affecting the resulting product's phase and structure. A structural examination verified that CoFe-LDHs with four distinct Co/Fe molar proportions exhibit a layered, plate-like morphology and a characteristic hydrotalcite-like structure. Elevated Fe content disrupts the hydrotalcite structure, resulting in the formation of magnetite particles. Electrochemical analysis reveals a strong correlation between the Co/Fe ratio and the specific capacitance of CoFe-LDHs. Among the samples, Co-Fe LDHs using a 2.35 Co/Fe ratio yield 728 F g^{-1} capacitance at 1 A g^{-1}. Combining it with AC as a negative material in an ASC can achieve 27.3 Wh kg^{-1} energy density at 823.5 W kg^{-1} power density. The results suggested that iron inhibits -Co(OH)$_2$ formation but also contributes to obtaining a large capacitance. However, excessive iron content may compromise the layered structure of LDHs and result in the deterioration of electrochemical performance. Consequently, to attain CoFe-LDHs with a stable structure and high electrochemical efficiency, the amount of Fe should be carefully regulated to maintain a relatively low value.

The formation of CoFe-LDHs was also demonstrated using a chemical co-precipitation method, applied as electrodes for supercapacitors [118]. Co/Fe molar ratio had a significant effect on electrochemical activity in this process. The results showed that the loose packed $Co_{0.74}Fe_{0.26}$-LDH nanoplatelets could expand the electroactive area for pseudocapacitive reactions and provide effective electrolyte-accessible channels for ion transport. In $Co_{0.74}Fe_{0.26}$-LDH, the total pore volume was 0.6 cm^3 g^{-1}, and the specific surface area was 202.9 m^2 g^{-1}. As a result, the interfacial area between liquid and solid is high, which results in improving the active materials' efficiency. The electrochemical measurement demonstrated that the CoFe-LDHs had an excellent capacitive performance that was relative to their composition. The largest specific capacitance of 869 F g^{-1} was accomplished by $Co_{0.74}Fe_{0.26}$-LDH in 1 M KOH electrolyte. At 1 A g^{-1}, over 1000 consecutive cycles, the $Co_{0.74}Fe_{0.26}$-LDH electrode was also shown to possess superior electrochemical stability further on than 99.5% of the initial capacitance due to its special molar ratio of Co^{II}/Fe^{III}. Therefore, a low-cost, environmentally friendly, and high-performance $Co_{0.74}Fe_{0.26}$-LDH, fabricated by a simple preparation process, is a potential electrode material for supercapacitors.

Considering the impact of the Co to Fe molar ratio on the electrochemical activity, Jo et al. have successfully designed CoFe-LDH nanosheets on nickel fabric (NFa) through a simple ECD technique with a constant potential of -1.0 V for 100 s [121], as depicted in Figure 9a. The composites with different ratios of Co-Fe precursors were synthesized by varying the mole ratio of Co and Fe. In addition, the distinct structure created during fabrication, which is a result of an adjustable chemical composition and a broad range of material properties, was effective in improving the efficiency of electrochemical energy storage devices. CoFe-LDH with a $Co_{0.5}Fe_{0.5}$ electrode was optimized with a well-designed LDH structure and exhibited outstanding electrochemical performance. In particular, the synthesized LDH morphology enhances the electronic structure as well as the electrical conductivity, offering a huge number of active sites and a rapid electron transfer process. Through the combination of a CoFe-LDH battery-type electrode and an AC capacitive-type electrode, a hybrid supercapacitor device was fabricated (Figure 9b). The as-fabricated HSC

based on conductive fabric exhibits superior energy storage performance with 70 $\mu F\ cm^{-2}$ areal capacitance at 2.0 mA cm^{-2}. In addition, the device displayed an energy density of 1.6 mW h cm^{-2} at 0.09 mW cm^{-2} power density and excellent stability of 91% over 2000 cycles of GCD measurements. Flexible devices are also suitable for use as power sources in flexible electronic devices due to their high degree of flexibility. In addition to providing a promising electrode for supercapacitors, this study also developed an electroactive material with a unique composition and structure.

By using a one-step electron capture device, Jiang et al. synthesized CoFe hydroxides grown on nickel foams with different CoFe atomic ratios [119]. Crystallinity and electrochemical characterization of the CoFe hydroxides are significantly affected by the initial Co/Fe ratios in the precursor solutions. Particles of Fe $(OH)_3$ have an average diameter of 200 nm. Adding Co ions improves crystallinity of CoFe hydroxide by forming a frame-like structure consisting of smaller particles. According to its morphology, $Co(OH)_2$ can be used as a network former to construct tridimensional frame networks. Two types of structure are observed in CoFe hydroxide with a Co/Fe ratio of 1:1 nanoflake-like network structure overall and nanoparticle with several mesopores. The as-prepared CoFe hydroxides have been applied for SC electrodes, showing superior electrochemical performance. The CoFe DH electrode, having a 1:1 CoFe ratio, achieved 2255.6 F g^{-1} specific capacitance at 1 A g^{-1} and 73.5% capacity retention after 2000 cycles at 10 A g^{-1}. Because of its particular structure and the synergistic effect between Co $(OH)_2$ network and Fe$(OH)_3$ particles, it has excellent electrochemical performance. The simple synthesis technique and high performance of CoFe hydroxide electrode materials make them a potential high-performance SC electrode material.
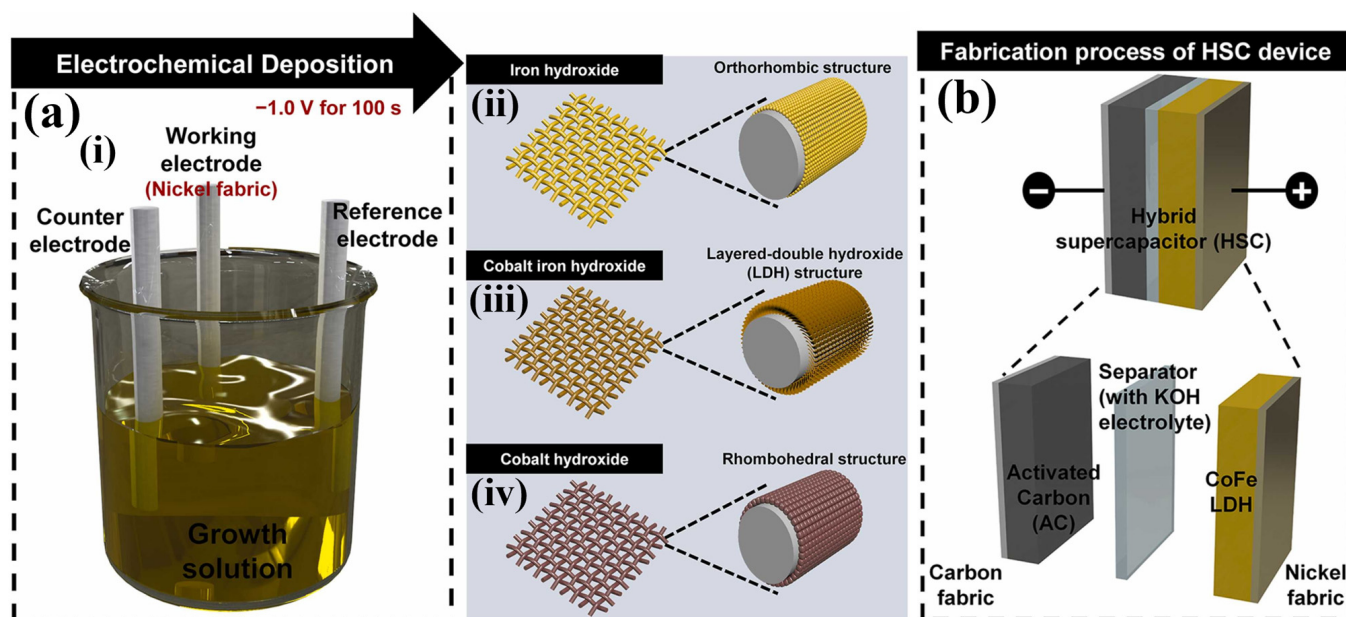
Figure 9. (**a**) Schematic illustration of (i) Preparation procedure of mono- and mixed-metal hydroxide via ECD method and fabricated electrodes of (ii) Fe$(OH)_2$, (iii) CoFe-LDH, and (iv) Co$(OH)_2$ [121]. (**b**) Fabrication process of HSC device. (**a**,**b**) are reprinted from Ref. [121], Copyright (2023), with permission from Elsevier.

Using a one-step liquid-phase reflux method, CoFe hydroxides with a ratio of Co/Fe of about 3:1 were synthesized [120]. The material consists of numerous well-defined platelets with uniform hexagonal shapes and a lateral dimension of 1.3 μm. For the CoFe hydroxide nanosheet electrode, a C_{sp} value of 2358.4 F g^{-1} was obtained at a current density of 0.5 A g^{-1}, and excellent capacitance retention of 83% was observed after 1400 cyclic voltammetry cycles, indicating good electrochemical stability. This can be assigned to the presence of metallic cobalt and iron, which effectively ameliorate the electri-

cal conductivity, consequently promoting charge/ion transport and leading to increased charge storage capacity. Notably, the cobalt element contributes to the electrode's higher specific capacity. Additionally, the distinctive nanostructures of these hydroxides offer a vast number of surface-active sites, thereby increasing the electrode's efficiency. Simultaneously, the amorphous nature of these material systems promotes the diffusion and reaction of electrolyte ions, enabling a uniform charging/discharging process throughout the electrode. These combined factors work together to provide an advanced electrochemical performance for the CoFe hydroxide nanosheet electrode. Furthermore, the fabricated solid device displayed 512 W kg^{-1} power density and 28.3 Wh kg^{-1} energy density. It may be used for flexible electronics and energy storage in the future due to its low cost and simplicity.

Regulating the intrinsic properties of the transition metal LDH material is a promising strategy to ameliorate the performance of supercapacitors. Li et al. have reported the CoFe-LDH array in a suit grown on NF substrate by a simple hydrothermal method and subsequently activated by electrochemical cyclic voltammetry [123], as shown in Figure 10a. The report demonstrates that the electrochemical activation can not only regulate the morphology and electronic structure of the CoFe-LDH but can also transform the original single crystal structure into the polycrystalline structure. The unique morphology (microflowers) of optimal CoFe-LDH-X (Figure 10b) is found to expose more active sites. Moreover, the existence of oxygen vacancies offers enhanced electrical conductivity with a large number of grain boundaries, which are beneficial for the improved electrochemical reaction process. Interestingly, after 200 cycles of CV activation of CoFe-LDH (CoFe-LDH-200), a significant enhancement in the specific capacitance of 4662.2 mF cm^{-2} and great cycle stability (133.8% after 10,000 cycles) was achieved. Using the proposed strategy, high-performance transition metal LDH electrode materials can be designed for future energy conversion and storage devices.

The creation of nanosized pores in layered materials can increase their active surface area and boost energy storage applications, according to Mahmood et al. [122]. Using this strategy, a unique synthetic strategy based on polyaniline (PANI)-doped 2D CoFe-LDH (CoFe-LDH/P) nanomaterials was developed through a hydrothermal method that causes the formation of pores at low temperature (80 °C), as shown in Figure 11a. It was found that, unlike all other polymers, PANI-optimized concentration creates nanopores on CoFe-LDH nanosheets. Ion diffusion is effective in CoFe-LDH/P because of its well-ordered pores that promote high accessibility of redox-active sites. In supercapacitor applications, the optimized CoFe-LDH/P2 cathode shows a specific capacitance of 1686 F g^{-1} and 1200 F g^{-1} at 1 and 30 A g^{-1}, as well as a high rate capability of 71.2% and a great cyclability of 98% over 10,000 cycles. Analysis of charge storage suggests a capacitive-type storage mechanism (69% capacitive at 1 mV s^{-1}) for the CoFe-LDH/P2 electrode. Moreover, Figure 11b shows an asymmetric aqueous supercapacitor made of CoFe-LDH/P2//AC that has an impressive energy density (75.9 Wh kg^{-1}) and outstanding stability (97.5%) at 10,000th cycle as can be observed from Figure 11c. The observations made and the chemical principles unveiled in the reported study by Mahmood et al. indicate that creating nanosized pores in transition metal-based 2D materials can increase the edge sites and surface area and improve the mass transfer. This opens up a new avenue for the development of porous 2D materials at low temperatures for use in aqueous energy storage systems.
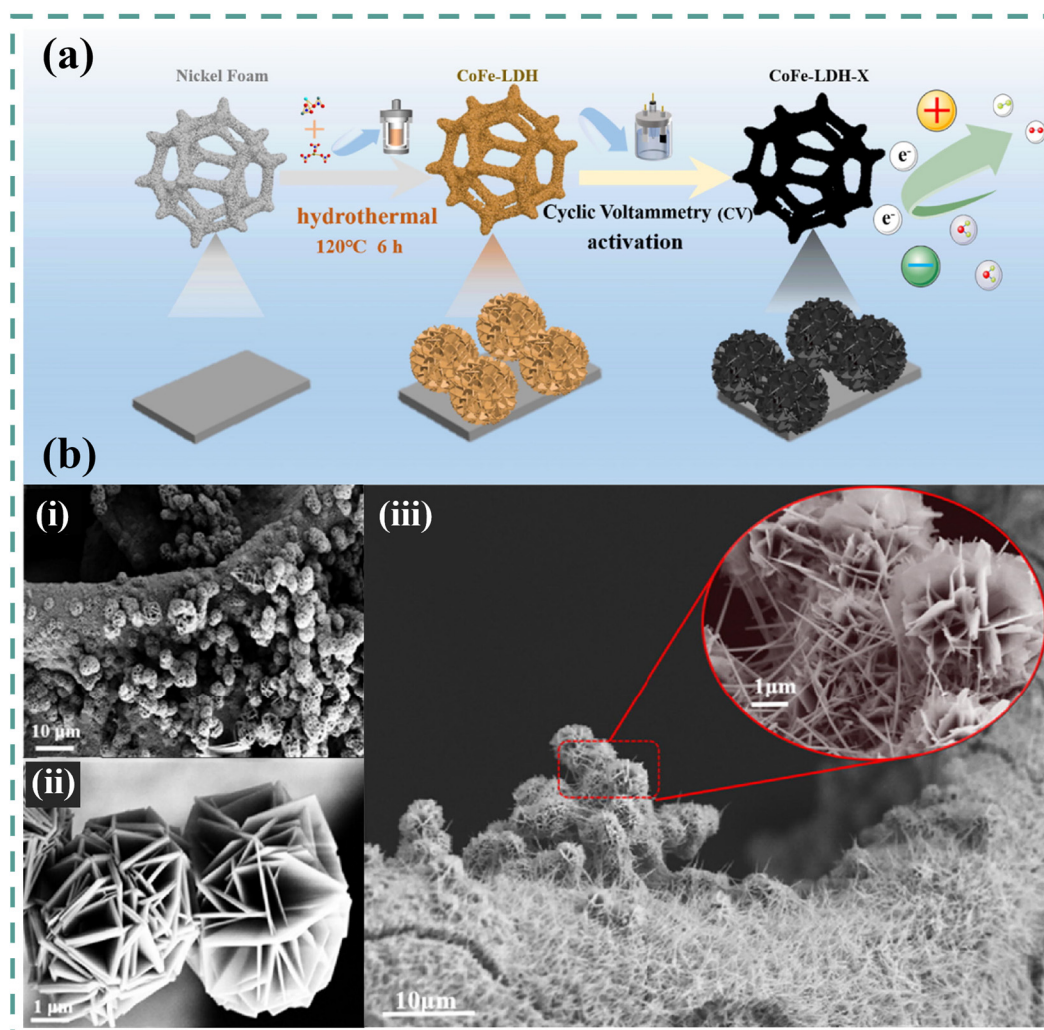
Figure 10. (**a**) The elaboration procedure of CoFe-LDH-X. (**b**) SEM images of (i,ii) CoFe-LDH and (iii) CoFe-LDH-200. (**a**,**b**) are reprinted from Ref. [123], Copyright (2023), with permission from Elsevier.

In supercapacitor devices, high energy and power densities are crucial because of their potential practical applications in different kinds of electronic devices. To achieve balanced properties, CoFe-LDH can be used to fabricate other composite electrode materials. An ASC with high capacitive performance has been developed by Gao et al. using electrodeposition coating method and the facile acid corrosion route, in which the positive and negative electrodes were made from NiO@CoFe-LDH and commercially available pen ink/graphene/carbon nanotubes (PGC), respectively [67]. It resulted in higher capacity and ultrastable rate capability because of the synergy that occurred between NiO ravines with high capacitance and wrinkled porous CoFe-LDH. Interestingly, CoFe-LDHs have been shown to have ultra-stable rates (retaining 94% from 4 to 25 mA cm^{-2}) and can be used to balance transition metal oxides and hydroxides. It was found that the ASC constructed in this study exhibited a large specific capacitance of about 205 F g^{-1} at 1 A g^{-1} and retained 60% of the capacitance at 20 A g^{-1}. It is also notable that it displays an extremely high energy density of 64.1 Wh kg^{-1} and a power density of 15 kW kg^{-1} in addition to a high degree of cyclability after 3000 cycles (90% capacitance retention). Additionally, as a demonstration of its potential application in micro- and nano-energy storage devices, the ASC drives LEDs, motor propellers, and even a toy car.
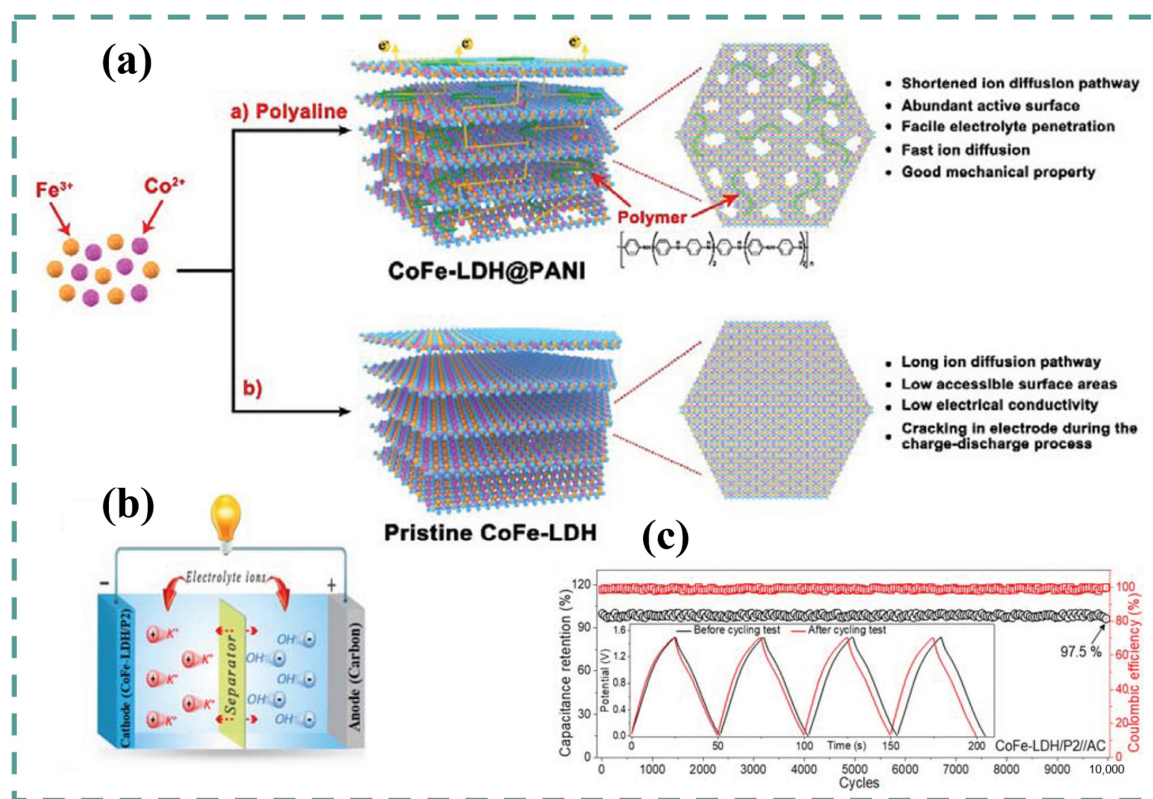
Figure 11. (**a**) Synthesis process and structure transformation of pristine and PANI doped CoFe-LDH. The pores and green sparks on the final product indicate the active sites. (**b**) Schematic representation of CoFe-LDH/P2//AC working principle. (**c**) Cycling stability performance for 10,000 cycles (inset exhibits the first and the last four cycles). (**a**–**c**) are reprinted from Ref. [122], Copyright (2023), with permission from John Wiley and Sons.

5. Ni-Co-Fe LDH

Supercapacitor electrodes made from mixed-metal hydroxide (MMH) exhibit superior performance as a result of the synergistic effect caused by mixed-metal elements, as compared to electrodes made from single-metal hydroxide (SMH). A number of energy storage devices have been developed using MMH electroactive materials. Due to their unique structural and chemical composition, they have strong electrochemical properties. Using a rational microstructure construction and combining multiple components, electrode materials can be displayed in ASCs in an extensible manner. Recently, ternary metal compounds have received considerable attention due to their high electrochemical activity and multiple valence states. Based on the excellent characteristics of Ni (which can offer a large specific capacity), Co (which can possess strong electrical conductivity), and Fe (which can stabilize the structure and provide more active sites) elements, the Ni-Co-Fe codoping approach is not only conducive to stabilizing the electronic structure of LDHs but can also improve the stability of the electrode materials to obtain better electrochemical performance than single Ni-, Co-, or Fe-doped LDH materials [124–131]. Cobalt-doped NiFe-LDH (Fe-Ni$_3$Co$_2$ LDH) assembled from one-dimensional (1D) nanoneedle subunits and FeSe$_2$/C is synthesized via a facile, one-pot self-template method [115], as illustrated in Figure 12a. The morphology of Fe-Ni$_3$Co$_2$ LDH nanospheres is shown in Figure 12b–d. The Fe-Ni$_3$Co$_2$ LDH electrode showed outstanding capacitance retention of 116.6% over 5000 cycles. Significantly, the fabricated all-solid-state ASC (Figure 12e), based on the Fe-Ni$_3$Co$_2$ LDH positive electrode and the FeSe$_2$/C negative electrode, (Fe-Ni$_3$Co$_2$ LDH//FeSe$_2$/C) delivers 83.9 mF cm^{-2} areal capacity at 0.3 mA, 22.3 μWh cm^{-2} energy density at a power density of 2076 μW cm^{-2}, and a stability 84.8% over 5000 cycles at 0.3 mA (Figure 12f). In addition, the device has good mechanical flexibility after bending from 0° to 180°. Based on the density

functional theory (DFT) calculations, the high electrochemical activity of Fe-Ni$_3$Co$_2$ LDH is mainly attributed to cobalt doping, which can modify the electronic structure and narrow the bandgap, thereby bringing enhanced conductivity, facile electron transfer, and abundant active sites.

As part of a supercapacitive energy storage application, Pourfarzad et al. synthesized Fe$_2$O$_3$/Graphene as a negative electrode and NiCoFe–LDH on NF as a positive electrode [125]. By using cyclic voltammetric methods to change the Ni, Co, and Fe amounts in NiCoFe-LDHs, the electrochemical efficiency has been explored and optimized. It has been determined that the NiCoFe-LDH electrode material, having a 2:1:1 Ni:Co:Fe ratio, has the highest specific capacitance because of the synergistic effect of Fe, Co, and Ni, which increases the conductivity, and the insulators oxidation rate (such as Ni(OH)$_2$), which facilitates the penetration of OH$^-$ and thereby accelerates the kinetics of the process by facilitating Co^{IV} active site formation. At a density of current of 1 A g^{-1}, NiCoFe-LDH nanocomposite exhibits a specific capacitance of 3130 F g^{-1}. This research has focused also on designing and constructing a SC with great power and energy density. There is a power density of 91.5 kW kg^{-1} and a total energy density of 101 Wh kg^{-1} in the designed supercapacitor. Additionally, this device's specific capacity was only 17.5% lost after 5000 cycles, indicating 82.5% stability.

Developing stable and efficient thin films that store and convert energy effectively has gained considerable attention for SCs. Rohit et al. developed hierarchical nanosheet-based ternary NiCoFe-LDH thin films using an inexpensive and facile electrodeposition process [128]. The NiCoFe-LDH exhibited, at 0.4 A g^{-1} current density, a specific capacity of 360 A g^{-1}, a 51% capacity retention at 10 A g^{-1}, and 84% stability performance after 2000 cycle tests.

Wang et al. devised a distinctive NiCoFe-LDH/carbon nanofiber (NiCoFe-LDH/CNFs-0.5) composite using a straightforward in situ growth method for supercapacitors [124]. Employing the two resulting materials as SC electrodes, the NiCoFe-LDH/CNFs-0.5 composite exhibited an elevated 114.2 m^2 g^{-1} specific surface area, a 1203 F g^{-1} specific capacitance at 1 A g^{-1}, and a 77.1% rate capability from 1 A g^{-1} to 10 A g^{-1}, all of which were significantly greater than the values for pure NiCoFe-LDH. Additionally, the NiCoFe-LDH/CNFs-0.5 composite showcased over 1000 cycles a remarkable long-term cyclic stability of 94.4% at 20 A g^{-1}. The ASC constructed using activated carbon (AC) as the negative electrode and NiCoFe-LDH/CNFs-0.5 as the positive electrode demonstrated an 84.9 F g^{-1} specific capacitance at 1 A g^{-1}, along with a high energy density of 30.2 Wh kg^{-1} at 800.1 W kg^{-1} power density. Most notably, this device maintained its cycling performance, retaining 82.7% capacity at a current density of 10 A g^{-1} over 2000 cycles. The excellent electrochemical performance of the NiCoFe-LDH/CNFs-0.5 composite suggests its considerable potential for use in high-power and energy storage devices.

To examine the metal ratios effect on the electrochemical performance of LDHs, Liao et al. elaborated porous Ni$_x$Co$_{1-x}$Fe-LDHS 2D nanosheets utilizing a concise hydrothermal technique [129]. The team optimized the molar ratios of NiCoFe-LDH samples, examining the variations in structural, morphological, and electrochemical properties and comparing them with their binary analogs. Their findings revealed that the increase in nickel content causes an increase in the LDH's specific capacity. Consequently, the NiCoFe-LDH material exhibited a substantial 425.56 mAh g^{-1} capacitance at 1 A g^{-1}, maintaining 94.52% capacitance at 8000 cycles at 10 A g^{-1}. Furthermore, the asymmetric NiCoFe-LDH//AC HSC device exhibited, at 1 A g^{-1}, 1.26 Wh kg^{-1} of power density and 51.81 Wh kg^{-1} of energy density. Conductivity of electrode material remained excellent after 10,000 CV cycles. As a consequence, NiCoFe-LDH is a potential candidate for SC applications because it has superior stability. This study offers guidance for the development of ternary LDH materials that can be used in electrochemical energy storage devices. Consequently, the ternary NiCoFe-LDH holds promise as a more effective electrode material compared to binary LDH in the realm of supercapacitors.
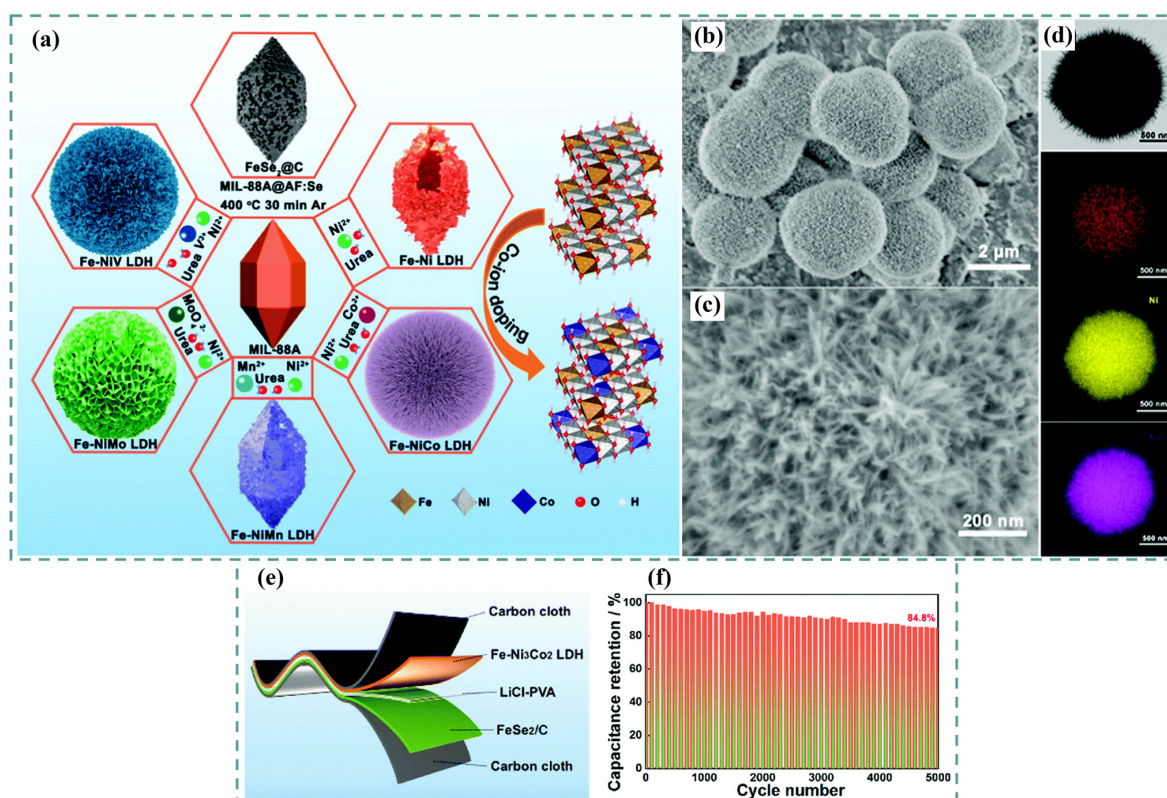
Figure 12. (**a**) Schematic representation of the formation of MIL-88A, Fe–Ni_3M_x LDH (M = Co, V, Mo, and Mn), and $FeSe_2$/C derived from MIL-88A [115]. (**b**,**c**) SEM images of Fe–Ni_3Co_2 LDH [115]. (**d**) TEM and the corresponding elemental mapping images of Fe, Ni, and Co of Fe–Ni_3Co_2 LDH [115]. (**e**) Components of an ASC based on Fe–Ni_3Co_2 LDH and $FeSe_2$/C as positive and negative electrodes, respectively [115]. (**f**) Cycling stability performance of ASC device at 0.3 mA for 5000 cycles [115].

Lee et al. also validated that NiCoFe hydroxide can be used in hybrid supercapacitors with high energy density [126]. Using a controlled molar ratio of Ni and Co, they successfully prepared ternary NiCoFe hydroxide by facile electrodeposition in Figure 13a. Optimum Ni/Co/Fe (3:1:1) molar ratios led to high energy and power densities for the hybrid supercapacitor, as represented in Figure 13d,e. When the nickel ratio is high, the metal hydroxide exhibits increased specific capacitance, and when cobalt is high, it displays a higher rate capacity. Upon adding inexpensive iron with a minimal cobalt ratio, the proposed material can be used as a low-cost, high-performance SC electrode. Based on AC and NiCoFe hydroxide, an aqueous HSC device has been fabricated (Figure 13b). The device displays, at 1 A g^{-1}, a high 1321 F g^{-1} capacitance of current density with high capacitance retention, over 10,000 continuous cycles, of 88.57% with good coulombic efficiency at 10 A g^{-1}. The as-prepared NiCoFe/AC HSC as well presents a greatest of 73.07 Wh kg^{-1} energy density at 1.07 kW kg^{-1} power density and an energy density of 14.02 Wh kg^{-1} at a maximum power density of 6.97 kW kg^{-1} over a large voltage window (1.6 V). Additionally, it displays after 50,000 cycles a satisfactory capacitance retention of 75.5% with a high coulombic efficiency, as shown in Figure 13c. As a guideline, this approach is useful in preparing electrochemical energy storage devices using ternary metal hydroxide electrodes.

As previously noted, LDHs have attracted significant interest within the energy storage domain due to their exceptional 2D hydrotalcite-like architecture, highly reversible redox dynamics, and tunable composition. At the same time, nanomaterials constructed by ultrathin nanosheets have enhanced conductivity, rich electrochemical active sites, and fast charge transfer channels, showing better electrochemical properties. Wang et al. designed three-dimensional NiCoFe-LDH vertical nanosheet arrays (denoted NiFeCo-LDH Na)

assembled by the tight interconnection of 2D nanosheets using a Ni-coordinated zeolitic imidazolate framework (Ni-ZIF–L) as a sacrificial template via facile ion exchange and etching reaction processes under hydrothermal conditions [131], as illustrated in Figure 14a. The as-prepared NiFeCo-LDH NA exhibits a characteristic 2D/3D porous structure, providing a substantial surface area that enhances active site exposure to electrolytes and promotes ion diffusion channels for redox reactions. Continuous charge–discharge processes are effectively limited by the hierarchical mesoporous structure. Therefore, this design improves the electrochemical utilization, accelerates reaction kinetics, and achieves superior electrochemical properties. Electrochemical tests show that the NiFeCo-LDH NA based electrode shows a superior specific capacity of 1495 C g^{-1} at 1 A g^{-1} and has great cycling stability (89% capacitance retention over 10,000 cycles at 10 A g^{-1}). The constructed HSC (NiFeCo-LDH NA//AC), shown in Figure 14b, attains an impressive 34.4 Wh kg^{-1} energy density at 935.5 W kg^{-1} power density while maintaining excellent cycling performance, maintaining over 96% of the initial capacitance (Figure 14c), and demonstrating nearly 99% coulombic efficiency after 15,000 cycles. This work not only proves that ternary LDHs can be used as good energy storage materials but also provides a new way to prepare nanomaterials with specific morphology.
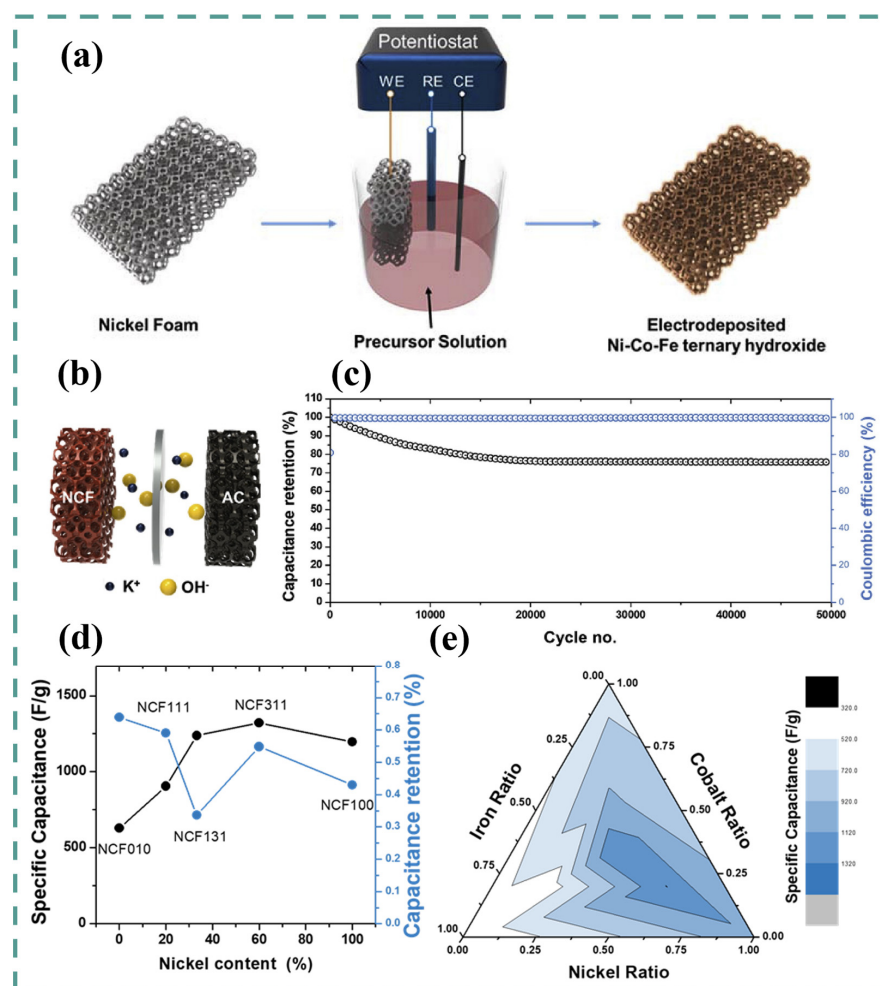
Figure 13. (**a**) Preparation procedure of Ni–Co–Fe hydroxide. (**b**) Schematic illustration of NCF311/AC HSC configuration. (**c**) Cycling stability performance and coulombic efficiency of HSC device at 10 A g^{-1} for 50,000 cycles. (**d**) Evolution of specific capacitance and capacitance retention at various current densities (from 1 to 20 A g^{-1}) versus Ni content. (**e**) Ternary diagram of the specific capacitance as a function of the Ni/Co/Fe ratio. (**a**–**e**) are reprinted from Ref. [126], Copyright (2023), with permission from Elsevier.

Intelligently developing self-supporting heterogeneous nanostructured electrode materials is a potent approach to enhance the electrochemical performance and mechanical strength of ASCs. Ren et al. presented a straightforward method to synthesize self-supporting petal-like NiFeCo-S (Sulfides) @NiFeCo-TH (Ternary Hydroxide) heterogeneous ultrathin nanosheets on nickel-iron foam (NIF) through an inventive electro-oxidation, sulfuration, and adjustable Co^{2+} exchange process [127], as illustrated in Figure 15a. The multicomponent ultrathin nanosheets offer numerous electrochemical interfaces/active sites, a brief ion/electron transport path, and exceptional structural stability, making them excellent supercapacitor electrode materials. The uniquely nanostructured NiFeCo-S@NiFeCo-TH lamellar hybrid (Figure 15b) yields a high 174 mAh g^{-1} specific capacitance at 10 mA cm^{-2} and a remarkable 68.3% rate capability at 100 mA cm^{-2} current density. The possible mechanism behind NiFeCo-S@NiFeCo-TH//NIF performance is represented in Figure 15c. Crucially, the assembled NiFeCo-S@NiFeCo-TH/NIF//AC all-solid-state ASC device demonstrates 56.3 Wh kg^{-1} energy density at 543 W kg^{-1} power density and outstanding cycling performance of 90.1% at the 4000th cycle. In addition to creating self-supporting transition metal nanostructured electrodes that can be used to store and convert energy, this fabrication strategy displays broad application potential.
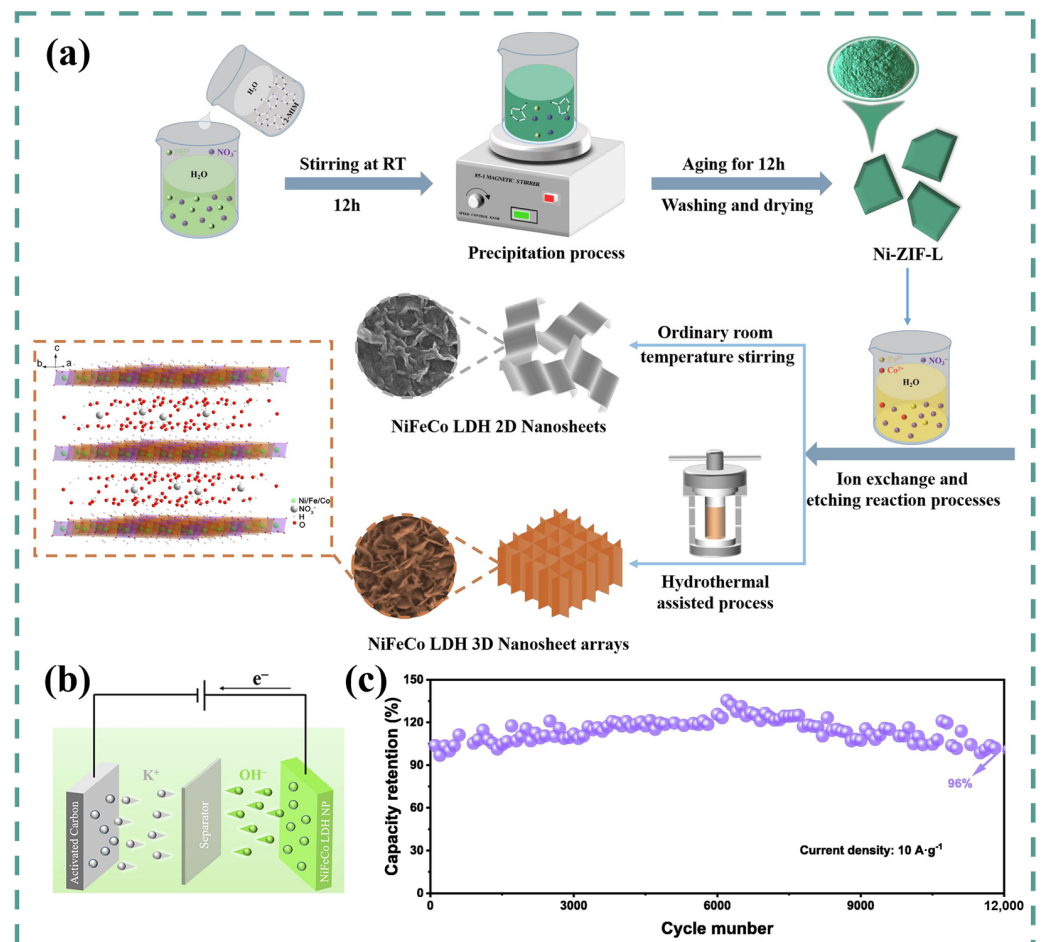
Figure 14. (**a**) Elaboration procedure of NiFeCo-LDH nanoplate arrays. (**b**) Schematic illustration of NiFeCo-LDH NA//AC HSC. (**c**) Cycling stability performance of NiFeCo-LDH NA//AC HSC at 10 A g^{-1} for 12,000 cycles. (**a**–**c**) are reprinted from Ref. [131], Copyright (2023), with permission from Elsevier.
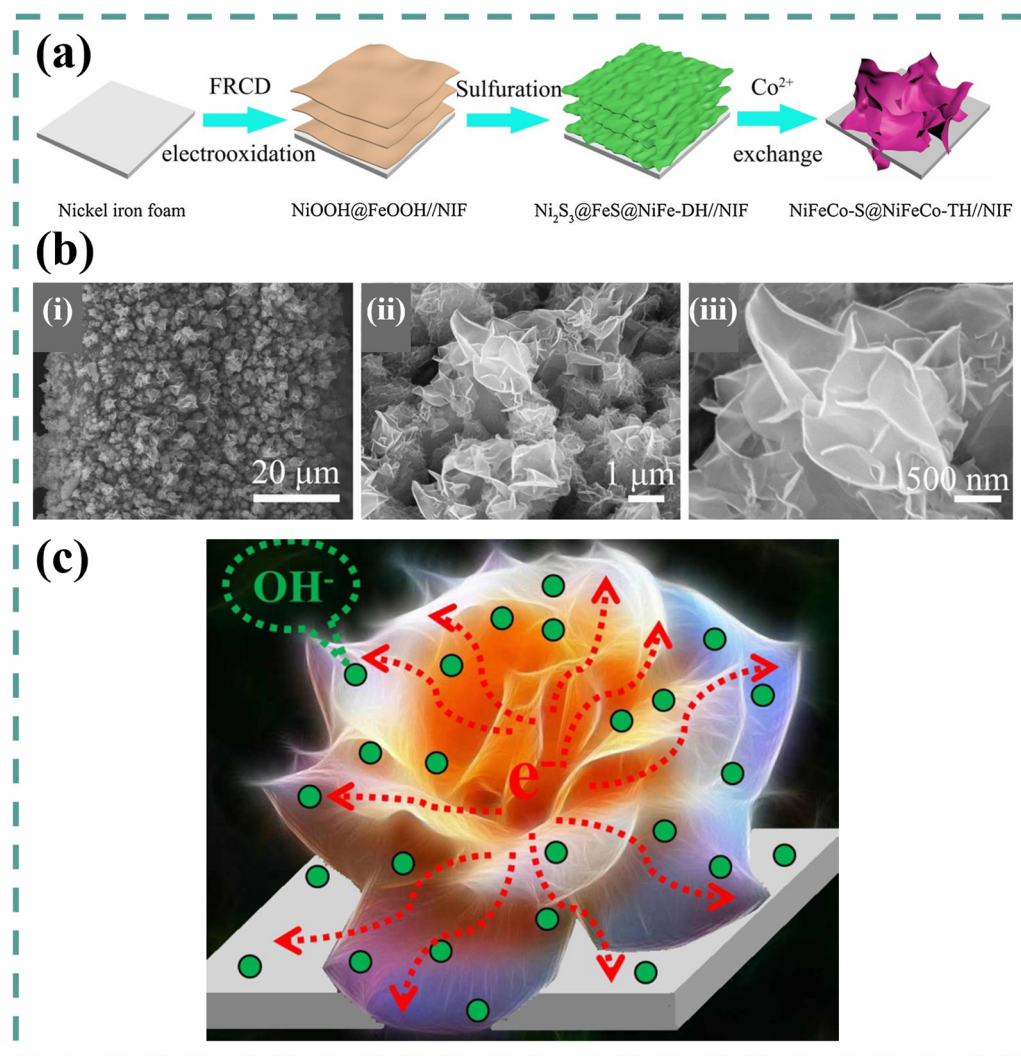
Figure 15. (**a**) Elaboration procedure of NiFeCo-S@NiFeCo-TH//NIF. (**b**) SEM images of NiFeCo-S@NiFeCo-TH//NIF at different magnifications (i–iii). (**c**) Schematic representation of the possible mechanism behind NiFeCo-S@NiFeCo-TH//NIF performance. (**a**–**c**) are reprinted from Ref. [127], Copyright (2023), with permission from Elsevier.

Zhao and colleagues prepared a nanocomposite consisting of ternary $NiCo_2Fe_x$ LDH anchored to graphitic carbon nitride (g-C_3N_4) via a hydrothermal route [130], as illustrated in Figure 16a. In this distinct material, Fe played a crucial role in boosting the energy storage performance of $NiCo_2Fex$-LDH. Notably, the substantial improvement in electrochemical performance following the incorporation of Fe into the $NiCo_2$-LDH structure was studied through theoretical calculations as shown in Figure 16b. The results revealed that the $NiCo_2$-LDH has a smaller band gap after Fe is added, facilitating rapid electron and ion transport. The electrochemical tests for this material indicated that the $NiCo_2Fe_{1.0}$-LDH@g-C_3N_4 electrode achieved a high 1550 F g^{-1} specific capacitance at 1 A g^{-1} current density, far exceeding that of the $NiCo_2$-LDH@g-C_3N_4 electrode. The assembled $NiCo_2Fe_{1.0}$-LDH@g-C_3N_4//AC asymmetric supercapacitor device (Figure 16c) exhibited an impressive specific capacitance of 129.64 F g^{-1}. Moreover, the device produced 35 Wh kg^{-1} energy density corresponding to 701 W kg^{-1} of power density, while maintaining excellent stability performance (92.7% capacitance retention after 5000 cycles), as shown in (Figure 16d). The $NiCo_2Fe_{1.0}$-LDH@g-C_3N_4//AC ASC was able to power a blue LED effortlessly. The experimental results in this study offer valuable insights for designing and comprehending novel LDH structure electrode materials for energy storage applications.
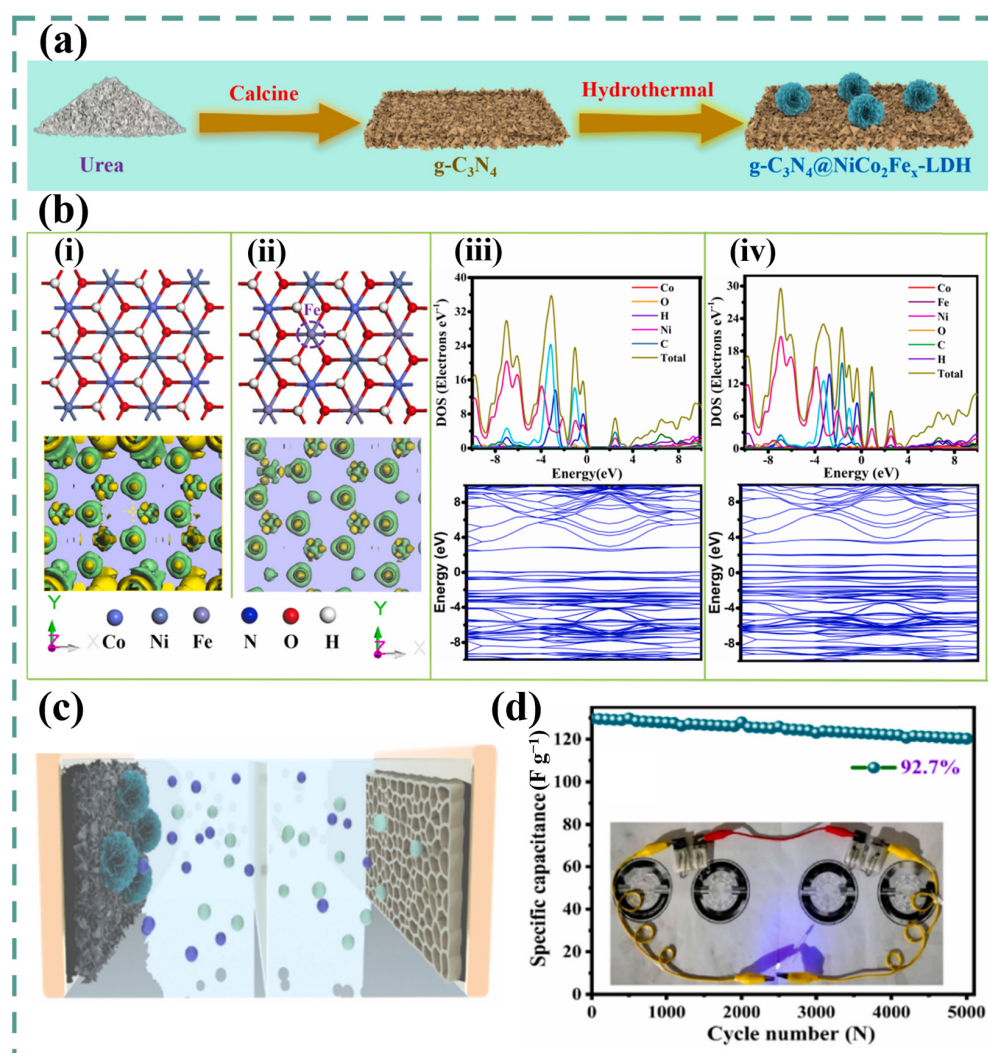
Figure 16. (**a**) The preparation procedure of NiCo$_2$Fe$_x$-LDH@g-C$_3$N$_4$. (**b**) Atomic structure models and the differential charge density (i,ii), total density of state (DOS), and band structures (iii,iv) of NiCo$_2$-LDH with and without the incorporation of Fe. (**c**) Graphical illustration of NiCo$_2$Fe$_{1.0}$-LDH@g-C$_3$N$_4$//AC ASC device. (**d**) Cycling stability performance for 5000 cycles (inset shows a pair of ASC devices in series that could illuminate a LED). (**a**–**d**) are reprinted from Ref. [130], Copyright (2023), with permission from Elsevier.

6. Ternary and Quaternary LDH

Binary LDHs are commonly used in supercapacitor applications [67,105–114,116–123]. However, their lower electrical conductivity and limited active sites restrict their potential for various energy-related applications. To overcome these limitations, ternary LDHs and quaternary LDHs can be formed by incorporating a third and fourth metal cation, respectively, which results in increased conductivity and a higher number of electrochemically active sites [132–136,155]. Elgendy et al. successfully fabricated a binder-free nickel-zinc-iron LDH (Ni-Zn-Fe LDH) through a one-step successive ionic layer adsorption and reaction (SILAR) technique [133]. The Ni-Zn-Fe LDH exhibited at 5 mV s^{-1} a high 1452.3 F g^{-1} specific capacitance and an outstanding cycling performance of 112.5% over 1000 cycles. The reason for this is the large specific surface area of 119.789 m^2 g^{-1} and mesoporous structure with pores sized around 3.69 nm, allowing electrolyte ions to extensively interact with the electroactive material surface. The assembled ASC (AC//Ni-Zn-Fe LDH) attained 14.9 Wh kg^{-1} energy density, 1077.6 W kg^{-1} power density, and at 1.5 A g^{-1} current density 95% cycling performance over 1000 cycles.

Metal hydroxides are versatile and appealing electrode materials owing to their merits such as easy room-temperature synthesis, nanostructure formation, higher conductivity, crystallite or non-crystallite formation, porous structures, etc. Nanostructured ternary transition metal (M = Mo, Co, Fe) hydroxides (TTMHs) were successfully grown on NF via template-free single-step electrodeposition for supercapacitor applications [135], as illustrated in Figure 17a. Interestingly, numerous element ratios of Mo^{5+}, Co^{2+}, and Fe^{3+} in the electrode position precursor solutions manifested novel nanostructures; viz. nanosheets, nanoflakes, nanoparticles, and nanograss-like structures evolved for different precursor solutions. A working electrode with composition Mo:Co:Fe = 6.0:2.0:2.0 ($M_6C_2F_2$) showed a high 3354.7 mF cm^{-2} areal capacitance at 1.0 mA cm^{-2} with superior stability of 91% over 3000 cycles. The possible mechanism of the electrode–electrolyte interface behavior in $M_6C_2F_2$ is represented in Figure 17b. An ASC device was made by MoCoFe hydroxide and AC as positive and negative electrodes, respectively, (Figure 18a) and exhibited an enormous energy and power density of 1.27×10^{-3} Wh cm^{-3} and 3.75 W cm^{-3}, respectively; it also intimated good stability of 80.5% after 2000 cycles. The superior performance of the ASC device is due to the unique composition of the hybrid electrodes (with nanostructured morphology) and synergistic effects. The present investigation demonstrates a simple strategy for preparing potential TTMHs composite electrodes with the evolution of different morphologies for supercapacitor application.
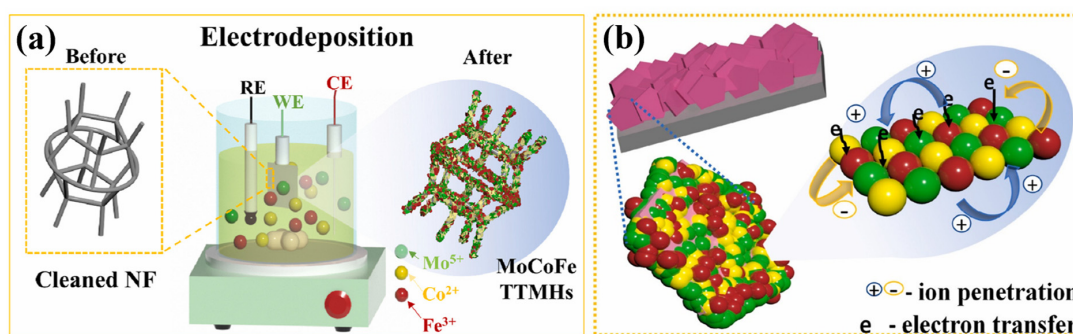
Figure 17. (**a**) Synthesis procedure of MoCoFe TTMHs. (**b**) Mechanism of the electrode–electrolyte interface behavior in $M_6C_2F_2$. (**a**,**b**) are reprinted from Ref. [135], Copyright (2023), with permission from Elsevier.

By aligning interconnected garland-like NiFeMn hydroxide on rGO membranes coated with NF (NiFeMn hydroxide/rGO/NF), a hierarchical web-like microstructure was elaborated through a one-pot two-step hydrothermal approach [134]. As a result of the redox reaction between GO and NF, the rGO membrane forms on NF through the first step at 50 °C. Then, urea decomposed and generated $NH_3 \cdot H_2O$ at 135 °C, which reacted with metal cations to obtain an amorphous NiFeMn ternary hydroxide. The unique microporous structure of NiFeMn hydroxide/rGO/Ni foam endows its larger surface area, more nanochannels for charge/mass transportation, and more electroactive sites exposed at the electrode/electrolyte interfaces. The NiFeMn hydroxide/rGO/NF demonstrates a remarkable capacitance of 2121 F g^{-1} at 0.61 A g^{-1}, 81.1% capacity retention over 5000 cycles at 0.91 A g^{-1}, and outstanding rate capability. The assembled ASC with AC and NiFeMn hydroxide/rGO/NF exhibits an extremely high 40.73 Wh m^2 of energy density at 79.38 W m^2 power density, indicating its promising potential for energy storage applications.

Although LDH materials have delivered numerous merits, such as high theoretical specific capacity, environmental friendliness, low cost, and ease of synthesis, the shortcomings of poor stability performance and unsatisfactory rate capability limit their practical applications. Controllable preparation of electrode materials possessing exquisite microstructure is considered as one of the most efficient strategies to enhance electrochemical performance. A gold-supported nanostructured NiFeCoPr hydroxide was synthesized by directly elec-

trodepositing praseodymium-doped nickel−cobalt−iron hydroxide onto a gold-deposited nickel foam (NF) substrate by Zhang et al. [132]. The active material NiFeCoPrO has an ultrathin nanostructure with an amorphous nature. The resultant monolithic NiFeCoPrO-Au/NF electrode displays a high 1792 F g^{-1} specific capacitance at 10 A g^{-1} current density, excellent rate capability (1445 F g^{-1} at 70 A g^{-1}), and eminent capacitance retention (99.5% after 30,000 cycles). This study provides an example of high-performance materials for use as supercapacitor electrodes and a general consideration of their chemical composition, dopants, support, and morphology to provoke further studies with improved performance.
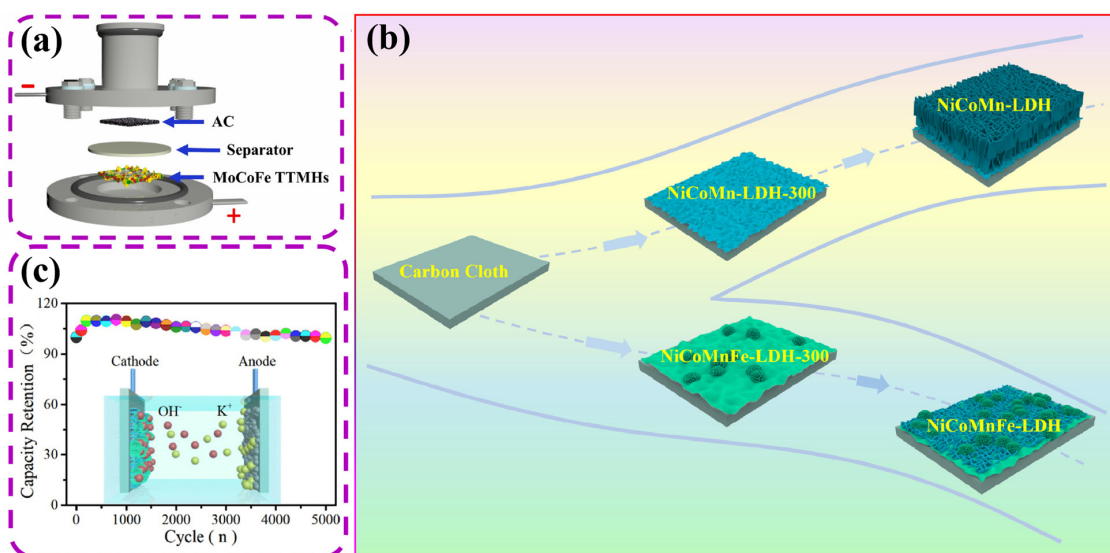
Figure 18. (**a**) Components of ASC device based on the MoCoFe TTMH positive electrode and the AC negative electrode. Reprinted from Ref. [135], Copyright (2023), with permission from Elsevier. (**b**) Growth pattern of the NiCoMn-LDH and NiCoMnFe-LDH materials grown on carbon cloth. (**c**) Cycling stability performance for 5000 cycles at 200 mV s^{-1} (inset shows a schematic illustration of the NiCoMnFe-LDH//AC AHSC configuration). (**b**,**c**) are reprinted from Ref. [136], Copyright (2023), with permission from Elsevier.

A unique quaternary nickel-cobalt-manganese-iron LDH (NiCoMnFe-LDH) material with a delicate microstructure design of combining dense nanosheets grown on NiCoMnFe-LDH thin films and outspread nanospheres assembled by tiny nanosheets was electrodeposited on carbon cloth by introducing a moderate amount of ion elements and regulating the growth time by Zhao et al. [136], as illustrated in Figure 18b. Ternary NiCoMn-LDH material was also prepared under the same condition for comparison, which shows a distinct morphology feature of thick nanosheets stacking. The NiCoMnFe-LDH electrode delivers more outstanding electrochemical properties than NiCoMn-LDH, an excellent specific capacity of 1836 mC cm^{-2} at 3 mA cm^{-2}, an ideal rate capability of about 81% of the capacity retention rate at 20 mA cm^{-2}, and a brilliant cycle lifespan of merely 1.7% capacity loss after 5000 continuous CV cycles. Moreover, the as-assembled NiCoMnFe-LDH//AC aqueous hybrid supercapacitor device (AHSC) possesses a satisfactory 31.3 Wh kg^{-1} energy density at 375 W kg^{-1} power density, and it reveals an ideal cycling lifespan with 99.5% of the capacity retention after 5000 consecutive tests, as shown in Figure 18c. The ease of fabrication and brilliant energy storage characteristics enable this AHSC to be a strong candidate for practical applications.

The outcomes of the electrochemical evaluations for pristine FeOOH and its assorted composites are outlined in Table 1. Of all the composites, the NiFe-LDH@CoS$_2$@Ni nanospheres-based composite, in particular, exhibits exceptional ultrahigh capacitance of 3880 F g^{-1} and maintains a cycling performance of 81.9% following 10,000 cycles [111].

Table 1. Assessment of diverse iron oxyhydroxide (FeOOH)-based materials for use as supercapacitor electrodes.

Material/Substrate	Synthesis Method	Structure/Morphology	Electrolyte	Potential Window	Specific Capacitance or Storage Capacity/Current Density or Scan Rate	Cycling Performance (N° of Cycles, Current Density)	Energy Density	Power Density	Ref.
FeOOH QDs/FGS composite/Ti foil	Facile chemical reaction	Heterostructure/self-assembled FeOOH mesoporous nanofilm tightly anchored on FGS	1 M Li_2SO_4	-0.8–0 V vs. Ag/AgCl	365 F g^{-1}/1 A g^{-1}	89.7% (20,000th, 4 A g^{-1})	-	-	[97]
FeOOH/NF	One-step electrodeposition	Amorphous nanostructured/fish-scale-like	3 M KOH	-1.1–-0.3 V vs. Hg/HgO	867 F g^{-1} at 5 mV s^{-1}	92.3% (200th)	86.4 Wh kg^{-1}	11.6 kW kg^{-1}	[88]
FeOOH/NF	One-pot hydrothermal route	3D porous structure/nanoflakes	1 M KOH	-0.1–0.5 V vs. Hg/HgO	1300 F g^{-1}/2 A g^{-1}	91% (2000th, 4 A g^{-1})	-	-	[98]
FeOOH/CFC	Hydrothermal growth + subsequent electrochemical transformation of α-Fe$_2$O$_3$	Nanoparticles	2 M KOH	-1.2–0 V vs. SCE	1066 F g^{-1}/1 A g^{-1}	91% (10,000th, 30 A g^{-1})	104.3 Wh kg^{-1}	1.27 kW kg^{-1}	[66]
γ-FeOOH/CNFP	Galvanostatic electrodeposition	Fluffy nanoflakes/porous morphology	1 M KOH	-1.5–0 V vs. SCE	3.48 C cm^{-2} at 10 mA cm^{-2}	92% (3000th, 50 mA cm^{-2})	1515 mW h cm^{-2}	9 mW cm^{-2}	[87]
α-FeOOH/NF	Two-step hydrothermal method + etching process	Nanorods	1 M Na_2SO_4	-1.0–0 V vs. SCE	224.6 F g^{-1}/1 A g^{-1}	92.5% (4000th, 5 A g^{-1})	51.5 Wh kg^{-1}	9.1 kW kg^{-1}	[24]
FeOOH/NF	Dropwise wet chemistry	Parallel and hollow	1 M Na_2SO_4	-0.8–0 V vs. SCE	186.8 F g^{-1}/0.5 A g^{-1}	93.1% (4000th, 5 A g^{-1})	20.7 Wh kg^{-1}	10 kW kg^{-1}	[99]
α-FeOOH nanorods/GO composite/NF	One-pot hydrothermal method	Nanorods	1 M KOH	-0.9–0 V vs. Hg/HgO	127 F g^{-1}/10 A g^{-1}	85% (2000th, 5 A g^{-1})	-	-	[85]
FeOOH@MWCNT	Facile synthesis method	Nanofilm/Nanoflowers	0.5 M Na_2SO_4	-0.85–0 V vs. Ag/AgCl	345 F g^{-1}/1 A g^{-1}	76.4% (5000th, 1 A g^{-1})	-	-	[101]
α-FeOOH-MWCNT composite/NF	PELLI strategies	Particles	0.5 M Na_2SO_4	-0.8–0 V vs. SCE	5.86 F cm^{-2} at 2 mV s^{-1}	-	-	-	[84]
FeOOH/MoSe$_2$/NF	Hydrothermal method + chemical blending technique	Nanorods	6 M KOH	0–1.0 V vs. Ag/AgCl (for device)	132 F g^{-1}/1 A g^{-1} (for device)	100% (3000th) (for device)	18.3 Wh kg^{-1}	1174 W kg^{-1}	[100]
FeOOH@Gr	Bioinspired method at the air-solution interface	Nanowires	2 M KOH	-1.2–0 V vs. Hg/HgO	25.5 mF cm^{-2} at 0.1 V s^{-1} (for device)	83.5% (10,000th) (for device)	1.04 mWh cm^{-3}	0.445 W cm^{-3}	[102]

Table 1. *Cont.*

Material/Substrate	Synthesis Method	Structure/Morphology	Electrolyte	Potential Window	Specific Capacitance or Storage Capacity/Current Density or Scan Rate	Cycling Performance (N° of Cycles, Current Density)	Energy Density	Power Density	Ref.
FeOOH@Gr	Gas-liquid diffusion method at the air-solution interface	Nanowires	2 M KOH	-1.25–0 V vs. Hg/HgO	1150.3 F g^{-1}/3.0 A g^{-1}	~100% (1000th)	0.67 mWh cm^{-3}	41.7 mW cm^{-3}	[103]
FeOOH/MnO$_2$/NF	Facile chemical reaction	Film/nanospheres	1 M Na$_2$SO$_4$	0–0.8 V vs. Ag/AgCl	350.2 F g^{-1}/0.5 A g^{-1}	95.6% (10,000th, 15 A g^{-1})	5 × 10^{-4} mWh cm^{-2}	0.04 mW cm^{-2}	[68]
Al(OH)$_3$/MnO$_2$/FeOOH/SS	Layer by Layer method	Mesoporous reindeer moss-like	1 M Na$_2$SO$_4$	-1.1–1.05 V vs. Ag/AgCl	2557 C g^{-1} at 5 mV s^{-1}	~70% (1000th, 5 mA)	443.67 Wh kg^{-1}	13.53 kW kg^{-1}	[104]
NiFe LDH/NF	One-step hydrothermal method	Porous nanostructure/Nanosheet arrays	1 M KOH	0–0.7 V vs. SCE	2708 F g^{-1}/5 A g^{-1}	42.6% (500th, 10 A g^{-1})	50.2 Wh kg^{-1}	800 W kg^{-1}	[106]
NiFe-LDH/NF	Two-step hydrothermal method + sulfidation modification	Nanosheets	1 M KOH	-1.0–0 V vs. Hg/HgO	992 mF cm^{-2} at 2 mA cm^{-2}	64.5% (2000th, 4 mA cm^{-2})	39.9 Wh kg^{-1}	211.4 W kg^{-1}	[109]
NiFe-LDH/Glassy carbon electrode	Sonochemical route	Spherical nanostructures	6 M KOH	0–0.4 V vs. SCE	168 F g^{-1}/1.5 Ag^{-1}	-	-	-	[107]
NiFe-LDH	Ultrasonication and mechanical stirring	Nanosheets	6 M KOH	-0.2–0.5 V vs. SCE	1923 F g^{-1} at 3 A g^{-1}	98% (1000th, 10 A g^{-1})	49.13 Wh kg^{-1}	400 W kg^{-1}	[116]
NiFe-LDH/MXene	One-step hydrothermal method	Interconnected network structure	1 M KOH	-0.4–1.0 V vs. Calomel E	720.2 F g^{-1}/1 A g^{-1}	86% (1000th)	42.4 Wh kg^{-1}	758.27 W kg^{-1}	[112]
NiFe-LDH/CC	One-step hydrothermal approach	Interconnected nanoflakes	3 M KOH	0–0.6 V vs. Ag/AgCl	984 F g^{-1}/1 A g^{-1}	87.6% (7000th, 12 A g^{-1})	-	-	[113]
NiFe LDH/GHA/NF	Hydrothermal method + freeze-drying treatment	Hexagonal platelets	6 M KOH	0–0.5 V vs. Hg/HgO	1196 F g^{-1}/1 A g^{-1}	80% (2000th, 10 A g^{-1})	17.6 Wh kg^{-1}	650 W kg^{-1}	[105]
NiFe-LDH/RGO/CNFs/NF	One-step hydrothermal method	Nanoplates	6 M KOH	0–0.57 V vs. Hg/HgO	1330.2 F g^{-1}/1 A g^{-1}	97.1% (2500th, 8 A g^{-1}) (for device)	33.7 Wh kg^{-1}	785.8 W kg^{-1}	[108]
NiFe-LDH/rGO/NF	Two-step electrodeposition method	Nanosheets	2 M KOH	0–0.5 V vs. SCE	1462.5 F g^{-1}/5 A g^{-1}	64.7% (2000th, 15 A g^{-1})	17.71 Wh kg^{-1}	348.49 W kg^{-1}	[110]
rGO-FeO-CNT-NiFeLDH	Hydrothermal + CVD + ECD	Thin layer	2M KOH	-1.2–0 V vs. Ag/AgCl	411.9 F g^{-1} at 5 mV s^{-1}	144.89% (3200th) (for device)	41.4 Wh kg^{-1}	5600 W kg^{-1}	[114]

Table 1. *Cont.*

Material/Substrate	Synthesis Method	Structure/Morphology	Electrolyte	Potential Window	Specific Capacitance or Storage Capacity/Current Density or Scan Rate	Cycling Performance (N° of Cycles, Current Density)	Energy Density	Power Density	Ref.
NiFe-LDH@CoS$_2$@Ni	Two-step hydrothermal method	Flower-like nanospheres	6 M KOH	0–0.7 V vs. Hg/HgO	3880 F g^{-1}/1.17 A g^{-1}	81.9% (10,000th, 20 mA cm^{-2})	15.84 Wh kg^{-1}	375.16 W kg^{-1}	[111]
CoFe-LDH/NF	Co-precipitation + I$_2$ partial oxidation process	Hydrotalcite-like/layered plate-like	2 M KOH	−0.15–0.45 V vs. Ag/AgCl	728 F g^{-1}/1 A g^{-1}	65.3% (5000th, 2 A g^{-1})	27.3 W h kg^{-1}	823.5 W kg^{-1}	[117]
CoFe-LDHs/NF	Co-precipitation	Layer hexagonal/Nanoflakes	1 M KOH	−0.2–0.5 V vs. Hg/HgO	869 F g^{-1}/1 g^{-1}	99.5% (1000th, 1 A g^{-1})	-	-	[118]
CoFe-LDH/NFa	ECD	Nanosheets	1 M KOH	0–0.55 V vs. Ag/AgCl	70 µF cm^{-2} at 2 mA cm^{-2} (for device)	91% (2000th, 3 mA cm^{-2}) (for device)	1.6 mWh cm^{-2}	0.09 mW cm^{-2}	[121]
CoFe Hydroxides	One-step ECD	Frame-like structure	1 M KOH	0–0.7 V vs. SCE	2255.6 F g^{-1}/1 A g^{-1}	73.5% (2000th, 10 A g^{-1})	-	-	[119]
CoFe hydroxides	One-step liquid-phase reflux	Hexagonal plate-like structure	6 M KOH	0–0.45 V vs. SCE	2358.4 F g^{-1}/0.5 A g^{-1}	83% (1400th, 0.5 A g^{-1})	28.3 Wh kg^{-1}	512 W kg^{-1}	[120]
CoFe-LDH/NF	Hydrothermal + CV	Microflowers	3 M KOH	0–0.6 V vs. Hg/HgO	4662.2 mF cm^{-2}	133.8% (10,000th)	-	-	[123]
CoFe-LDH/P	Hydrothermal	Nanosheets	6 M KOH	−0.1–0.7 V vs. Ag/AgCl	1686 F g^{-1}/1 A g^{-1}	98% (10,000th)	75.9 Wh kg^{-1}	1124 W kg^{-1}	[122]
NiO@CoFe-LDH/NF	Acid corrosion route + electrodeposition coating process	3D open porous structure/uniform wrinkled cross-linked	2 M KOH	0–1.5 V vs. SCE (for device)	205 F g^{-1}/1 A g^{-1} (for device	90% (3000th, 1 A g^{-1}) (for device)	64.1 W h kg^{-1}	15 kW kg^{-1}	[67]
NiCoFe-LDH	One-pot self-template method	Nanospheres	3 M LiCl	0–1.0 V vs. SCE	83.9 mF cm^{-2} at 0.3 mA (for device)	116.6% (5000th)	22.3 µWh cm^{-2}	2076 µW cm^{-2}	[115]
NiCoFe-LDH/NF	Cyclic voltametric method	Layer structure	3 M KOH	0–0.4 V vs. Ag/AgCl	3130 F g^{-1}/1 A g^{-1}	82.5% (5000th)	101 Wh kg^{-1}	91.5 kW kg^{-1}	[125]
NiCoFe-LDH/SS	Electrodeposition	Nanosheets	2 M KOH	−0.2–0.4 V vs. Ag/AgCl	360 C g^{-1}/0.4 A g^{-1}	84% (2000th)	-	-	[128]
NiCoFe-LDH/CNFs	In situ growth approach with hydrothermal	Nanosheets	6 M KOH	0–0.6 V vs. Hg/HgO	1203 F g^{-1}/1 A g^{-1}	94.4% (1000th, 20 A g^{-1})	30.2 W h kg^{-1}	800.1 W kg^{-1}	[124]
NiCoFe-LDH/NF	Hydrothermal	Two-dimensional porous nanosheets	2 M KOH	0–0.6 V vs. SCE	425.56 mAh g^{-1}/1 A g^{-1}	94.52% (8000th, 10 A g^{-1})	51.81 Wh kg^{-1}	1.26 Wh kg^{-1}	[129]
NiCoFe hydroxide	Electrodeposition	Nanosheets	1 M KOH	0–0.6 V vs. Hg/HgO	1321 F g^{-1}/1 A g^{-1}	88.57% (10,000th, 10 A g^{-1})	73.07 Wh kg^{-1}	1.07 kW kg^{-1}	[126]

Table 1. *Cont.*

Material/Substrate	Synthesis Method	Structure/Morphology	Electrolyte	Potential Window	Specific Capacitance or Storage Capacity/Current Density or Scan Rate	Cycling Performance (N° of Cycles, Current Density)	Energy Density	Power Density	Ref.
NiCoFe-LDH NA/NF	Ion exchange + etching reaction under hydrothermal conditions	2D/3D porous structure/Nanosheets	2 M KOH	0–0.6 V vs. SCE	1495 C g^{-1}/1 A g^{-1}	89% (10,000th, 10 A g^{-1})	34.4 W h kg^{-1}	935.5 W kg^{-1}	[131]
NiFeCo-S@NiFeCo-TH/NIF	Electro-oxidation + sulfuration + controllable Co^{2+} exchange process	Nanosheets	2 M KOH	−0.1–0.6 V vs. SCE	174 mAh g^{-1} at 10 mA cm^{-2}	90.1% (4000th) (for device)	56.3 Wh kg^{-1}	543 W kg^{-1}	[127]
NiCoFe-LDH@g-C$_3$N$_4$/NF	Hydrothermal	Nanosheets	6 M KOH	0–0.5 V vs. SCE	1550 F g^{-1}/1 A g^{-1}	92.7% (5000th) (for device)	35 Wh kg^{-1}	701 W kg^{-1}	[130]
Ni-Zn-Fe LDH	SILAR method	Ash-like	6 M KOH	0–0.45 V vs. Ag/AgCl	1452.3 F g^{-1} at 5 mV s^{-1}	112.5% (1000th)	14.9 Wh kg^{-1}	1077.6 W kg^{-1}	[133]
MoCoFe hydroxide	Single-step electrodeposition technique	Nanosheet-like	1 M KOH	0–0.5 V vs. Ag/AgCl	3354.7 mF cm^{-2} at 1.0 mA cm^{-2}	91% (3000th, 10 mA cm^{-2})	1.27 × 10^{-3} Wh cm^{-3}	3.75 W cm^{-3}	[135]
NiFeMn hydroxide/rGO/NF	One-pot two-step hydrothermal method	Hierarchical web-like microstructure	2 M KOH	0–0.5 V vs. Hg/HgO	2121 F g^{-1}/0.61 A g^{-1}	81.1% (5000th, 0.91 A g^{-1})	40.73 W h m^{-2}	79.38 W m^{-2}	[134]
NiFeCoPrO	Electrodeposition	Ultrathin nanostructure/amorphous nature	3 M KOH	−0.2–0.4 V vs. Ag/AgCl	1792 F g^{-1}/10 A g^{-1}	99.5% (30,000th)	-	-	[132]
NiCoMnFe-LDH	Electrodeposition	Thin film	2 M KOH	0–0.5 V vs. SCE	1836 mC cm^{-2} at 3 mA cm^{-2}	98.3% (5000th)	31.3 Wh kg^{-1}	375 W kg^{-1}	[136]

7. Conclusions

In recent times, there has been a marked surge in interest surrounding the development of high-performance electrode materials for supercapacitors. This can be attributed to the need for negative electrodes boasting characteristics such as widespread availability, high specific capacitance, exceptional redox activity, expansive operating potential, eco-friendliness, and low cost, all of which contribute to an enhanced energy density in supercapacitors. Iron oxyhydroxide (FeOOH) materials have demonstrated their exceptional capabilities as anode materials for supercapacitors, and this comprehensive review provides the-state-of-the-art progress and development of FeOOH-based materials employed as both negative and positive electrodes for supercapacitors.

An in-depth examination of the supercapacitive performance of the FeOOH electrode is conducted, with particular attention paid to the influence of factors such as synthesis method, crystallinity, morphology, dispersibility, surface area, and substrate on its electrochemical properties. As well as discussing approaches to deal with the challenges caused by FeOOH's low surface area, the review also discusses how to increase its electrical conductivity. One such approach involves the controlled synthesis of electrode materials through a customizable three-dimensional porous structure based on diatoms, which expands the surface area and active sites in contact with the electrolyte, prevents aggregation, and ultimately results in exceptional electrochemical properties. In addition to promoting easy liquid electrolyte penetration, this 3D porous structure also prevents electrode volume changes during charging and discharging. Moreover, the amorphous nature of electrode materials enhances the reaction and diffusion of electrolyte ions, enabling isotropic charging processes as well as discharging processes. FeOOH electrode materials synthesized with a hollow parallel nanostructure have been found to outperform conventional activated graphene or FeOOH nanoneedle materials.

This review also explores the enhancement of supercapacitive performance, considering factors such as specific capacitance, power density, energy density, cycling life, and rate capability, that result from the synergistic effects of composite materials. These composite materials, through their synergistic effect, augment the specific surface area, inhibit particle agglomeration, and increase conductivity.

Furthermore, the review delves into the supercapacitive performance of Fe-based binary, ternary, and quaternary hydroxides and layered double hydroxides (LDHs). Although binary LDHs/hydroxides are commonly utilized in supercapacitor applications, their limited electrical conductivity and active sites hinder their potential in various energy-related applications. To circumvent these limitations, ternary and quaternary LDHs/hydroxides can be created by incorporating third and fourth metal cations, respectively, leading to enhanced conductivity and a greater number of electrochemically active sites. Nevertheless, the development of binder-free Fe-based binary LDH composites with unique architectures, such as flower-like structures of ultrathin nanosheets, is considered a promising strategy for achieving superior capacitive performance. These distinctive structures offer an abundance of active sites, a superior specific surface area, shortened diffusion distances between electrolyte ions and substrates, and accelerated electron transport.

Additionally, this review offers a comprehensive analysis of the asymmetric cell performance of FeOOH-based materials, examining various positive and negative electrodes. Asymmetric configurations employing FeOOH-based electrodes yield high energy densities that rival those of commercial batteries and pave the way for the development of cost-effective, high energy density devices.

Author Contributions: Writing—original draft preparation, Y.E.I.; writing—original draft preparation, A.L.; writing—review and editing, S.S.K.; writing—review and editing, S.K.N.; writing—review and editing, B.G.P.; supervision, project administration, B.G.P. All authors have read and agreed to the published version of the manuscript.

Data Availability Statement: Not applicable as this article is a survey/review.

Conflicts of Interest: The authors declare that they do not have any competing financial interest or personal relationships that might influence their work.

References

1. Lalwani, S.; Karade, S.; Eum, J.-H.; Kim, H. Maximizing Redox Charge Storage via Cation (V)–Anion (S) Dual Doping on Nickel Diselenide Nanodiscs for Hybrid Supercapacitors. *ACS Appl. Energy Mater.* **2021**, *4*, 2430–2439. [CrossRef]
2. Global Energy Crisis—Topics. Available online: https://www.iea.org/topics/global-energy-crisis (accessed on 23 February 2023).
3. Friedlingstein, P.; O'Sullivan, M.; Jones, M.W.; Andrew, R.M.; Gregor, L.; Hauck, J.; Le Quéré, C.; Luijkx, I.T.; Olsen, A.; Peters, G.P.; et al. Global Carbon Budget 2022. *Earth Syst. Sci. Data* **2022**, *14*, 4811–4900. [CrossRef]
4. Nations, U. Net Zero Coalition. Available online: https://www.un.org/en/climatechange/net-zero-coalition (accessed on 23 February 2023).
5. Net Zero by 2050—Analysis. Available online: https://www.iea.org/reports/net-zero-by-2050 (accessed on 23 February 2023).
6. The Paris Agreement | UNFCCC. Available online: https://unfccc.int/process-and-meetings/the-paris-agreement (accessed on 23 February 2023).
7. Hu, B.; Xu, J.; Fan, Z.; Xu, C.; Han, S.; Zhang, J.; Ma, L.; Ding, B.; Zhuang, Z.; Kang, Q.; et al. Covalent Organic Framework Based Lithium–Sulfur Batteries: Materials, Interfaces, and Solid-State Electrolytes. *Adv. Energy Mater.* **2023**, *13*, 2203540. [CrossRef]
8. Li, L.; Cheng, H.; Zhang, J.; Guo, Y.; Sun, C.; Zhou, M.; Li, Q.; Ma, Z.; Ming, J. Quantitative Chemistry in Electrolyte Solvation Design for Aqueous Batteries. *ACS Energy Lett.* **2023**, *8*, 1076–1095. [CrossRef]
9. Javed, M.S.; Najam, T.; Hussain, I.; Idrees, M.; Ahmad, A.; Imran, M.; Shah, S.S.A.; Luque, R.; Han, W. Fundamentals and Scientific Challenges in Structural Design of Cathode Materials for Zinc-Ion Hybrid Supercapacitors. *Adv. Energy Mater.* **2023**, *13*, 2202303. [CrossRef]
10. Zhang, X.; Han, R.; Liu, Y.; Li, H.; Shi, W.; Yan, X.; Zhao, X.; Li, Y.; Liu, B. Porous and Graphitic Structure Optimization of Biomass-Based Carbon Materials from 0D to 3D for Supercapacitors: A Review. *Chem. Eng. J.* **2023**, *460*, 141607. [CrossRef]
11. Eisa, T.; Abdelkareem, M.A.; Jadhav, D.A.; Mohamed, H.O.; Sayed, E.T.; Olabi, A.G.; Castaño, P.; Chae, K.-J. Critical Review on the Synthesis, Characterization, and Application of Highly Efficient Metal Chalcogenide Catalysts for Fuel Cells. *Prog. Energy Combust. Sci.* **2023**, *94*, 101044. [CrossRef]
12. Vinodh, R.; Atchudan, R.; Kim, H.-J.; Yi, M. Recent Advancements in Polysulfone Based Membranes for Fuel Cell (PEMFCs, DMFCs and AMFCs) Applications: A Critical Review. *Polymers* **2022**, *14*, 300. [CrossRef]
13. Zeng, Y.; Yu, M.; Meng, Y.; Fang, P.; Lu, X.; Tong, Y. Iron-Based Supercapacitor Electrodes: Advances and Challenges. *Adv. Energy Mater.* **2016**, *6*, 1601053. [CrossRef]
14. Ma, X.; Jing, Z.; Feng, C.; Qiao, M.; Xu, D. Research and Development Progress of Porous Foam-Based Electrodes in Advanced Electrochemical Energy Storage Devices: A Critical Review. *Renew. Sustain. Energy Rev.* **2023**, *173*, 113111. [CrossRef]
15. Vlad, A.; Singh, N.; Galande, C.; Ajayan, P.M. Design Considerations for Unconventional Electrochemical Energy Storage Architectures. *Adv. Energy Mater.* **2015**, *5*, 1402115. [CrossRef]
16. Zhang, S.; Pan, N. Supercapacitors Performance Evaluation. *Adv. Energy Mater.* **2015**, *5*, 1401401. [CrossRef]
17. Burke, A. Ultracapacitors: Why, How, and Where Is the Technology. *J. Power Sources* **2000**, *91*, 37–50. [CrossRef]
18. Zhi, M.; Xiang, C.; Li, J.; Li, M.; Wu, N. Nanostructured Carbon–Metal Oxide Composite Electrodes for Supercapacitors: A Review. *Nanoscale* **2013**, *5*, 72–88. [CrossRef] [PubMed]
19. Raza, W.; Ali, F.; Raza, N.; Luo, Y.; Kim, K.-H.; Yang, J.; Kumar, S.; Mehmood, A.; Kwon, E.E. Recent Advancements in Supercapacitor Technology. *Nano Energy* **2018**, *52*, 441–473. [CrossRef]
20. Sial, Q.A.; Kalanur, S.S.; Seo, H. Lamellar Flower Inspired Hierarchical Alpha Manganese Vanadate Microflowers for High-Performance Flexible Hybrid Supercapacitors. *Ceram. Int.* **2022**, *48*, 24989–24999. [CrossRef]
21. Kumar, N.; Kim, S.-B.; Lee, S.-Y.; Park, S.-J. Recent Advanced Supercapacitor: A Review of Storage Mechanisms, Electrode Materials, Modification, and Perspectives. *Nanomaterials* **2022**, *12*, 3708. [CrossRef]
22. Krishna Roy, B.; Tahmid, I.; Ur Rashid, T. Chitosan-Based Materials for Supercapacitor Applications: A Review. *J. Mater. Chem. A* **2021**, *9*, 17592–17642. [CrossRef]
23. Chaichi, A.; Venugopalan, G.; Devireddy, R.; Arges, C.; Gartia, M.R. A Solid-State and Flexible Supercapacitor That Operates across a Wide Temperature Range. *ACS Appl. Energy Mater.* **2020**, *3*, 5693–5704. [CrossRef]
24. Li, K.; Liu, X.; Zheng, T.; Jiang, D.; Zhou, Z.; Liu, C.; Zhang, X.; Zhang, Y.; Losic, D. Tuning MnO_2 to FeOOH Replicas with Bio-Template 3D Morphology as Electrodes for High Performance Asymmetric Supercapacitors. *Chem. Eng. J.* **2019**, *370*, 136–147. [CrossRef]
25. Qiao, Y.; Liu, G.; Xu, R.; Hu, R.; Liu, L.; Jiang, G.; Demir, M.; Ma, P. $SrFe_{1-X}Zr_xO_{3-\delta}$ Perovskite Oxides as Negative Electrodes for Supercapacitors. *Electrochim. Acta* **2023**, *437*, 141527. [CrossRef]
26. Guo, W.; Yu, C.; Li, S.; Song, X.; Huang, H.; Han, X.; Wang, Z.; Liu, Z.; Yu, J.; Tan, X.; et al. A Universal Converse Voltage Process for Triggering Transition Metal Hybrids In Situ Phase Restruction toward Ultrahigh-Rate Supercapacitors. *Adv. Mater.* **2019**, *31*, 1901241. [CrossRef] [PubMed]

27. Omar, N.; Daowd, M.; Hegazy, O.; Al Sakka, M.; Coosemans, T.; Van den Bossche, P.; Van Mierlo, J. Assessment of Lithium-Ion Capacitor for Using in Battery Electric Vehicle and Hybrid Electric Vehicle Applications. *Electrochim. Acta* **2012**, *86*, 305–315. [CrossRef]

28. Conway, B.E. *Electrochemical Supercapacitors: Scientific Fundamentals and Technological Applications*; Springer Science & Business Media: Berlin, Germany, 2013; ISBN 978-1-4757-3058-6.

29. Reis, S.; Grosso, R.; Kosctiuk, J.; Franchetti, M.; Oliveira, F.; Souza, A.; Gonin, C.; Freitas, H.; Monteiro, R.; Parreira, L.; et al. Effect of Zr^{4+} on Lithium-Ion Conductivity of Garnet-Type $Li_{5+x}La_3(Nb_{2-x}Zr_x)O_{12}$ Solid Electrolytes. *Batteries* **2023**, *9*, 137. [CrossRef]

30. Yang, Z.; Trask, S.E.; Wu, X.; Ingram, B.J. Effect of Si Content on Extreme Fast Charging Behavior in Silicon–Graphite Composite Anodes. *Batteries* **2023**, *9*, 138. [CrossRef]

31. Palneedi, H.; Peddigari, M.; Hwang, G.-T.; Jeong, D.-Y.; Ryu, J. High-Performance Dielectric Ceramic Films for Energy Storage Capacitors: Progress and Outlook. *Adv. Funct. Mater.* **2018**, *28*, 1803665. [CrossRef]

32. El Issmaeli, Y.; Lahrichi, A.; Nzaba Madila, E.E.; Lamcharfi, T.; Abdi, F.; Duong, A. Novel Dielectric Response in B-Site Zirconium-Doped $CaCu_3Ti_4O_{12}$ Ceramics: A Structural, Optical and Electrical Study. *Solid State Sci.* **2022**, *134*, 107050. [CrossRef]

33. McCloskey, B.D. Expanding the Ragone Plot: Pushing the Limits of Energy Storage. *J. Phys. Chem. Lett.* **2015**, *6*, 3592–3593. [CrossRef]

34. Zhou, L.; Li, C.; Liu, X.; Zhu, Y.; Wu, Y.; van Ree, T. 7—Metal Oxides in Supercapacitors. In *Metal Oxides in Energy Technologies*; Wu, Y., Ed.; Metal Oxides; Elsevier: Amsterdam, The Netherlands, 2018; pp. 169–203. ISBN 978-0-12-811167-3.

35. Vinodh, R.; Babu, R.S.; Sambasivam, S.; Gopi, C.V.V.M.; Alzahmi, S.; Kim, H.-J.; de Barros, A.L.F.; Obaidat, I.M. Recent Advancements of Polyaniline/Metal Organic Framework (PANI/MOF) Composite Electrodes for Supercapacitor Applications: A Critical Review. *Nanomaterials* **2022**, *12*, 1511. [CrossRef]

36. Vandeginste, V. A Review of Fabrication Technologies for Carbon Electrode-Based Micro-Supercapacitors. *Appl. Sci.* **2022**, *12*, 862. [CrossRef]

37. Haider, W.A.; Tahir, M.; He, L.; Yang, W.; Minhas-khan, A.; Owusu, K.A.; Chen, Y.; Hong, X.; Mai, L. Integration of VS2 Nanosheets into Carbon for High Energy Density Micro-Supercapacitor. *J. Alloys Compd.* **2020**, *823*, 151769. [CrossRef]

38. Zhou, W.; Liu, Z.; Chen, W.; Sun, X.; Luo, M.; Zhang, X.; Li, C.; An, Y.; Song, S.; Wang, K.; et al. A Review on Thermal Behaviors and Thermal Management Systems for Supercapacitors. *Batteries* **2023**, *9*, 128. [CrossRef]

39. Dutta, A.; Mitra, S.; Basak, M.; Banerjee, T. A Comprehensive Review on Batteries and Supercapacitors: Development and Challenges since Their Inception. *Energy Storage* **2023**, *5*, e339. [CrossRef]

40. Lee, J.-H.; Yang, G.; Kim, C.-H.; Mahajan, R.L.; Lee, S.-Y.; Park, S.-J. Flexible Solid-State Hybrid Supercapacitors for the Internet of Everything (IoE). *Energy Environ. Sci.* **2022**, *15*, 2233–2258. [CrossRef]

41. Han, J.; Li, Q.; Wang, J.; Ye, J.; Fu, G.; Zhai, L.; Zhu, Y. Heteroatoms (O, N)-Doped Porous Carbon Derived from Bamboo Shoots Shells for High Performance Supercapacitors. *J. Mater. Sci. Mater. Electron.* **2018**, *29*, 20991–21001. [CrossRef]

42. Echeverry-Montoya, N.A.; Prías-Barragán, J.J.; Tirado-Mejía, L.; Agudelo, C.; Fonthal, G.; Ariza-Calderón, H. Fabrication and Electrical Response of Flexible Supercapacitor Based on Activated Carbon from Bamboo. *Phys. Status Solidi C* **2017**, *14*, 1600258. [CrossRef]

43. Fasakin, O.; Dangbegnon, J.K.; Momodu, D.Y.; Madito, M.J.; Oyedotun, K.O.; Eleruja, M.A.; Manyala, N. Synthesis and Characterization of Porous Carbon Derived from Activated Banana Peels with Hierarchical Porosity for Improved Electrochemical Performance. *Electrochim. Acta* **2018**, *262*, 187–196. [CrossRef]

44. Liu, B.; Zhang, L.; Qi, P.; Zhu, M.; Wang, G.; Ma, Y.; Guo, X.; Chen, H.; Zhang, B.; Zhao, Z.; et al. Nitrogen-Doped Banana Peel–Derived Porous Carbon Foam as Binder-Free Electrode for Supercapacitors. *Nanomaterials* **2016**, *6*, 18. [CrossRef]

45. Shang, T.; Xu, Y.; Li, P.; Han, J.; Wu, Z.; Tao, Y.; Yang, Q.-H. A Bio-Derived Sheet-like Porous Carbon with Thin-Layer Pore Walls for Ultrahigh-Power Supercapacitors. *Nano Energy* **2020**, *70*, 104531. [CrossRef]

46. Seo, M.-K.; Park, S.-J. Electrochemical Characteristics of Activated Carbon Nanofiber Electrodes for Supercapacitors. *Mater. Sci. Eng. B* **2009**, *164*, 106–111. [CrossRef]

47. Yuan, S.; Fan, W.; Wang, D.; Zhang, L.; Miao, Y.-E.; Lai, F.; Liu, T. 3D Printed Carbon Aerogel Microlattices for Customizable Supercapacitors with High Areal Capacitance. *J. Mater. Chem. A* **2021**, *9*, 423–432. [CrossRef]

48. Yang, X.; Kong, L.; Cao, M.; Liu, X.; Li, X. Porous Nanosheets-Based Carbon Aerogel Derived from Sustainable Rattan for Supercapacitors Application. *Ind. Crop. Prod.* **2020**, *145*, 112100. [CrossRef]

49. Lee, K.; Shabnam, L.; Faisal, S.N.; Hoang, V.C.; Gomes, V.G. Aerogel from Fruit Biowaste Produces Ultracapacitors with High Energy Density and Stability. *J. Energy Storage* **2020**, *27*, 101152. [CrossRef]

50. Long, S.; Feng, Y.; He, F.; Zhao, J.; Bai, T.; Lin, H.; Cai, W.; Mao, C.; Chen, Y.; Gan, L.; et al. Biomass-Derived, Multifunctional and Wave-Layered Carbon Aerogels toward Wearable Pressure Sensors, Supercapacitors and Triboelectric Nanogenerators. *Nano Energy* **2021**, *85*, 105973. [CrossRef]

51. Yao, B.; Peng, H.; Zhang, H.; Kang, J.; Zhu, C.; Delgado, G.; Byrne, D.; Faulkner, S.; Freyman, M.; Lu, X.; et al. Printing Porous Carbon Aerogels for Low Temperature Supercapacitors. *Nano Lett.* **2021**, *21*, 3731–3737. [CrossRef] [PubMed]

52. Kim, T.-W.; Park, S.-J. Synthesis of Reduced Graphene Oxide/Thorn-like Titanium Dioxide Nanofiber Aerogels with Enhanced Electrochemical Performance for Supercapacitor. *J. Colloid Interface Sci.* **2017**, *486*, 287–295. [CrossRef]

53. Sathish Kumar, P.; Prakash, P.; Srinivasan, A.; Karuppiah, C. A New Highly Powered Supercapacitor Electrode of Advantageously United Ferrous Tungstate and Functionalized Multiwalled Carbon Nanotubes. *J. Power Sources* **2021**, *482*, 228892. [CrossRef]

54. Awata, R.; Shehab, M.; El Tahan, A.; Soliman, M.; Ebrahim, S. High Performance Supercapacitor Based on Camphor Sulfonic Acid Doped Polyaniline/Multiwall Carbon Nanotubes Nanocomposite. *Electrochim. Acta* **2020**, *347*, 136229. [CrossRef]

55. Ovhal, M.M.; Kumar, N.; Hong, S.-K.; Lee, H.-W.; Kang, J.-W. Asymmetric Supercapacitor Featuring Carbon Nanotubes and Nickel Hydroxide Grown on Carbon Fabric: A Study of Self-Discharging Characteristics. *J. Alloys Compd.* **2020**, *828*, 154447. [CrossRef]

56. Zhang, W.; Yang, W.; Zhou, H.; Zhang, Z.; Zhao, M.; Liu, Q.; Yang, J.; Lu, X. Self-Discharge of Supercapacitors Based on Carbon Nanotubes with Different Diameters. *Electrochim. Acta* **2020**, *357*, 136855. [CrossRef]

57. Kim, M.; Lee, B.; Li, M.; Noda, S.; Kim, C.; Kim, J.; Song, W.-J.; Lee, S.W.; Brand, O. All-Soft Supercapacitors Based on Liquid Metal Electrodes with Integrated Functionalized Carbon Nanotubes. *ACS Nano* **2020**, *14*, 5659–5667. [CrossRef] [PubMed]

58. Lee, S.-Y.; Kim, J.-I.; Park, S.-J. Activated Carbon Nanotubes/Polyaniline Composites as Supercapacitor Electrodes. *Energy* **2014**, *78*, 298–303. [CrossRef]

59. Ni, G.; Qin, F.; Guo, Z.; Wang, J.; Shen, W. Nitrogen-Doped Asphaltene-Based Porous Carbon Fibers as Supercapacitor Electrode Material with High Specific Capacitance. *Electrochim. Acta* **2020**, *330*, 135270. [CrossRef]

60. Heo, Y.-J.; Park, M.; Kang, W.-S.; Rhee, K.Y.; Park, S.-J. Preparation and Characterization of Carbon Black/Pitch-Based Carbon Fiber Paper Composites for Gas Diffusion Layers. *Compos. Part B Eng.* **2019**, *159*, 362–368. [CrossRef]

61. Shimanoe, H.; Mashio, T.; Nakabayashi, K.; Inoue, T.; Hamaguchi, M.; Miyawaki, J.; Mochida, I.; Yoon, S.-H. Manufacturing Spinnable Mesophase Pitch Using Direct Coal Extracted Fraction and Its Derived Mesophase Pitch Based Carbon Fiber. *Carbon* **2020**, *158*, 922–929. [CrossRef]

62. Yang, C.-M.; Kim, B.-H. Highly Conductive Pitch-Based Carbon Nanofiber/MnO_2 Composites for High-Capacitance Supercapacitors. *J. Alloys Compd.* **2018**, *749*, 441–447. [CrossRef]

63. Wang, Y.; Ding, Y.; Guo, X.; Yu, G. Conductive Polymers for Stretchable Supercapacitors. *Nano Res.* **2019**, *12*, 1978–1987. [CrossRef]

64. Libich, J.; Máca, J.; Vondrák, J.; Čech, O.; Sedlaříková, M. Supercapacitors: Properties and Applications. *J. Energy Storage* **2018**, *17*, 224–227. [CrossRef]

65. Han, H.; Sial, Q.A.; Kalanur, S.S.; Seo, H. Binder Assisted Self-Assembly of Graphene Oxide/Mn2O3 Nanocomposite Electrode on Ni Foam for Efficient Supercapacitor Application. *Ceram. Int.* **2020**, *46*, 15631–15637. [CrossRef]

66. Owusu, K.A.; Qu, L.; Li, J.; Wang, Z.; Zhao, K.; Yang, C.; Hercule, K.M.; Lin, C.; Shi, C.; Wei, Q.; et al. Low-Crystalline Iron Oxide Hydroxide Nanoparticle Anode for High-Performance Supercapacitors. *Nat. Commun.* **2017**, *8*, 14264. [CrossRef]

67. Gao, L.; Cao, K.; Zhang, H.; Li, P.; Song, J.; Surjadi, J.U.; Li, Y.; Sun, D.; Lu, Y. Rationally Designed Nickel Oxide Ravines@iron Cobalt-Hydroxides with Largely Enhanced Capacitive Performance for Asymmetric Supercapacitors. *J. Mater. Chem. A* **2017**, *5*, 16944–16952. [CrossRef]

68. Lu, Q.; Liu, L.; Yang, S.; Liu, J.; Tian, Q.; Yao, W.; Xue, Q.; Li, M.; Wu, W. Facile Synthesis of Amorphous $FeOOH/MnO_2$ Composites as Screen-Printed Electrode Materials for All-Printed Solid-State Flexible Supercapacitors. *J. Power Sources* **2017**, *361*, 31–38. [CrossRef]

69. Zheng, W.; Sun, S.; Xu, Y.; Yu, R.; Li, H. Facile Synthesis of NiAl-LDH/MnO_2 and NiFe-LDH/MnO_2 Composites for High-Performance Asymmetric Supercapacitors. *J. Alloys Compd.* **2018**, *768*, 240–248. [CrossRef]

70. Wei, G.; Du, K.; Zhao, X.; Li, C.; Li, J.; Ren, K.; Huang, Y.; Wang, H.; Yao, S.; An, C. Integrated FeOOH Nanospindles with Conductive Polymer Layer for High-Performance Supercapacitors. *J. Alloys Compd.* **2017**, *728*, 631–639. [CrossRef]

71. Chen, Y.-C.; Lin, Y.-G.; Hsu, Y.-K.; Yen, S.-C.; Chen, K.-H.; Chen, L.-C. Novel Iron Oxyhydroxide Lepidocrocite Nanosheet as Ultrahigh Power Density Anode Material for Asymmetric Supercapacitors. *Small* **2014**, *10*, 3803–3810. [CrossRef] [PubMed]

72. Lee, J.S.; Shin, D.H.; Jun, J.; Lee, C.; Jang, J. Fe3O4/Carbon Hybrid Nanoparticle Electrodes for High-Capacity Electrochemical Capacitors. *ChemSusChem* **2014**, *7*, 1676–1683. [CrossRef] [PubMed]

73. Qu, Q.; Yang, S.; Feng, X. 2D Sandwich-like Sheets of Iron Oxide Grown on Graphene as High Energy Anode Material for Supercapacitors. *Adv. Mater.* **2011**, *23*, 5574–5580. [CrossRef]

74. Lu, X.; Zeng, Y.; Yu, M.; Zhai, T.; Liang, C.; Xie, S.; Balogun, M.-S.; Tong, Y. Oxygen-Deficient Hematite Nanorods as High-Performance and Novel Negative Electrodes for Flexible Asymmetric Supercapacitors. *Adv. Mater.* **2020**, *32*, 2003125. [CrossRef]

75. Zeng, Y.; Han, Y.; Zhao, Y.; Zeng, Y.; Yu, M.; Liu, Y.; Tang, H.; Tong, Y.; Lu, X. Advanced Ti-Doped Fe_2O_3@PEDOT Core/Shell Anode for High-Energy Asymmetric Supercapacitors. *Adv. Energy Mater.* **2015**, *5*, 1402176. [CrossRef]

76. Yang, P.; Ding, Y.; Lin, Z.; Chen, Z.; Li, Y.; Qiang, P.; Ebrahimi, M.; Mai, W.; Wong, C.P.; Wang, Z.L. Low-Cost High-Performance Solid-State Asymmetric Supercapacitors Based on MnO_2 Nanowires and Fe_2O_3 Nanotubes. *Nano Lett.* **2014**, *14*, 731–736. [CrossRef]

77. Wu, M.-S.; Lee, R.-H. Electrochemical Growth of Iron Oxide Thin Films with Nanorods and Nanosheets for Capacitors. *J. Electrochem. Soc.* **2009**, *156*, A737. [CrossRef]

78. Liu, T.; Ling, Y.; Yang, Y.; Finn, L.; Collazo, E.; Zhai, T.; Tong, Y.; Li, Y. Investigation of Hematite Nanorod–Nanoflake Morphological Transformation and the Application of Ultrathin Nanoflakes for Electrochemical Devices. *Nano Energy* **2015**, *12*, 169–177. [CrossRef]

79. Lin, Y.; Wang, X.; Qian, G.; Watkins, J.J. Additive-Driven Self-Assembly of Well-Ordered Mesoporous Carbon/Iron Oxide Nanoparticle Composites for Supercapacitors. *Chem. Mater.* **2014**, *26*, 2128–2137. [CrossRef]

80. Chaudhari, N.K.; Chaudhari, S.; Yu, J.-S. Cube-like α-Fe$_2$O$_3$ Supported on Ordered Multimodal Porous Carbon as High Performance Electrode Material for Supercapacitors. *ChemSusChem* **2014**, *7*, 3102–3111. [CrossRef] [PubMed]

81. Shivakumara, S.; Penki, T.R.; Munichandraiah, N. Synthesis and Characterization of Porous Flowerlike α-Fe$_2$O$_3$ Nanostructures for Supercapacitor Application. *ECS Electrochem. Lett.* **2013**, *2*, A60. [CrossRef]

82. Chen, L.-F.; Yu, Z.-Y.; Ma, X.; Li, Z.-Y.; Yu, S.-H. In Situ Hydrothermal Growth of Ferric Oxides on Carbon Cloth for Low-Cost and Scalable High-Energy-Density Supercapacitors. *Nano Energy* **2014**, *9*, 345–354. [CrossRef]

83. Barik, R.; Jena, B.K.; Mohapatra, M. Metal Doped Mesoporous FeOOH Nanorods for High Performance Supercapacitors. *RSC Adv.* **2017**, *7*, 49083–49090. [CrossRef]

84. Chen, R.; Puri, I.K.; Zhitomirsky, I. High Areal Capacitance of FeOOH-Carbon Nanotube Negative Electrodes for Asymmetric Supercapacitors. *Ceram. Int.* **2018**, *44*, 18007–18015. [CrossRef]

85. Wei, Y.; Ding, R.; Zhang, C.; Lv, B.; Wang, Y.; Chen, C.; Wang, X.; Xu, J.; Yang, Y.; Li, Y. Facile Synthesis of Self-Assembled Ultrathin α-FeOOH Nanorod/Graphene Oxide Composites for Supercapacitors. *J. Colloid Interface Sci.* **2017**, *504*, 593–602. [CrossRef]

86. Chen, L.-F.; Yu, Z.-Y.; Wang, J.-J.; Li, Q.-X.; Tan, Z.-Q.; Zhu, Y.-W.; Yu, S.-H. Metal-like Fluorine-Doped β-FeOOH Nanorods Grown on Carbon Cloth for Scalable High-Performance Supercapacitors. *Nano Energy* **2015**, *11*, 119–128. [CrossRef]

87. Nguyen, T.; Montemor, M.F. γ-FeOOH and Amorphous Ni–Mn Hydroxide on Carbon Nanofoam Paper Electrodes for Hybrid Supercapacitors. *J. Mater. Chem. A* **2018**, *6*, 2612–2624. [CrossRef]

88. Chen, J.; Xu, J.; Zhou, S.; Zhao, N.; Wong, C.-P. Amorphous Nanostructured FeOOH and Co–Ni Double Hydroxides for High-Performance Aqueous Asymmetric Supercapacitors. *Nano Energy* **2016**, *21*, 145–153. [CrossRef]

89. Nie, Y.; Yang, T.; Luo, D.; Liu, Y.; Ma, Q.; Yang, L.; Yao, Y.; Huang, R.; Li, Z.; Akinoglu, E.M.; et al. Tailoring Vertically Aligned Inorganic-Polymer Nanocomposites with Abundant Lewis Acid Sites for Ultra-Stable Solid-State Lithium Metal Batteries. *Adv. Energy Mater.* **2023**, *13*, 2204218. [CrossRef]

90. Ma, J.; Guo, Z.; Han, X.; Guo, K.; Li, H.; Fang, P.; Wang, X.; Xin, J. Reduced Graphene Oxide/FeOOH-Based Asymmetric Evaporator for the Simultaneous Generation of Clean Water and Electrical Power. *Carbon* **2023**, *201*, 318–327. [CrossRef]

91. Yang, P.-Q.; Ko, T.-E.; Tseng, C.-M.; Wang, W.-H.; Huang, C.-C.; Tsai, J.-E.; Fu, Y.-C.; Li, Y.-Y. FeOOH-Carbon Nanotube-FeCo/Nitrogen-Doped Porous Carbon as an Excellent Bifunctional Catalyst for Achieving High Power Performance in Rechargeable Zinc-Air Batteries. *J. Ind. Eng. Chem.* **2023**, *121*, 338–347. [CrossRef]

92. Tang, M.; Liu, X.; Ali, A.; He, Y.; Shen, P.; Ouyang, Y. Operando Spectroscopies Capturing Surface Reconstruction and Interfacial Electronic Regulation by FeOOH@Fe$_2$O$_3$@Ni(OH)$_2$ Heterostructures for Robust Oxygen Evolution Reaction. *J. Colloid Interface Sci.* **2023**, *636*, 501–511. [CrossRef] [PubMed]

93. Vishwanathan, S.; Moolayadukkam, S.; Gangaiah, V.K.; Matte, H.S.S.R. Amorphous MnO$_2$-Modified FeOOH Ternary Composite with High Pseudocapacitance As Anode for Lithium-Ion Batteries. *ACS Appl. Energy Mater.* **2023**, *6*, 2022–2030. [CrossRef]

94. Liu, Y.; Ding, M.; Tian, Y.; Zhao, G.; Huang, J.; Xu, X. In-Situ Growth of 3D Hierarchical γ-FeOOH/Ni3S2 Heterostructure as High Performance Electrocatalyst for Overall Water Splitting. *J. Colloid Interface Sci.* **2023**, *639*, 24–32. [CrossRef] [PubMed]

95. Wang, H.; Ren, X.; Chen, J.; Xu, W.; He, Q.; Wang, H.; Zhan, F.; Chen, L. Recent Advances of Emerging Oxyhydroxide for Electrochemical Energy Storage Applications. *J. Power Sources* **2023**, *554*, 232309. [CrossRef]

96. Mohapatra, M.; Anand, S. Synthesis and Applications of Nano-Structured Iron Oxides/Hydroxides—A Review. *Int. J. Eng. Sci. Technol.* **2010**, *2*, 127–146. [CrossRef]

97. Liu, J.; Zheng, M.; Shi, X.; Zeng, H.; Xia, H. Amorphous FeOOH Quantum Dots Assembled Mesoporous Film Anchored on Graphene Nanosheets with Superior Electrochemical Performance for Supercapacitors. *Adv. Funct. Mater.* **2016**, *26*, 919–930. [CrossRef]

98. Yang, L.; Liu, Y.; Li, J.; Du, G. One-Pot Hydrothermal Synthesis of Amorphous FeOOH on Ni Foam for High Performance Supercapacitors. *J. Alloys Compd.* **2018**, *763*, 134–140. [CrossRef]

99. Wang, T.; Li, K.; Le, Q.; Zhu, S.; Guo, X.; Jiang, D.; Zhang, Y. Tuning Parallel Manganese Dioxide to Hollow Parallel Hydroxyl Oxidize Iron Replicas for High-Performance Asymmetric Supercapacitors. *J. Colloid Interface Sci.* **2021**, *594*, 812–823. [CrossRef]

100. Tanwar, S.; Arya, A.; Sharma, A.L. MoSe2-FeOOH Nanocomposite as Hybrid Electrode Material for High-Performance Symmetric Supercapacitor. *Mater. Res. Bull.* **2023**, *160*, 112144. [CrossRef]

101. Sun, C.; Pan, W.; Zheng, D.; Zheng, Y.; Zhu, J.; Liu, C. Low-Crystalline FeOOH Nanoflower Assembled Mesoporous Film Anchored on MWCNTs for High-Performance Supercapacitor Electrodes. *ACS Omega* **2020**, *5*, 4532–4541. [CrossRef]

102. Li, N.; Zhi, C.; Zhang, H. High-Performance Transparent and Flexible Asymmetric Supercapacitor Based on Graphene-Wrapped Amorphous FeOOH Nanowire and Co(OH)$_2$ Nanosheet Transparent Films Produced at Air-Water Interface. *Electrochim. Acta* **2016**, *220*, 618–627. [CrossRef]

103. Li, N.; Huang, X.; Zhang, H. High Energy Density Transparent and Flexible Asymmetric Supercapacitor Based on a Transparent Metal Hydroxides@graphene Micro-Structured Film via a Scalable Gas-Liquid Diffusion Method. *J. Alloys Compd.* **2017**, *712*, 194–203. [CrossRef]

104. Parveen, S.; Kavyashree; Sharma, S.K.; Pandey, S.N. High Performance Solid State Symmetric Supercapacitor Based on Reindeer Moss-like Structured Al(OH)3/MnO$_2$/FeOOH Composite Electrode for Energy Storage Applications. *Energy* **2021**, *224*, 120137. [CrossRef]

105. Gao, X.; Lv, H.; Li, Z.; Xu, Q.; Liu, H.; Wang, Y.; Xia, Y. Low-Cost and High-Performance of a Vertically Grown 3D Ni–Fe Layered Double Hydroxide/Graphene Aerogel Supercapacitor Electrode Material. *RSC Adv.* **2016**, *6*, 107278–107285. [CrossRef]

106. Lu, Y.; Jiang, B.; Fang, L.; Ling, F.; Wu, F.; Hu, B.; Meng, F.; Niu, K.; Lin, F.; Zheng, H. An Investigation of Ultrathin Nickel-Iron Layered Double Hydroxide Nanosheets Grown on Nickel Foam for High-Performance Supercapacitor Electrodes. *J. Alloys Compd.* **2017**, *714*, 63–70. [CrossRef]

107. Sanati, S.; Rezvani, Z. Ultrasound-Assisted Synthesis of NiFe- Layered Double Hydroxides as Efficient Electrode Materials in Supercapacitors. *Ultrason. Sonochem.* **2018**, *48*, 199–206. [CrossRef]

108. Wang, F.; Wang, T.; Sun, S.; Xu, Y.; Yu, R.; Li, H. One-Step Synthesis of Nickle Iron-Layered Double Hydroxide/Reduced Graphene Oxide/Carbon Nanofibres Composite as Electrode Materials for Asymmetric Supercapacitor. *Sci. Rep.* **2018**, *8*, 8908. [CrossRef] [PubMed]

109. Xiao, T.; Wang, S.; Li, J.; Yang, N.; Li, W.; Xiang, P.; Jiang, L.; Tan, X. Sulfidation of NiFe-Layered Double Hydroxides as Novel Negative Electrodes for Supercapacitors with Enhanced Performance. *J. Alloys Compd.* **2018**, *768*, 635–643. [CrossRef]

110. Li, M.; Jijie, R.; Barras, A.; Roussel, P.; Szunerits, S.; Boukherroub, R. NiFe Layered Double Hydroxide Electrodeposited on Ni Foam Coated with Reduced Graphene Oxide for High-Performance Supercapacitors. *Electrochim. Acta* **2019**, *302*, 1–9. [CrossRef]

111. Tian, J.; Zhang, A.; Liu, R.; Huang, W.; Yuan, Z.; Zheng, R.; Wei, D.; Liu, J. Preparation of CoS2 Supported Flower-like NiFe Layered Double Hydroxides Nanospheres for High-Performance Supercapacitors. *J. Colloid Interface Sci.* **2020**, *579*, 607–618. [CrossRef] [PubMed]

112. Zhou, H.; Wu, F.; Fang, L.; Hu, J.; Luo, H.; Guan, T.; Hu, B.; Zhou, M. Layered NiFe-LDH/MXene Nanocomposite Electrode for High-Performance Supercapacitor. *Int. J. Hydrogen Energy* **2020**, *45*, 13080–13089. [CrossRef]

113. Shakir, I.; Almutairi, Z.; Shar, S.S. Fabrication of Carbon Cloth Supported Ni@Fe Double Hydroxide Based Electrode for Flexible Supercapacitor Applications. *Ceram. Int.* **2021**, *47*, 17427–17434. [CrossRef]

114. Hsiao, C.; Lee, C.; Tai, N. High Retention Supercapacitors Using Carbon Nanomaterials/Iron Oxide/Nickel-Iron Layered Double Hydroxides as Electrodes. *J. Energy Storage* **2022**, *46*, 103805. [CrossRef]

115. Shao, W.; Wang, Q.; Huang, C.; Zhang, D. High Valence State Metal-Ion Doped Fe–Ni Layered Double Hydroxides for Oxygen Evolution Electrocatalysts and Asymmetric Supercapacitors. *Mater. Adv.* **2022**, *3*, 1816–1824. [CrossRef]

116. Wang, Y.; Chen, Z.; Zhang, M.; Liu, Y.; Luo, H.; Yan, K. Green Fabrication of Nickel-Iron Layered Double Hydroxides Nanosheets Efficient for the Enhanced Capacitive Performance. *Green Energy Environ.* **2022**, *7*, 1053–1061. [CrossRef]

117. Ma, K.; Cheng, J.P.; Zhang, J.; Li, M.; Liu, F.; Zhang, X. Dependence of Co/Fe Ratios in Co-Fe Layered Double Hydroxides on the Structure and Capacitive Properties. *Electrochim. Acta* **2016**, *198*, 231–240. [CrossRef]

118. Wu, Y.-J.; Zhang, W.-T.; Liu, Z.-W.; Chen, R.-F. Synthesis of Co$_{1-x}$Fe$_x$ Hydroxide Nanoplatelets and Its Electrochemical Performances as Supercapacitor Electrode Materials. *Electrochemistry* **2016**, *84*, 2–6. [CrossRef]

119. Jiang, L.; Sui, Y.; Qi, J.; Chang, Y.; He, Y.; Meng, Q.; Wei, F.; Sun, Z.; Jin, Y. Structure Dependence of Fe-Co Hydroxides on Fe/Co Ratio and Their Application for Supercapacitors. *Part. Part. Syst. Charact.* **2017**, *34*, 1600239. [CrossRef]

120. Fang, X.; Han, S.; Liu, D.; Zhu, Y. Two-Dimensional CoFe Hydroxides Nanostructure as Positive Material for Asymmetric Supercapacitor. *Chem. Phys. Lett.* **2020**, *746*, 137282. [CrossRef]

121. Jo, S.; Jayababu, N.; Kim, D. Rational Design of Cobalt-Iron Bimetal Layered Hydroxide on Conductive Fabric as a Flexible Battery-Type Electrode for Enhancing the Performance of Hybrid Supercapacitor. *J. Alloys Compd.* **2022**, *904*, 164082. [CrossRef]

122. Mahmood, A.; Zhao, B.; Javed, M.S.; He, D.; Cheong, W.-C.; Han, D.; Niu, L. Unprecedented Dual Role of Polyaniline for Enhanced Pseudocapacitance of Cobalt–Iron Layered Double Hydroxide. *Macromol. Rapid Commun.* **2022**, *43*, 2100905. [CrossRef] [PubMed]

123. Li, X.; Zhang, L.; Chai, H.; Zhang, Y.; Wang, R.; Xie, M.; Xu, Y.; Chen, J.; Jiao, Y. Electrochemical Activation Strategy Assisted Morphology Engineering Co-Fe Layered Double Hydroxides for Oxygen Hydrogen Evolution and Supercapacitor. *J. Colloid Interface Sci.* **2023**, *632*, 186–195. [CrossRef] [PubMed]

124. Wang, F.; Sun, S.; Xu, Y.; Wang, T.; Yu, R.; Li, H. High Performance Asymmetric Supercapacitor Based on Cobalt Nickle Iron-Layered Double Hydroxide/Carbon Nanofibres and Activated Carbon. *Sci. Rep.* **2017**, *7*, 4707. [CrossRef]

125. Pourfarzad, H.; Shabani-Nooshabadi, M.; Ganjali, M.R.; Kashani, H. Synthesis of Ni–Co-Fe Layered Double Hydroxide and Fe$_2$O$_3$/Graphene Nanocomposites as Actively Materials for High Electrochemical Performance Supercapacitors. *Electrochim. Acta* **2019**, *317*, 83–92. [CrossRef]

126. Lee, S.C.; Liu, S.; Shinde, P.A.; Chung, K.Y.; Chan Jun, S. A Systematic Approach to Achieve High Energy Density Hybrid Supercapacitors Based on Ni–Co–Fe Hydroxide. *Electrochim. Acta* **2020**, *353*, 136578. [CrossRef]

127. Ren, X.; Zhou, Y.; Du, Y.; Jiang, Y.; Chen, Y.; Wan, J.; Ma, F. Facile Ion Exchange to Construct Ni-Fe-Co Sulfides and Hydroxides Ultrathin Nanosheets with Rich Interfaces for Advanced All-Solid-State Asymmetric Supercapacitors. *Appl. Surf. Sci.* **2020**, *514*, 145951. [CrossRef]

128. Rohit, R.C.; Jagadale, A.D.; Shinde, S.K.; Kim, D.-Y.; Kumbhar, V.S.; Nakayama, M. Hierarchical Nanosheets of Ternary CoNiFe Layered Double Hydroxide for Supercapacitors and Oxygen Evolution Reaction. *J. Alloys Compd.* **2021**, *863*, 158081. [CrossRef]

129. Liao, F.; Yang, G.; Cheng, Q.; Mao, L.; Zhao, X.; Chen, L. Rational Design and Facile Synthesis of Ni-Co-Fe Ternary LDH Porous Sheets for High-Performance Aqueous Asymmetric Supercapacitor. *Electrochim. Acta* **2022**, *428*, 140939. [CrossRef]

130. Zhao, Y.; Feng, Z.; Guo, Z.; Mu, J.; Che, H.; Zhang, Z.; Tian, T.; Xiaoliang, Z.; Li, S.; Wang, Y.; et al. Fe Incorporated Ternary Layered Double Hydroxides with Remarkably Improved Electrochemical Performance towards Asymmetric Supercapacitors. *Ceram. Int.* **2022**, *48*, 27369–27378. [CrossRef]

131. Wang, H.; He, Q.; Zhan, F.; Chen, L. Fe, Co-Codoped Layered Double Hydroxide Nanosheet Arrays Derived from Zeolitic Imidazolate Frameworks for High-Performance Aqueous Hybrid Supercapacitors and Zn-Ni Batteries. *J. Colloid Interface Sci.* **2023**, *630*, 286–296. [CrossRef]

132. Zhang, D.; Peng, L.; Yang, Z.; Yang, Y.; Li, H. Gold-Supported Nanostructured NiFeCoPr Hydroxide as a High-Performance Supercapacitor Electrode and Electrocatalyst toward the Oxygen Evolution Reaction. *Inorg. Chem.* **2019**, *58*, 15841–15852. [CrossRef]

133. Elgendy, A.; El Basiony, N.M.; El-Taib Heakal, F.; Elkholy, A.E. Mesoporous Ni-Zn-Fe Layered Double Hydroxide as an Efficient Binder-Free Electrode Active Material for High-Performance Supercapacitors. *J. Power Sources* **2020**, *466*, 228294. [CrossRef]

134. Yang, Y.J.; Chen, S.; Jiang, C.; Yang, P.; Wang, N.; Cheng, Y.; Liu, M. Hierarchical Web-like NiFeMn Ternary Hydroxides Microstructure Assembled on Reduced Graphene Oxide for Binder-Free Supercapacitor Electrode. *Diam. Relat. Mater.* **2022**, *125*, 109009. [CrossRef]

135. Nguyen, Q.T.; Nakate, U.T.; Chen, J.; Tran, D.T.; Park, S. Evolution of Novel Nanostructured MoCoFe-Based Hydroxides Composites toward High-Performance Electrochemical Applications: Overall Water Splitting and Supercapacitor. *Compos. Part B Eng.* **2023**, *252*, 110528. [CrossRef]

136. Zhao, N.; Feng, Y.; Chen, H. Exquisite Microstructure Design of Quaternary Nickel Cobalt Manganese Iron Layered Double Hydroxides for High Performance Hybrid Supercapacitors. *Electrochim. Acta* **2023**, *441*, 141756. [CrossRef]

137. Li, H.B.; Yu, M.H.; Wang, F.X.; Liu, P.; Liang, Y.; Xiao, J.; Wang, C.X.; Tong, Y.X.; Yang, G.W. Amorphous Nickel Hydroxide Nanospheres with Ultrahigh Capacitance and Energy Density as Electrochemical Pseudocapacitor Materials. *Nat. Commun.* **2013**, *4*, 1894. [CrossRef] [PubMed]

138. Li, H.; Gao, Y.; Wang, C.; Yang, G. A Simple Electrochemical Route to Access Amorphous Mixed-Metal Hydroxides for Supercapacitor Electrode Materials. *Adv. Energy Mater.* **2015**, *5*, 1401767. [CrossRef]

139. Ragni, R.; Cicco, S.R.; Vona, D.; Farinola, G.M. Multiple Routes to Smart Nanostructured Materials from Diatom Microalgae: A Chemical Perspective. *Adv. Mater.* **2018**, *30*, 1704289. [CrossRef] [PubMed]

140. Sun, X.W.; Zhang, Y.X.; Losic, D. Diatom Silica, an Emerging Biomaterial for Energy Conversion and Storage. *J. Mater. Chem. A* **2017**, *5*, 8847–8859. [CrossRef]

141. Geim, A.K.; Novoselov, K.S. The Rise of Graphene. *Nat. Mater* **2007**, *6*, 183–191. [CrossRef] [PubMed]

142. Wang, C.; Zhai, P.; Zhang, Z.; Zhou, Y.; Ju, J.; Shi, Z.; Ma, D.; Han, R.P.S.; Huang, F. Synthesis of Highly Stable Graphene-Encapsulated Iron Nanoparticles for Catalytic Syngas Conversion. *Part. Part. Syst. Charact.* **2015**, *32*, 29–34. [CrossRef]

143. Amiri, A.; Bruno, A.; Polycarpou, A.A. Configuration-Dependent Stretchable All-Solid-State Supercapacitors and Hybrid Supercapacitors. *Carbon Energy* **2023**, e320. [CrossRef]

144. Transparent, Flexible, and Solid-State Supercapacitors Based on Graphene Electrodes: APL Materials: Vol 1, No 1. Available online: https://aip.scitation.org/doi/full/10.1063/1.4808242 (accessed on 9 March 2023).

145. Bae, S.; Kim, H.; Lee, Y.; Xu, X.; Park, J.-S.; Zheng, Y.; Balakrishnan, J.; Lei, T.; Ri Kim, H.; Song, Y.I.; et al. Roll-to-Roll Production of 30-Inch Graphene Films for Transparent Electrodes. *Nat. Nanotech* **2010**, *5*, 574–578. [CrossRef]

146. Yoo, J.J.; Balakrishnan, K.; Huang, J.; Meunier, V.; Sumpter, B.G.; Srivastava, A.; Conway, M.; Mohana Reddy, A.L.; Yu, J.; Vajtai, R.; et al. Ultrathin Planar Graphene Supercapacitors. *Nano Lett.* **2011**, *11*, 1423–1427. [CrossRef]

147. Xu, P.; Kang, J.; Choi, J.-B.; Suhr, J.; Yu, J.; Li, F.; Byun, J.-H.; Kim, B.-S.; Chou, T.-W. Laminated Ultrathin Chemical Vapor Deposition Graphene Films Based Stretchable and Transparent High-Rate Supercapacitor. *ACS Nano* **2014**, *8*, 9437–9445. [CrossRef]

148. Li, N.; Yang, G.; Sun, Y.; Song, H.; Cui, H.; Yang, G.; Wang, C. Free-Standing and Transparent Graphene Membrane of Polyhedron Box-Shaped Basic Building Units Directly Grown Using a NaCl Template for Flexible Transparent and Stretchable Solid-State Supercapacitors. *Nano Lett.* **2015**, *15*, 3195–3203. [CrossRef] [PubMed]

149. Niu, Z.; Zhou, W.; Chen, J.; Feng, G.; Li, H.; Hu, Y.; Ma, W.; Dong, H.; Li, J.; Xie, S. A Repeated Halving Approach to Fabricate Ultrathin Single-Walled Carbon Nanotube Films for Transparent Supercapacitors. *Small* **2013**, *9*, 518–524. [CrossRef] [PubMed]

150. Zhao, M.; Zhao, Q.; Li, B.; Xue, H.; Pang, H.; Chen, C. Recent Progress in Layered Double Hydroxide Based Materials for Electrochemical Capacitors: Design, Synthesis and Performance. *Nanoscale* **2017**, *9*, 15206–15225. [CrossRef]

151. Mohapatra, L.; Parida, K. A Review on the Recent Progress, Challenges and Perspective of Layered Double Hydroxides as Promising Photocatalysts. *J. Mater. Chem. A* **2016**, *4*, 10744–10766. [CrossRef]

152. Abellán, G.; Carrasco, J.A.; Coronado, E.; Romero, J.; Varela, M. Alkoxide-Intercalated CoFe-Layered Double Hydroxides as Precursors of Colloidal Nanosheet Suspensions: Structural, Magnetic and Electrochemical Properties. *J. Mater. Chem. C* **2014**, *2*, 3723–3731. [CrossRef]

153. Wang, L.; Wang, D.; Dong, X.Y.; Zhang, Z.J.; Pei, X.F.; Chen, X.J.; Chen, B.; Jin, J. Layered Assembly of Graphene Oxide and Co–Al Layered Double Hydroxide Nanosheets as Electrode Materials for Supercapacitors. *Chem. Commun.* **2011**, *47*, 3556–3558. [CrossRef]

154. Li, M.; Cheng, J.P.; Fang, J.H.; Yang, Y.; Liu, F.; Zhang, X.B. NiAl-Layered Double Hydroxide/Reduced Graphene Oxide Composite: Microwave-Assisted Synthesis and Supercapacitive Properties. *Electrochim. Acta* **2014**, *134*, 309–318. [CrossRef]
155. Rohit, R.C.; Jagadale, A.D.; Lee, J.; Lee, K.; Shinde, S.K.; Kim, D.-Y. Tailoring the Composition of Ternary Layered Double Hydroxides for Supercapacitors and Electrocatalysis. *Energy Fuels* **2021**, *35*, 9660–9668. [CrossRef]